Scuola Internazionale Superiore Studi Avanzati -S.I.S.S.A
International School for Advanced Studies -I.S.A.S
Trieste, Italy

Regulation by calcium, voltage and permeant anions of TMEM16B/anoctamin2

Thesis submitted for the degree of
"Doctor Philosophiae"

CANDIDATE:

Giulia Betto

SUPERVISOR:

Prof. Anna Menini

SISSA – Via Bonomea 265 – 34136 Trieste - Italy

To mamma&babbo

DECLARATION

The work described in this Thesis was carried out at the International School for Advanced Studies, Trieste, between November 2008 and May 2014. The work was suspended from May 2012 to October 2013 because of maternity.

The work described in this Thesis is included in:

Valentina Cenedese, Giulia Betto, Fulvio Celsi, O. Lijo Cherian, Simone Pifferi, and Anna Menini

The voltage-dependence of the TMEM16B/anoctamin2 calcium- activated chloride channel is modified by mutations in the first putative intracellular loop.

J Gen Physiol. 2012 Apr;139(4):285-94. March, 2012.

I performed some of the experiments and data analysis.

Giulia Betto*, O.Lijo Cherian*, Simone Pifferi*, Valentina Cenedese, Anna Boccaccio, Anna Menini

Interaction between permeation and gating in the TMEM16B/anoctamin2 calcium-activated chloride channel.

J Gen Physiol, 2014 in press.

* These authors contributed equally to this paper.

I performed some of the experiments and data analysis.

ABSTRACT

Ca^{2+}- activated Cl^- channels (CaCCs) play important roles in many physiological processes, including olfactory transduction, modulation of light photoreceptor responses, epithelial secretion. The molecular identity of these channels has been elusive for a long time, but recently it was shown that two members of the TMEM16/anoctamin family, TMEM16A/anoctamin1 and TMEM16B/anoctamin2, are responsible for CaCCs in several cells. At present, little is known about the structure-function relations for TMEM16A and TMEM16B.

In the first part of this Thesis, we performed for the first time a site-directed mutagenesis study on TMEM16B to understand the molecular mechanisms of voltage and Ca^{2+} dependence. We mutated aminoacids in the first putative intracellular loop and measured the properties of the wild-type and mutant TMEM16B channels expressed in HEK 293T cells using the whole cell patch-clamp technique. In particular, we obtained three different mutants of TMEM16B: E367Q, ΔE_5 (deletion of the five consecutive glutamates $_{386}$EEEEE$_{390}$), and ΔEYE (deletion of three aminoacids $_{399}$EYE$_{401)}$ in the first intracellular loop. Ca^{2+} and voltage dependence of channel activation were not significantly modified in the ΔEYE mutant compared to the wild-type channel. E367Q and deletion of five glutamates modified the voltage dependence of the TMEM16B, shifting the conductance-voltage relation toward more positive voltages. None of these mutants affected the apparent Ca^{2+} affinity. These results show that glutamates E367 and $_{386}$EEEEE$_{390}$ in the first putative intracellular loop contribute to the voltage-dependent regulation of the TMEM16B channel.

In the second part of this Thesis, we studied the relation between permeation and gating of TMEM16B, using both the whole cell and the inside-out patch clamp techniques. The permeability ratio sequence substituting Cl^- with other anions at the extracellular or intracellular side was: SCN^-> I^-> NO_3^-> Br^-> Cl^-> F^-> gluconate. Activation and deactivation kinetics at 0.5 μM Ca^{2+} were affected by the presence of various anions. The time constants of deactivation became slower in the presence of anions more permeant than Cl^-, and faster with anions less permeant than Cl^-. The voltage-dependence of channel activation was also modified by anions. When external Cl^- was reduced by partial replacement with the less permeant gluconate, or

with sucrose, the conductance-voltage relation was shifted toward more positive voltages. Conversely, the substitution of Cl^- with more permeant anions shifted the conductance-voltage relation to more negative voltages. Moreover, in the presence of different extracellular anions the apparent affinity for Ca^{2+} increased with increasing the permeability ratios. We also investigated the effect of replacing Cl^- with SCN^- at the intracellular side of the channel and found similar gating modifications as from the extracellular side. These results provide the first evidence that gating of TMEM16B is modulated by permeant anions.

CONTENTS

ABBREVIATIONS

Anoctamin	ANion selective and eight (OCT) transmembrane segments
BK	Big conductance Ca^{2+} activated K^{+} Channel
CaCC	Calcium activated Chloride Channel
CaM	Calmodulin
cAMP	cyclic Adenosine MonoPhosphate
DIDS	4-4'diisothiocynostilbene-2-2'disulphonic acid
DRG	Dorsal Root Ganglia
DTT	Dithiolthreitol
FRT cell	Fisher Rat Thyroid cell
GFP	Green Fluorescent Protein
HEK cell	Human Embryonic Kidney cells
NFA	NiFlumic Acid

NPPB	5-nitro-2-(3-phenylpropylamino)benzoic acid
PCR	Polymerase Chain Reaction
PIP_3	Phosphatidylinositol-3,4,5-trisphoshate
SITS	4-acetamido-4'-isothiocynostilbene-2.2'disulphonic acid
TMEM16	Transmembrane protein with unknown function 16

1. INTRODUCTION

1.1. Ca^{2+}- activated Cl^- channels

Calcium-activated chloride currents (CaCCs) play important roles in cellular physiology. These channels were first described in *Xenopus* oocytes, where fertilization produces an increase in $[Ca^{2+}]_i$ causing the opening of CaCCs. The efflux of Cl^- through CaCCs in *Xenopus* oocytes produces a membrane depolarization, which has been shown to block the fusion of additional sperm, thus preventing polyspermy (Miledi, 1982; Barish, 1983).

CaCCs have been found in several cell types and are involved in many physiological processes, including epithelial secretion, membrane excitability in cardiac muscle and neurons, olfactory transduction, regulation of vascular tone, modulation of photoreceptor light responses (Hartzell et al., 2005).

CaCCs are activated by cytosolic Ca^{2+} and the movement of Cl^- depends on the membrane potential and on the Cl^- concentration gradient across the cellular membrane.

In airway epithelia, activation of CaCCs contributes to the control of the level of mucous hydration, which is important for protection against infection. Since intracellular Cl^- concentration is high, the activation of CaCCs causes an efflux of Cl^-, which is followed by Na^+ efflux, resulting in secretion of NaCl and transepithelial water transport. Moreover, CaCCs play a role in exocrine secretion in many types of glands (Kidd and Thorn, 2000; Melvin et al., 2005).

In smooth muscle cells, CaCC activity is involved in signal amplification leading to cell contraction. A Ca^{2+} increase activates CaCCs, producing an efflux of Cl^-. The membrane depolarization allows the activation of voltage-gated Ca^{2+} channels that mediate further Ca^{2+} influx and increase muscle contraction (Leblanc et al., 2005).

In dorsal root ganglion (DRG) neurons, spinal cord neurons and in neurons of the autonomic nervous system, CaCCs are thought to regulate neuronal excitability, although the mechanism is poorly established. In DRG neurons, opening of these channels would depolarize the cell membranes or produce

after-depolarization following an action potential (Scott et al., 1995; De Castro et al., 1997; Frings et al., 2000; Hartzell et al., 2005). On the other hand, in spinal cord neurons, intracellular Cl^- is low and the activation of CaCCs would stabilize the resting membrane potential or hyperpolarize the cell membrane (Scott et al., 1995).

In olfactory sensory neurons (OSNs), CaCCs mediate depolarization and are thought to play a key role in the amplification of the initial receptor current or in stabilizing the response to odorants in the presence of various ionic conditions (Kleene and Gesteland, 1991; Kleene, 1993; Kurahashi and Yau, 1994; Schild and Restrepo, 1998; Boccaccio and Menini, 2007; Kleene, 2008). In taste cells, CaCCs have been proposed to contribute to hyperpolarization and to adaptation (Taylor and Roper, 1994; Herness and Sun, 1999).

CaCCs are also found in neurons and glia cells of retina. In photoreceptors, they are activated in response to depolarization-evoked Ca^{2+} influx during the dark current. It has been suggested that they are necessary to stabilize the presynaptic membrane potential during synaptic activity (Lalonde et al., 2008).

CaCCs in different cell systems could display different characteristics but some biophysical hallmark features common to native channels have been identified (Hartzell et al., 2005).

They are activated by cytosolic Ca^{2+} with half maximal concentration ($K_{1/2}$) for activation in the submicromolar range. $K_{1/2}$ values may be different in specific tissue; for example it has been reported that $K_{1/2}$ value in pulmonary artery endothelial cells was 283 nM at +100 mV (Nilius et al., 1997), 0.9 nM at +120 mV in *Xenopus* oocytes (Kuruma and Hartzell, 2000), or 63 nM at +97 mV in rat parotid acinar cells (Arreola et al., 1996). The Hill coefficient was higher than 1, suggesting than more than one Ca^{2+} is necessary to activate the channel. CaCCs exhibit outward rectification at low intracellular Ca^{2+} and become linear at higher Ca^{2+} concentrations (Arreola et al., 1996; Kuruma and Hartzell, 2000; Reisert et al., 2003). See figure 1.1.

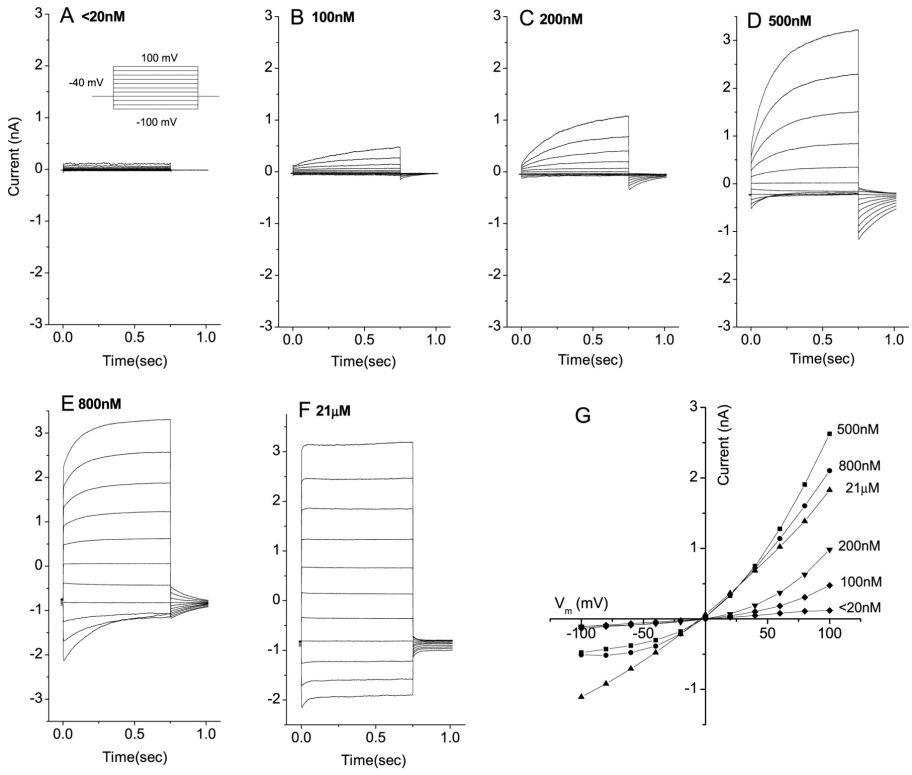

Figure 1.1. Properties of Ca^{2+} activated Cl^- channel. Each panel reports traces of CaCCs recorded in the whole cell configuration from mouse kidney medullary collecting duct cell line with different Ca^{2+} concentration in the pipette solution. Cells were voltage clamped and the voltage was stepped from a holding potential of -40 mV to different voltages between -100 and +100 mV for 0.75 s with a 20 mV increment for each step, followed by a step to -40 mV. Panel G shows the steady-state current-voltage relationship (Qu et al., 2003).

These channels are relatively nonselective among anions. The Na^+ permeability is about 10% that of Cl^- (Jentsch, 2002). CaCCs preferentially permeate large anions, with the following anion permeability sequence $SCN^- > NO_3^- > I^- > Br^- > Cl^- > F^-$ (Large and Wang, 1996; Qu and Hartzell, 2000).

Moreover, permeant anions could influence the activation of CaCCs (Greenwood and Large, 1999; Perez-Cornejo and Arreola, 2004).

There are no specific blockers for CaCCs (Verkman and Galietta, 2009). The most used blockers for native CaCCs are NFA (niflumic acid) and flufenamic acid (White and Aylwin, 1990) that block CaCCs in Xenopus oocytes at 10 μ M (Qu and Hartzell, 2001). Other less efficient blockers for CaCCs are tamoxifen, DIDS, SITS, NPPB, A9C (Frings et al., 2000).

The electrophysiological characteristics of CaCCs have been studied since 1980s but the physiological role of these channels in many tissues is still unclear (Hartzell et al., 2005). Moreover, the molecular identity of the protein has remained elusive for a long time until, in 2008, three different groups using different approaches identified TMEM16A as a major component of CaCCs (Caputo et al., 2008; Schroeder et al., 2008; Yang et al., 2008).

1.2. TMEM16/Anoctamin family

The TMEM16 gene family was first identified by bioinformatic analysis (Katoh and Katoh, 2003). The term 'TMEM16' stands for 'transmembrane protein with unknown function 16'. However, members of the TMEM16 family were already known with different names for being involved in some tumors (West et al., 2004; Galindo and Vacquier, 2005; Huang et al., 2006; Espinosa et al., 2008; Kashyap et al., 2009). TMEM16 proteins are well conserved among eukaryotes; humans and mice have 10 genes named TMEM16A-K, sharing considerable homology (Galindo and Vacquier, 2005). See figure 1.2.

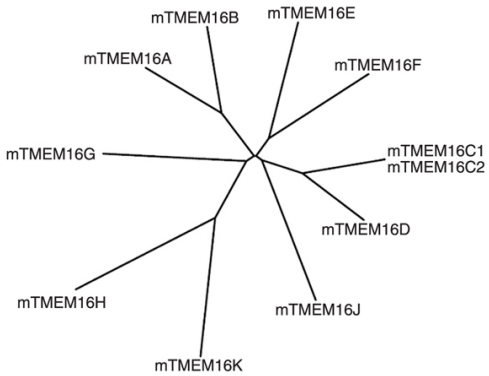

Figure 1.2. Phylogenetic tree of the mouse TMEM16 family members (Flores et al., 2009).

Mammalian subfamilies TMEM16A and B are closely related, as are C and D, H and K (Hartzell et al., 2009). Current data suggest that members of TMEM16 protein family are involved in both normal vertebrate development

and disease. The existence of multiple TMEM16 paralogs in mice and humans might have evolved to allow tissue-specific expression of proteins with similar function (Galindo and Vacquier, 2005; Rock and Harfe, 2008; Duran and Hartzell, 2011).

In 2008, three independent laboratories using different approaches reported that the TMEM16A protein is able to form a CaCC (Caputo et al., 2008; Schroeder et al., 2008; Yang et al., 2008). Yang et al. (2008), named the family Anoctamin because TMEM16A/ANO1 forms anion selective channels (AN) and hydropathy analysis indicated that the protein has eight (OCT) transmembrane segments (Yang et al., 2008). TMEM16B/ANO2 has also been shown to function as a CaCC (Schroeder et al., 2008; Stephan et al., 2009; Pifferi et al., 2009; Stöhr et al., 2009). However, it is still unclear if all the members of the family are able to form CaCCs. Almaca et al. (2009) suggested that TMEM16F/ANO6, TMEM16H/ANO8 and TMEM16J/ANO9 form swelling activated Cl^- channels implicated in the control of cell volume (Almaça et al., 2009). However, different results were found by Scudieri et al. (2012), who did not measure an increase in anion transport or membrane current when TMEM16F/ANO6, TMEM16G/ANO7, TMEM16H/ANO8, TMEM16J/ANO9 or TMEM16K/ANO10, were transfected in HEK 293 cells (Scudieri et al., 2012). In 2010, Schreiber et al. (2010) showed that TMEM16H/ANO8 inhibits TMEM16A/ANO1 current (Schreiber et al., 2010). TMEM16F/ANO6 has been shown to be involved in phospholipid scramblase activity (Suzuki et al., 2010), but also to constitute a CaCC or a pore-forming subunit of an anion channel (Grubb et al., 2013). Morevover, Yang et al. (2012) showed that TMEM16F/ANO6 forms a Ca^{2+}-activated cation channel critical for Ca^{2+}-dependent scramblase activity (Yang et al., 2012)

In the Introduction of this Thesis, I will mainly report results about TMEM16A and TMEM6B, the only two members of the family known to be CaCCs.

1.3. Expression of TMEM16A and TMEM16B

The expression of TMEM16A and TMEM16B has been investigated in several studies. Huang et al. (2009) raised an antibody specific for mouse TMEM16A, as shown by the absence of staining in immunohistochemistry experiments in knockout mice for TMEM16A. These authors found that TMEM16A was expressed in the apical membrane of acinar cells of salivary glands and of the pancreas, in the airway smooth muscle cells, in the apical membranes of epithelial cells in exocrine glands, trachea and in the interstitial cells of Cajal. TMEM16A is also expressed in the supporting cells in the olfactory and vomeronasal epithelium (Billig et al., 2011; Dauner et al., 2012; Dibattista et al., 2012; Maurya and Menini, 2013) and in microvilli of vomeronasal sensory neurons (Dibattista et al., 2012).

TMEM16B is expressed in the cilia of olfactory sensory neurons (Stephan et al., 2009; Hengl et al., 2010; Rasche et al., 2010; Billig et al., 2011; Dauner et al., 2012), in presynaptic terminals of retinal photoreceptors (Stöhr et al., 2009; Billig et al., 2011; Dauner et al., 2013), and in hippocampal cells (Huang et al., 2012).

Studies with knockout mice for TMEM16A or TMEM16B (Rock and Harfe, 2008; Billig et al., 2011) or knockdown of these proteins confirmed a reduction in CaCC activity in several tissues (Flores et al., 2009; Galietta, 2009; Hartzell et al., 2009; Kunzelmann et al., 2011; Pifferi et al., 2012; Sanders et al., 2012; Scudieri et al., 2012; Huang et al., 2012).

1.4. Topology of TMEM16 family

The TMEM16 family does not share any significant sequence homology with other known ion channel families. Within the TMEM16 family, the primary sequence identity between TMEM16A and TMEM16B is relatively high (around 60%) but decreases progressively with the other TMEM16 proteins: TMEM16F, G, H, J and K are only 20-30% identical (Galietta, 2009). Bioinformatic hydropathy analysis predicts that TMEM16 proteins have eight

transmembrane domains (TM), with cytosolic N and C termini, and a N-linked glycosylation site in the last extracellular loop (except for TMEM16K) (Hartzell et al., 2009; Kunzelmann et al., 2009; Flores et al., 2009; Galietta, 2009). A region located between transmembrane domains 5 and 6 was proposed to form a re-entrant loop exposed to the extracellular membrane side and to be part of the channel pore. In TMEM16A, mutations of some basic aminoacids in this region, such as R610E, altered ion selectivity (Yang et al., 2008), although another study did not confirm the change in ion selectivity (Yu et al., 2012). Hartzell's group proposed a different topology in which the re-entrant loop is exposed to the intracellular side of the membrane, forming the third intracellular loop. Indeed, mutagenesis of two aminoacids in this region, E702 and E705, modified Ca^{2+} sensitivity of TMEM16A (Yu et al., 2012). See figure 1.3.

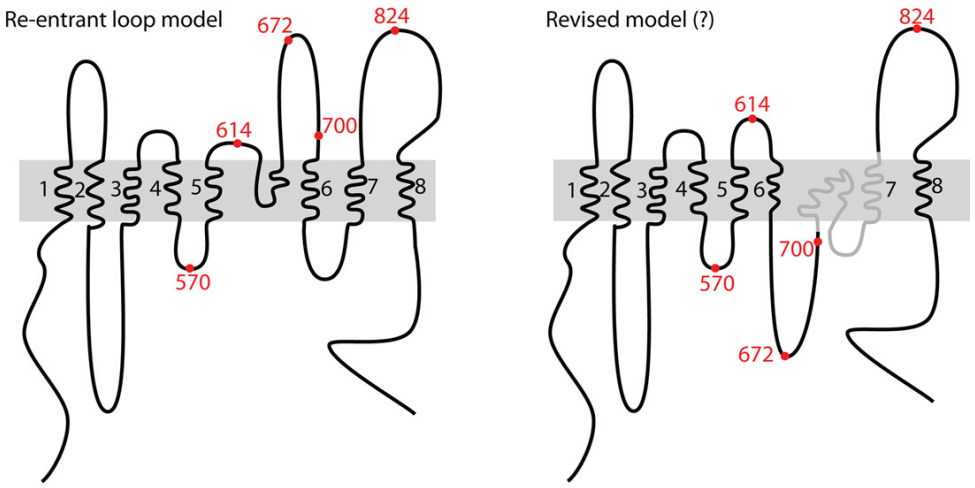

Figure 1.3. Topology of TMEM16A channel. On the left the old version of the structure where the re-entrant loop between transmembrane 5 and 6 is on the extracellular side of the channel; on the right the revised model where the third re-entrant loop is on the intracellular side of the channel (Yu et al., 2012).

1.5. Alternative splicing

Both TMEM16A and TMEM16B have various protein isoforms generated by alternative splicing (Caputo et al., 2008; Ferrera et al., 2009; Ponissery Saidu et al., 2013).

Galietta's group identified the presence of different TMEM16A isoforms. They found a basic minimal isoform, named TMEM16A (0), formed by 840 residues with all putative transmembrane domains. This basic structure can be expanded by addition of four alternative segments. Segment *a* with 116 residues at the N-terminus; segment *b* with 22 residues located before the first transmembrane domain; segment *c* with 4 residues and segment *d* with 26 residues located in the first intracellular loop, connecting the second and the third transmembrane domains. All these protein isoforms make functional channels with different biophysical characteristics, which will be described in Section 1.7 (Caputo et al., 2008; Ferrera et al., 2009; Galietta, 2009; Ferrera et al., 2010, 2011). See figure 1.4.

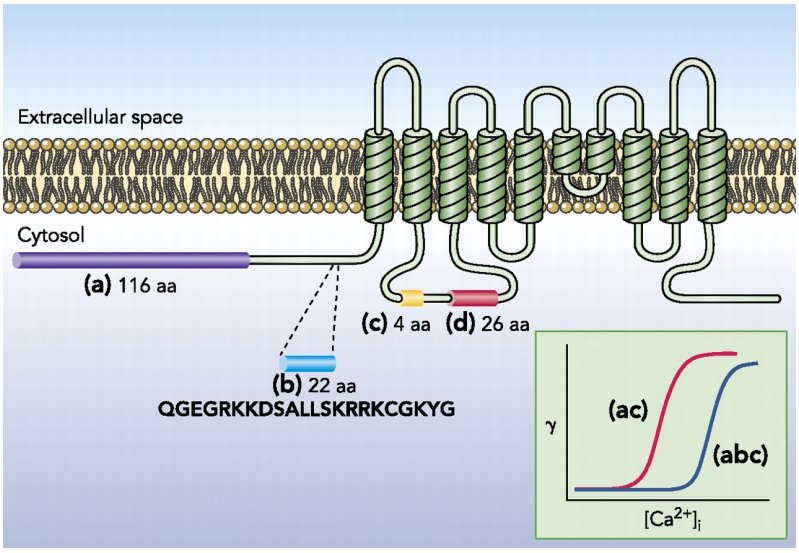

Figure 1.4. Here the position and the size of the four alternative segments (*a, b, c, d*). Segment b can modulate the Ca^{2+} sensitivity of TMEM16A Cl^- conductance (ϒ). The Ca^{2+} sensitivity of TMEM16A (*abc*) is fourfold lower than TMEM16 (*ac*) (Ferrera et al., 2010).

TMEM16B also has several isoforms. The olfactory and the retinal isoforms differ in the inclusion (retinal) or exclusion (olfactory) of exon 14 (previously annotated as exon 13 in Stephan et al., 2009). Moreover, in the olfactory epithelium alternative splicing occurs at exon 4 (previously annotated as exon 3 in Stephan et al., 2009), generating TMEM16B variants either with or

without exon 4 (Stephan et al., 2009; Ponissery Saidu et al., 2013). Exon 4 encodes a 33 residues segment within the cytoplasmic N terminus which is required for channel function in the heterologous system. In addition, also two alternative starting exons were identified. Therefore, with two alternative starting exons and alternative splicing of exon 4, four olfactory TMEM16B isoforms are possible: isoform *A*, isoform *B*, isoform $A_{\Delta 4}$ and Isoform $B_{\Delta 4}$ (Ponissery Saidu et al., 2013).

Alternative splicing could explain the various properties reported for CaCCs in different cell types (Hartzell et al., 2005; Ferrera et al., 2009, 2010; Scudieri et al., 2012).

1.6. Stoichiometry

TMEM16A interacts with itself to form a homodimer (Fallah et al., 2011; Sheridan et al., 2011; Tien et al., 2013) and the multimerization seems to occur before the channel is trafficked to the membrane (Sheridan et al., 2011). Tien et al. (2013) showed that TMEM16A, TMEM16B and TMEM16F form homodimeric structures. Dimerization occurs in the cytosolic N-terminal region and it is crucial for channel assembly and function (Tien et al., 2013). In addition, TMEM16A coimmunoprecipitated with TMEM16B and viceversa (but not with TMEM16F), indicating that the closely related homologs TMEM16A and TMEM16B can interact.

1.7. Biophysical properties of TMEM16A and TMEM16B

a. Ca^{2+} sensitivity

TMEM16A and TMEM16B show most of the electrophysiological properties of ‘classical’ CaCCs (Galietta, 2009; Hartzell et al., 2009; Romanenko et al.,

2010; Duran and Hartzell, 2011; Huang et al., 2012; Pifferi et al., 2012; Scudieri et al., 2012).

In TMEM16A, the affinity of the channel for Ca^{2+} depends on the splice variants (Ferrera et al., 2009). Galietta's group showed that at the membrane potential of +100 mV, $K_{1/2}$ for Ca^{2+} was 332 nM for (*abc*) and 85 nM for (*ac*) and that in both cases $K_{1/2}$ was slightly voltage dependent. See figure 1.5.

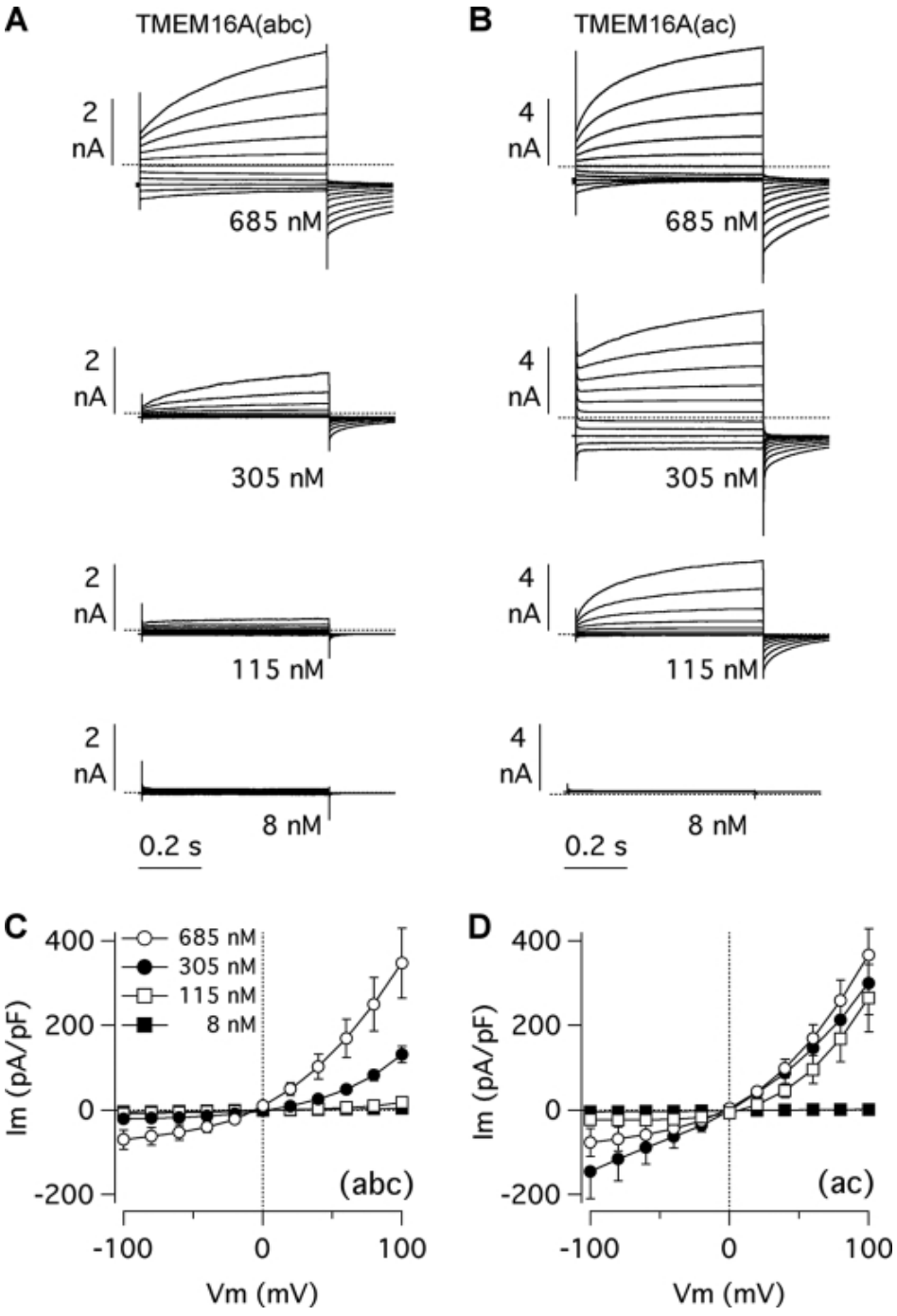

Figure 1.5. In panel **A** and **B** whole cell currents recorded at different intracellular Ca^{2+} in FRT cells with stable expression of (*abc*) and (*ac*) variants of TMEM16A. In **C** and **D** current-voltage relationships for the two isoforms (Ferrera et al., 2009).

Therefore, when segment *b* (26 amino acids in the N- terminal) was excluded, the Ca^{2+} sensitivity changed of about 4-fold, resulting in Cl^- currents requiring lower Ca^{2+} concentrations to be activated (Ferrera et al., 2009; Galietta, 2009; Ferrera et al., 2011). $K_{1/2}$ for (*ab*) was in the range 290-360 nM at voltages between -40 to +100 mV, showing that upon exclusion of segment *c* (residues EAVK in the first intracellular loop) the channel was not affected by membrane potential (Ferrera et al., 2009). The Hill coefficient was always higher than one, indicating cooperativity.

Another study, from Hartzell's group, found that deletion of the same segment *c* (EAVK) severely decreased the apparent Ca^{2+} sensitivity (Xiao et al., 2011).

The analysis of the primary sequence of TMEM16A or TMEM16B could not identify any canonical Ca^{2+} binding site (EF-hand). The first intracellular loop contains five consecutive glutamic acids resembling the 'Ca^{2+} bowl' of BK channel (Schreiber and Salkoff, 1997; Ferrera et al., 2010). However, mutations of the five glutamic acids did not modify the apparent Ca^{2+} affinity (Xiao et al., 2011).

It has been hypothesized that an auxiliary protein binds to and mediates TMEM16A activation upon an increase in intracellular Ca^{2+}. Tian et al. (2011) reported that calmodulin could be co-immunoprecipitated with TMEM16A and that calmodulin inhibitors decreased whole cell currents of TMEM16A (Tian et al., 2011). However, more recent studies showed that calmodulin is not necessary for activation of TMEM16A (Terashima et al., 2013; Yu et al., 2014).

In TMEM16B, studies were performed both with the retinal and with the olfactory isoforms. $K_{1/2}$ at +40 mV was 3.3 μM in the retinal isoform (Pifferi et al., 2009) and varied between 1.08 and 1.35 μM in the olfactory isoform (Stephan et al., 2009; Ponissery Saidu et al., 2013). TMEM16B Ca^{2+}

sensitivity was slightly voltage-dependent. The Hill coefficient was around 2, pointing to at least two binding sites for Ca^{2+} in the channel protein. See figure 5. It is of interest to note that $K_{1/2}$ at -40 mV differed in splice variants for TMEM16B differing at the N-terminal, indicating that the N-terminal of TMEM16B affects Ca^{2+} sensitivity (Ponissery Saidu et al., 2013).

Despite their high level of amino acid identity, TMEM16A and TMEM16B show different properties. Galietta's group replaced regions of TMEM16A with the equivalent regions of TMEM16B to look for a change in their properties. TMEM16A protein containing the first intracellular loop of TMEM16B did not show a decrease in apparent Ca^{2+} affinity. Instead, replacement of the region of the third intracellular loop changed the Ca^{2+} sensitivity of the chimeric TMEM16A protein (LOOP3 chimera) and it became more similar to that of TMEM16B. Indeed, the half-effective Ca^{2+} concentration of the LOOP3 chimera and TMEM16B at +100 mV was 2 and 3 μM respectively (Scudieri et al., 2013).

b. Voltage dependence

At low calcium concentrations, TMEM16A and TMEM16B are more activated at positive than at negative potentials; on the other hand, positive voltages lower the value of $K_{1/2}$, causing a higher Ca^{2+} sensitivity of these channels. Insights into the identification of the voltage-sensing module came from studies on TMEM16A splice variants. Galietta's group showed that the channel formed by the minimal TMEM16A (0) isoform, that has shorter intracellular domains, is both time and voltage independent (Caputo et al., 2008; Ferrera et al., 2011). Moreover, TMEM16A lacking segment *c* (EVAK) in the first cytosolic loop was less sensitive to voltage across the membrane, showing that the first cytosolic loop is involved in voltage dependent modulation of the channel (Ferrera et al., 2009; Xiao et al., 2011). Hartzell's group also mutated the five consecutive glutamic acids in alanine in the first intracellular loop and found that these mutations abilshed intrinsic voltage dependence of TMEM16A (Xiao et al., 2011).

For TMEM16B, the electrophysiological whole cell study of Pifferi et al. (2009), using HEK cells expressing TMEM16B shows that the channel at the steady state the current-voltage relationship at low calcium concentration had an outward rectification while it became linear increasing the Ca^{2+} concentration (Pifferi et al., 2009). The first study of structure-function relations for TMEM16B to identify regions involved in the voltage dependence of the channel is presented in the Results section of this Thesis.

c. Anion selectivity

Similarly to endogenous CaCCs, TMEM16A and TMEM16B favor permeation of bulkier anions, with SCN^-, NO_3^-, I^-, Br^- more permeant than Cl^- (Schroeder et al., 2008; Yang et al., 2008; Pifferi et al., 2009; Stephan et al., 2009; Sagheddu et al., 2010; Ferrera et al., 2011; Adomaviciene et al., 2013). See figure 1.6.

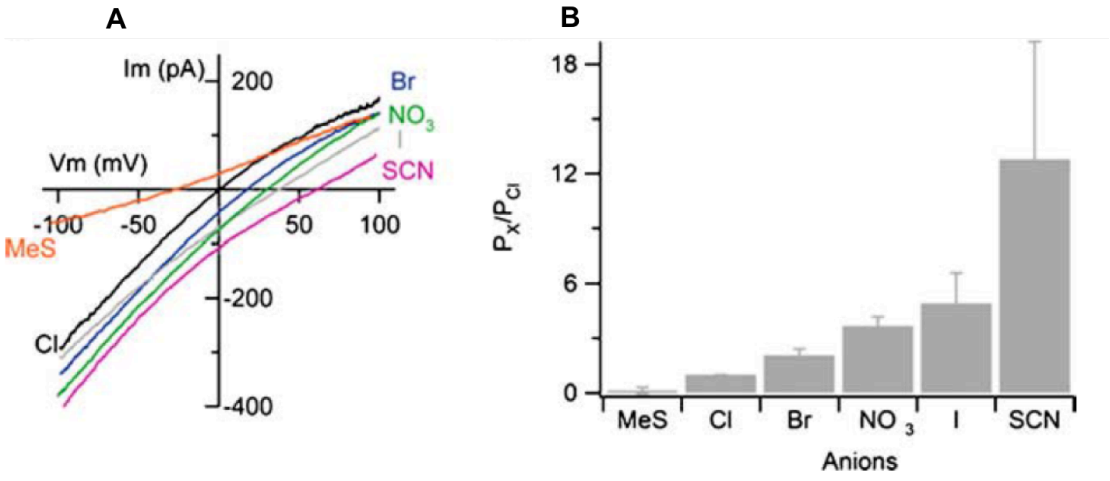

Figure 1.6. A Current–voltage relations for TMEM16B currents activated by 100 μM Ca^{2+} in an inside-out membrane patch, obtained from a ramp protocol. Bath solutions contained 140 mM NaCl or the Na salt of other anions, as indicated. Current traces were from the same patch; **B** Relative permeability ratios (P_X/P_{Cl}) calculated with the Goldman–Hodgkin–Katz equation (Pifferi et al., 2009).

It has also been shown that the anion selectivity of TMEM16A and TMEM16B changed during channel activation (Schroeder et al., 2008; Sagheddu et al., 2010). See figure 1.7.

Indeed, whole-cell recordings with flash photolysis of caged Ca^{2+} both for native olfactory CaCCs and for TMEM16B expressed in HEK cells, showed that the reversal potential for the external anions SCN^-, NO_3^-, I^-, which are more permeant than Cl^-, changed with time (Sagheddu et al., 2010). The dynamic change in permeability to more permenat anions was also observed in TMEM16A expressed in Axolotl oocytes (Schroeder et al., 2008), as well as in some cation channels such as TRPV1 and P2X (Khakh and Lester, 1999; Chung et al., 2008).

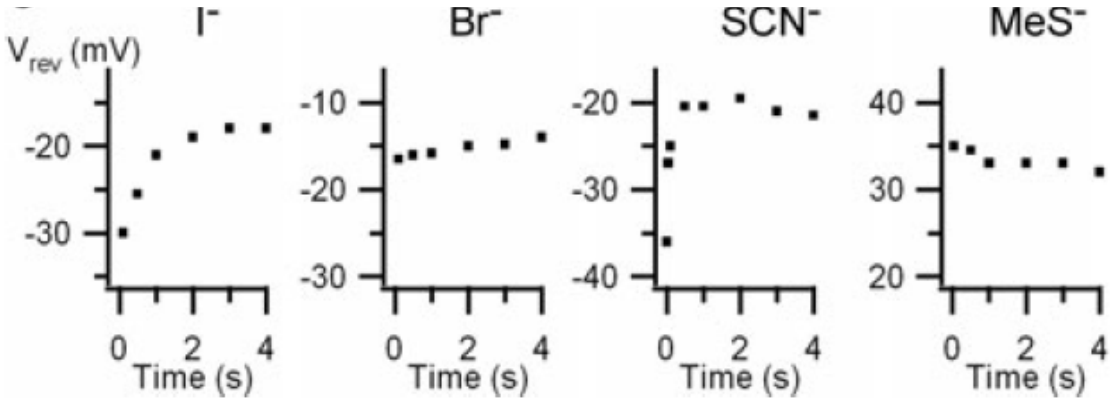

Figure 1.7. Currents recorded from a HEK 293T cell expressing TMEM16B using the uncaging technique for Ca^{2+} release in the whole cell configuration. External Cl^- was substituted with the anions indicated. V_{rev} as a function of time for external I- , Br-, SCN-, MeS-, each from a different cell (Sagheddu et al., 2010).

Moreover, recent studies reported that external anions modify gating of TMEM16A. Ferrera et al. (2011) showed that the membrane conductance

increased at all voltages when extracellular Cl^- was replaced with more permeant anions. Xiao et al. (2011) showed that the voltage dependent gating of TMEM16A was facilitated by anions such as SCN^- or NO_3^-, which are more permeant than Cl^-, or by an increase in extracellular Cl^- (Xiao et al., 2011).

d. Inactivation and Rundown

Inactivation is defined as slow decrease of the current amplitude in the presence of the constant Ca^{2+} concentration. When TMEM16B was activated by Ca^{2+}, it developed a current which inactivated. This process was reversible, voltage- and Ca^{2+} dependent and it was more evident at higher Ca^{2+} concentration and negative potentials (Stephan et al., 2009; Pifferi et al., 2009; Ponissery Saidu et al., 2013). In his recent work, Ponissery Saidu et al. (2013) showed that inactivation could be altered by co-expression of isoforms containing or lacking exon 4. When the isoform *A* of TMEM16B was co-expressed with the respective isoform lacking exon 4 ($A_{\Delta 4}$), the channel showed increased inactivation at -40 mV without any alteration at positive potentials. In contrast, when the TMEM16B isoform *B* was co-expressed with the respective isoform lacking exons 4 ($B_{\Delta 4}$), the channel inactivated more at both positive and negative voltages (Ponissery Saidu et al., 2013).

Another effect observed in inside-out excised patches, both for TMEM16A and TMEM16B is an irreversible rundown (Pifferi et al., 2009; Stephan et al., 2009; Ponissery Saidu et al., 2013; Yu et al., 2014). Rundown is a decrease in the current amplitude with time, upon subsequent application of Ca^{2+} and reaches a relatively stationary value afterwards. In the attempt to determine the rundown mechanisms in TMEM16A, Yu et al. (2014) performed experiments where purified brain CaM was applied at concentrations ranging from 1 to 25 μM to the cytosolic side of the patch, but the rundown never reversed or decreased (Yu et al., 2014). Pifferi et al., (2009) performed experiments on excised patch with TMEM16B adding several compounds, such as NO3, VO4, DTT, calmodulin, cAMP, PIP_3, to the cytoplasmic side of the patch but

none of them was effective in reducing the rundown (Pifferi et al., 2009). The molecular mechanisms of rundown are still not known. See figure 1.8.

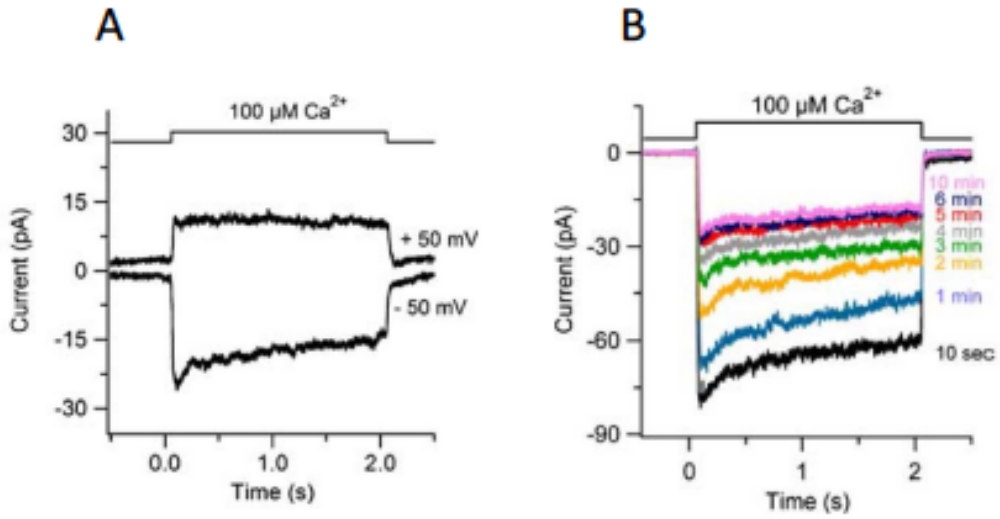

Figure 1.8. A An inside-out membrane patch was excised from HEK 293T cells transfected with TMEM16B and the cytoplasmic side was exposed to 100 µM Ca^{2+} at the time indicated in the upper trace A. Inactivation was voltage-dependent. Currents activated by 100 µM Ca^{2+} at -50 mV or +50 mV after 3 or 4 min from patch excision respectively. Current traces were from the same patch B. In **B** Rundown: repetitive applications of Ca^{2+} produced a current of decreasing amplitude. The holding potential was -50 mV. The number next to each trace indicates the initial time of Ca^{2+}application after patch excision (Pifferi et al., 2009).

6. AIM OF THE WORK

The molecular mechanisms of TMEM16B channel gating are unknown. The analysis of the primary sequence of TMEM16B does not contain any canonical voltage-sensing or Ca^{2+}-binding domains. However, the first intracellular loop contains several glutamates that could be involved in channel gating. The aim of the first part of this Thesis is to perform a first site-directed mutagenesis study on TMEM16B to contribute to the understanding of the molecular mechanisms underlying the channel voltage and Ca^{2+} dependence.

The aim of the second part of this Thesis is to investigate how permeant anions affect gating in TMEM16B.

3. MATERIALS AND METHODS

3.1. Cell culture and transfection

HEK-293T cells were grown in DMEM (Gibco, Italy) supplemented with 10% fetal bovine serum (Sigma, Italy) 100 UI/ml penicillin and 100 μg/ml streptomycin (Sigma, Italy) at 37°C in a humidified CO_2 incubator.

Full-length mouse TMEM16B cDNA in pCMV-Sport6 mammalian expression plasmid was obtained from RZPD (Germany; clone identification: IRAVp968H1167D, accession number NP_705817.1). Mutations were made using a PCR-based site-directed mutagenisis kit (Gene Tailor mutagenisis kit, Invitrogen, OR, USA) and confirmed by DNA sequencing.

2 μg TMEM16B or its mutants was transfected into cells using FuGENE 6 reagent (Roche diagnostics, Germany) according to the manufacturer's protocol. Cells were cotransfected with 0.2 μg eGFP (Clontech, Mountain View, CA, USA) for fluorescent identification of transfected cells.

Electrophysiological recordings were performed between 48 and 72 hours from transfection.

3.2. Experimental set up and recordings

HEK cells were visualized with an Olympus IX70 inverted microscope (Olympus, Japan) placed on an antivibration table (TMC, USA). A homemade Faraday cage provided an adequate electrical shielding. All recordings were performed using an Axopatch 1-D amplifier controlled by Clampex 9.2 via Digidata 1322A (Axon Instruments, USA). Data were sampled at 10 kHz and low-pass filtered at 4 kHz. Patch pipettes were made of borosilicate glass (WPI, USA) with a PP-830 puller (Narishige, Japan) and had a resistance of 3-5 MΩ. The pipette filled with the intracellular solution was inserted into a holder containing an Ag/AgCl electrode, connected to the headstage of a Axopatch 1-D amplifier. Headstage movements were controlled by a

mechanical micromanipulator (for coarse movements) and by a hydraulic micromanipulator (for fine movements) to bring the pipette close to the cell and obtain the GΩ seal. When Cl^- in the bath solution was replaced with other anions, the bath was grounded with a 1M KCl agar bridge connected with a Ag/AgCl reference electrode. Experiments were performed at room temperature.

3.3. The perfusion system

Rapid exchange of solution was achieved by translating the boundary between two flowing streams of solutions in front of the cell in the whole-cell configuration (or the excised patch in inside-out experiments). Streams of various solutions emerged from four glass tubes with ID of 0.90 mm (Vitro Dynamics, USA). Changes between the solutions was performed by using the Perfusion Fast-Step SF-77B (Warner Instrument Corp., USA) controlled by the Digidata 1322A (Axon Instruments, USA). The perfusion system was entirely gravity driven; the solutions were stored in 25-50 ml syringes and polyethylene tubes (ID 1.14 mm) were used for connection with the perfusion system or the recording chamber. The flow of solution was controlled by solenoid valves (manually controlled). The recording chamber was continuously bathed with mammalian Ringer solution while an aspiration tube, placed at the opposite site and connected with a trap bottle, controlled the level of solution in the recording chamber. See figure 3.1.

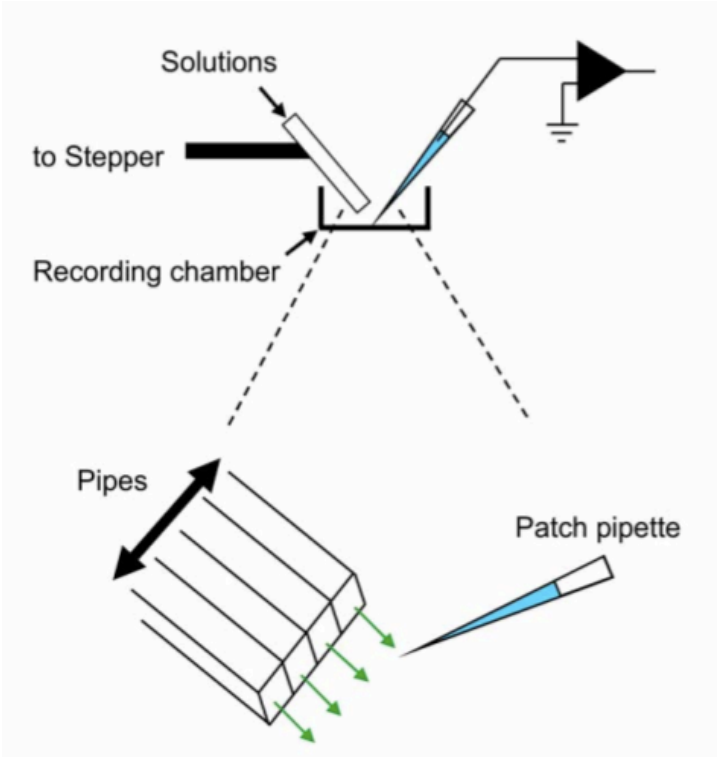

Figure 3.1. Perfusion system used for patch clamp experiments. Four parallel streams of solutions from glass pipes were delivered in front of the patch pipette. Stepping the pipe sideway, it was possible to rapidly change (about 20 ms) the solution bathing the cells attached to the patch pipette (scheme by Dott. Simone Pifferi).

3.4. Solutions

The composition of the standard extracellular mammalian Ringer was (in mM): 140 NaCl; 5 KCl; 2 $CaCl_2$; 1 $MgCl_2$, 10 glucose, and 10 HEPES, pH 7.4. For experiments on ion selectivity, NaCl of the Ringer solution was replaced with the sodium salt of different anions. For solutions containing NaF, divalent cations were omitted to avoid the precipitation of the insoluble salt. In some experiments with low extracellular Cl^- concentrations, the Ringer control solution contained (in mM): 140 NaCl; 2.5 K_2SO_4; 2 $CaSO_4$; 1 $MgSO_4$ and 10 HEPES, pH 7.4. For the 11 mM Cl^- and 1 mM Cl^- solutions, NaCl was replaced with equimolar amounts of Na-gluconate or sucrose. The osmolarity was adjusted with sucrose. The extracellular solutions were adjusted to pH 7.4

using NaOH or HCl.

Intracellular solutions contained different concentrations of free Ca^{2+}, calculated with the program WinMAXC (C.Patton, Stanford university, Palo Alto, CA USA) ((Patton et al., 2004). The composition is reported in the following table.

INTRACELLULAR SOLUTIONS

Free Ca^{2+} (µM)	CsCl (mM)	$CaCl_2$ (mM)	HEDTA (mM)	HEPES (mM)
0 Ca^{2+}	140	-	10	10
0.5 Ca^{2+}	140	1.242	10	10
1.5 Ca^{2+}	140	3.209	10	10
3.8 Ca^{2+}	140	5.866	10	10
13 Ca^{2+}	140	8.263	10	10
100 Ca^{2+}	140	9.98	10	10

The pH of the intracellular solutions was adjusted to 7.2 with CsOH.

All salts used were purchased from Sigma (Italy) except for K_2SO_4 from Carlo Erba (Rodano, Milano, Italy) and $CaSO_4$ from JT Baker (Milano, Italy).

3.5. Data analysis

Data are presented as mean ± SEM, with *n* indicating the number of cells. Statistical significance was determined using paired or unpaired t-tests, or ANOVA, as appropriate. When a statistically significant difference was determined with ANOVA, a post hoc Tukey test was done to evaluate which data groups showed significant differences. P values <0.05 were considered

significant. Data analysis and figures were made with Igor Pro software (Wavemetrics, USA).

4. RESULTS

Valentina Cenedese, Giulia Betto, Fulvio Celsi, O. Lijo Cherian, Simone Pifferi, and Anna Menini

The voltage-dependence of the TMEM16B/anoctamin2 calcium- activated chloride channel is modified by mutations in the first putative intracellular loop.

J Gen Physiol 2012; 139(4): 285-94

Giulia Betto, O. Lijo Cherian, Simone Pifferi, Valentina Cenedese, Anna Boccaccio, and Anna Menini

Interactions between permeantion and gating in the TMEM16B/anoctamin2 calcium-activated chloride channel.

J Gen Physiol, 2014 In Press.

Published March 12, 2012

The voltage dependence of the TMEM16B/anoctamin2 calcium-activated chloride channel is modified by mutations in the first putative intracellular loop

Valentina Cenedese, Giulia Betto, Fulvio Celsi, O. Lijo Cherian, Simone Pifferi, and Anna Menini

Neurobiology Sector, International School for Advanced Studies, and Italian Institute of Technology, SISSA Unit, 34136 Trieste, Italy

Ca^{2+}-activated Cl^- channels (CaCCs) are involved in several physiological processes. Recently, TMEM16A/anoctamin1 and TMEM16B/anoctamin2 have been shown to function as CaCCs, but very little information is available on the structure–function relations of these channels. TMEM16B is expressed in the cilia of olfactory sensory neurons, in microvilli of vomeronasal sensory neurons, and in the synaptic terminals of retinal photoreceptors. Here, we have performed the first site-directed mutagenesis study on TMEM16B to understand the molecular mechanisms of voltage and Ca^{2+} dependence. We have mutated amino acids in the first putative intracellular loop and measured the properties of the wild-type and mutant TMEM16B channels expressed in HEK 293T cells using the whole cell voltage-clamp technique in the presence of various intracellular Ca^{2+} concentrations. We mutated E367 into glutamine or deleted the five consecutive glutamates $_{386}$EEEEE$_{390}$ and $_{399}$EYE$_{401}$. The EYE deletion did not significantly modify the apparent Ca^{2+} dependence nor the voltage dependence of channel activation. E367Q and deletion of the five glutamates did not greatly affect the apparent Ca^{2+} affinity but modified the voltage dependence, shifting the conductance–voltage relations toward more positive voltages. These findings indicate that glutamates E367 and $_{386}$EEEEE$_{390}$ in the first intracellular putative loop play an important role in the voltage dependence of TMEM16B, thus providing an initial structure–function study for this channel.

INTRODUCTION

Ca^{2+}-activated Cl^- channels (CaCCs) are expressed in many cell types, where they play various physiological roles. For example, CaCCs are involved in fast block of polyspermy in *Xenopus laevis* oocytes, in the regulation of smooth muscle contraction, in fluid secretion from exocrine glands, in the control of excitability in cardiac myocytes, as well as in olfactory, taste, and phototransduction (Frings et al., 2000; Hartzell et al., 2005; Leblanc et al., 2005; Petersen, 2005; Wray et al., 2005; Bers, 2008; Kleene, 2008; Lalonde et al., 2008; Petersen and Tepikin, 2008; Duran et al., 2010; Kunzelmann et al., 2011a).

Despite the fact that CaCCs are broadly present in several tissues, their molecular identity had remained elusive until 2008, when three independent studies reported that the expression of TMEM16A/anoctamin1 was associated with CaCCs (Caputo et al., 2008; Schroeder et al., 2008; Yang et al., 2008). The TMEM16 family comprises 10 members, and another member of the family, TMEM16B/anoctamin2, has also been shown to function as a CaCC when heterologously expressed in axolotl oocytes (Schroeder et al., 2008) or in HEK 293T cells (Pifferi et al., 2009; Stephan et al., 2009; Stöhr et al., 2009; Rasche et al., 2010; Sagheddu et al., 2010).

The study of knockout mice for TMEM16A (Rock and Harfe, 2008) and for TMEM16B (Billig et al., 2011) further confirmed that CaCC activity was reduced or abolished in several cells (Flores et al., 2009; Galietta, 2009; Hartzell et al., 2009; Kunzelmann et al., 2011b, 2012; Huang et al., 2012; Pifferi et al., 2012; Sanders et al., 2012; Scudieri et al., 2012).

Hydropathy analysis indicates that TMEM16 proteins have eight putative transmembrane domains with both N- and C-terminal domains located at the intracellular side of the membrane, and the predicted topology has been experimentally confirmed for TMEM16G/anoctamin7 (Das et al., 2008). At present, TMEM16A and TMEM16B have been shown to function as CaCCs, whereas it is unclear whether the other members of the family are CaCCs (Duran and Hartzell, 2011; Huang et al., 2012; Scudieri et al., 2012). Furthermore, splice variants have been identified both for TMEM16A (Caputo et al., 2008; Ferrera et al., 2009, 2011) and for TMEM16B

Correspondence to Anna Menini: menini@sissa.it

S. Pifferi's present address is Max Delbrück Center for Molecular Medicine, 13125 Berlin, Germany.

Abbreviations used in this paper: CaCC, Ca^{2+}-activated Cl^- channel; WT, wild type.

The Rockefeller University Press $30.00
J. Gen. Physiol. Vol. 139 No. 4 285–294
www.jgp.org/cgi/doi/10.1085/jgp.201110764

Published March 12, 2012

(Stephan et al., 2009). However, although the functional properties of different isoforms have been extensively investigated for TMEM16A, only preliminary data have been presented for TMEM16B (Saidu, S.P., A.B. Stephan, S.M. Caraballo, H. Zhao, and J. Reisert. 2010. Association for Chemoreception Sciences Meeting. Abstr. P68).

At present, very little is known about the structure–function relations for these channels. The analysis of the sequence of TMEM16A and TMEM16B did not reveal any canonical voltage-sensing or Ca^{2+}-binding domains (Yang et al., 2008), but a comparison among the biophysical properties of the TMEM16A splice variants pointed to the functional relevance of the first putative intracellular loop (Caputo et al., 2008; Ferrera et al., 2009, 2011). Moreover, a recent study performed site-directed mutagenesis experiments on TMEM16A modifying some amino acids in the first putative intracellular loop and found that deletion of EAVK affected both the Ca^{2+} and voltage dependence of TMEM16A (Xiao et al., 2011).

Here, we aimed to perform a first site-directed mutagenesis investigation of TMEM16B to contribute to the understanding of the molecular mechanisms underlying the channel voltage and Ca^{2+} dependence. We identified some acidic amino acids in the first intracellular loop of TMEM16B ($_{367}$E, $_{386}$EEEEE$_{390}$, $_{399}$EYE$_{401}$), which are conserved in TMEM16A, where some of them have been studied (Xiao et al., 2011). We mutated or deleted the indicated glutamates and made a comparison between the electrophysiological properties measured in the whole cell configuration of the wild-type (WT) TMEM16B and its mutants. We have found that $_{367}$E and $_{386}$EEEEE$_{390}$ contribute to the voltage-dependent regulation of the TMEM16B channel.

MATERIALS AND METHODS

Site-directed mutagenesis of TMEM16B and heterologous expression

Full-length mouse TMEM16B cDNA in pCMV-Sport6 mammalian expression plasmid was obtained from RZPD (clone identification, IRAVp968H1167D; NCBI Protein database accession no. NP_705817.1). Mutations were made using a PCR-based site-directed mutagenesis kit (Gene Tailor; Invitrogen) and confirmed by DNA sequencing. HEK 293T cells (American Type Culture Collection) were transfected with 2 µg TMEM16B by using transfection reagent (FuGENE 6; Roche). Cells were co-transfected with 0.2 µg enhanced green fluorescent protein (eGFP; Takara Bio Inc.) for fluorescent identification of transfected cells. After 24 h, transfected cells were replated at a lower density and used for patch-clamp experiments between 48 and 72 h from transfection.

Electrophysiological recordings and ionic solutions

Current recordings from HEK 293T cells expressing TMEM16B or its mutants were performed in the whole cell voltage-clamp configuration, as described previously (Pifferi et al., 2006, 2009). Patch pipettes were made of borosilicate glass (World Precision Instruments, Inc.) and pulled with a PP-830 puller (Narishige). Patch pipettes filled with the intracellular solution had a resistance of ~3–5 MΩ when immersed in the bath solution. Currents were recorded with an Axopatch 1D or Axopatch 200B amplifier controlled by Clampex 9 or 10 via a Digidata 1332A or 1440 (Molecular Devices). Data were low-pass filtered at 5 kHz and sampled at 10 kHz. Experiments were performed at room temperature (20–25°C). As reported previously (Pifferi et al., 2006), control experiments in nontransfected and only eGFP-transfected cells did not show any significant Ca^{2+}-activated current.

The standard extracellular solution contained (in mM): 140 NaCl, 5 KCl, 2 $CaCl_2$, 1 $MgCl_2$, 10 glucose, and 10 HEPES, adjusted to pH 7.4 with NaOH. The intracellular solution filling the patch pipette contained (in mM): 140 CsCl, 10 HEPES, and 10 HEDTA, adjusted to pH 7.2 with CsOH, and no added Ca^{2+} for the nominally 0 Ca^{2+} solution, or various added Ca^{2+} concentrations, as calculated with the program WinMAXC (Patton et al., 2004), to obtain free Ca^{2+} in the range between 0.5 and 100 µM. The free Ca^{2+} concentrations were experimentally determined by Fura-4F (Invitrogen) measurements by using a luminescence spectrophotometer (LS-50B; PerkinElmer), as described previously (Pifferi et al., 2006). The total Cl^- concentration was 158 mM in the extracellular solution, whereas in the pipette solution it ranged from 140 mM in 0 Ca^{2+} to 160 mM in 100 µM Ca^{2+}, with a calculated

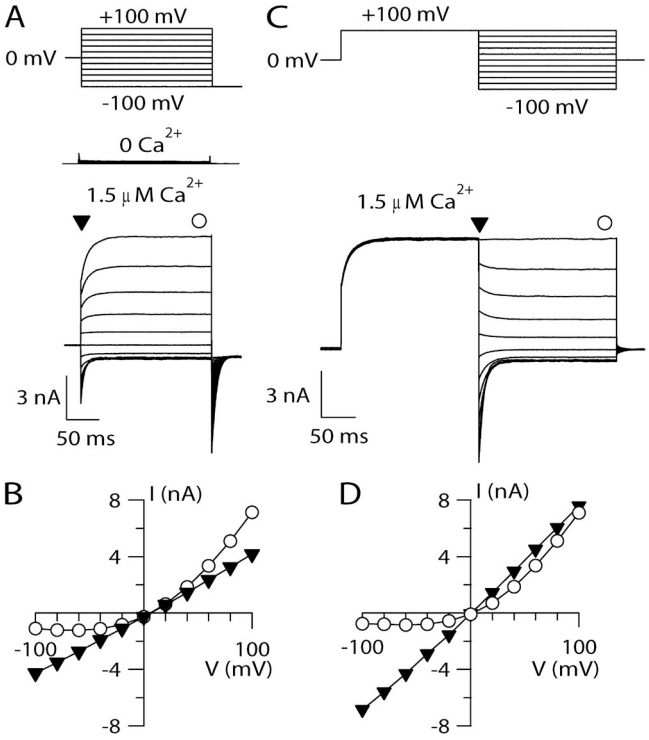

Figure 1. I-V relations of TMEM16B. (A) Representative whole cell voltage-clamp recordings obtained with an intracellular solution containing nominally 0 Ca^{2+} or 1.5 µM Ca^{2+}, as indicated. Voltage steps of 200-ms duration were given from a holding voltage of 0 mV to voltages between −100 and +100 mV in 20-mV steps, followed by a step to −100 mV, as indicated in the top part of the panel. (B) Steady-state I-V relation measured at the end of the voltage steps (circles) or instantaneous I-V measured at the beginning of each voltage step (inverted triangles) from the cell shown in B. (C) Representative recordings at 1.5 µM Ca^{2+} obtained with a voltage protocol consisting of a prepulse to +100 mV from a holding voltage of 0 mV, followed by voltage steps between −100 and +100 mV in 20-mV steps, as shown in the top part of the panel. (D) I-V relations measured from tail currents (inverted triangles) or at the steady state (circles).

Published March 12, 2012

equilibrium potential for Cl^- of −1.5 and +1.9 mV, respectively. All chemicals, unless otherwise stated, were purchased from Sigma-Aldrich.

In most experiments, we applied voltage steps of 200-ms duration from a holding potential of 0 mV ranging from −100 to +100 mV (or from −200 to +200 mV), followed by a step to −100 mV. A single-exponential function was fitted to tail currents to extrapolate the current value at the beginning of the step to −100 mV. In another set of experiments, channels were activated by a 200-ms pulse to +100 mV, and then rapidly closed by the application of hyperpolarizing steps. Single-exponential functions were fitted to tail currents at each voltage step.

Membrane capacitance and series resistance were compensated with the amplifier during the experiments. Membrane current density was calculated by dividing the current by the cell capacitance. The conductance, *G*, was calculated as $G = I/(V - V_{rev})$, where *I* is the tail current, V is the membrane voltage, and V_{rev} is the current reversal potential. Because in our experimental conditions the calculated equilibrium potential for Cl^- ranged between −1.5 and +1.9 mV and the measured V_{rev} was close to 0 mV, V_{rev} was set to 0 mV in all calculations.

Data analysis

Data are presented as mean ± SEM, with *n* indicating the number of cells. Statistical significance was determined using paired or unpaired *t* tests or ANOVA, as appropriate. When a statistically significant difference was determined with ANOVA, a post-hoc Tukey test was done to evaluate which data groups showed significant differences. P-values of <0.05 were considered significant. Data analysis and figures were made with Igor Pro software (WaveMetrics).

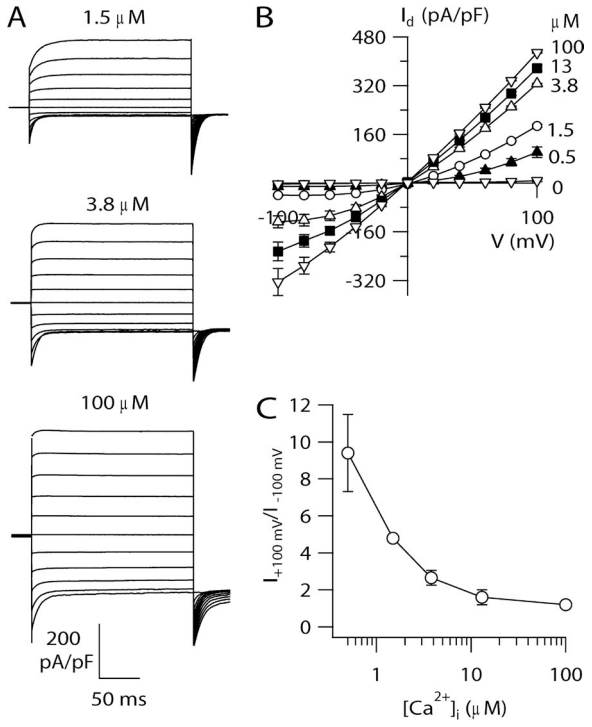

Figure 2. Ca^{2+}-dependent rectification of TMEM16B. (A) Whole cell currents activated by the indicated $[Ca^{2+}]_i$. Voltage protocol as in Fig. 1 A. (B) Average steady-state I-V relations from several cells (n = 3–6). (C) Average ratios between steady-state currents measured at +100 and −100 mV at various $[Ca^{2+}]_i$ (n = 3–6).

RESULTS

TMEM16B activation by Ca^{2+} and voltage

To study the activation of TMEM16B by $[Ca^{2+}]_i$ and voltage, we performed whole cell voltage-clamp recordings on HEK 293T cells transiently transfected with TMEM16B using intracellular solutions containing different free $[Ca^{2+}]_i$. Fig. 1 A shows that voltage steps between −100 and +100 mV from a holding voltage of 0 mV elicited very small currents with a nominally 0-Ca^{2+} pipette solution (8 ± 3 pA/pF at +100 mV; n = 8), whereas it induced large outward currents in the presence of 1.5 µM Ca^{2+}.

In the presence of Ca^{2+}, depolarizing voltage steps elicited an instantaneous outward current, indicating that channels were open at the holding potential of 0 mV, followed by a time-dependent outward relaxation (see also Fig. 5). Hyperpolarizing voltage steps induced instantaneous inward currents followed by a relaxation toward less negative values, in agreement with previous results (Pifferi et al., 2009; Stöhr et al., 2009; Rasche et al., 2010). The I-V relation measured at the steady state showed a pronounced outward rectification, whereas the instantaneous I-V curve measured at the beginning of each step was linear (Fig. 1 B). A similar result was obtained by activating TMEM16B with a different voltage protocol: channels were first activated by a 200-ms prepulse to +100 mV, and then tail currents were induced by voltage steps between −100 and +100 mV in 20-mV steps (Fig. 1 C). The I-V relation obtained by plotting the tail currents measured at the beginning of each step versus the step voltage was linear, whereas the steady-state I-V curve showed an outward rectification (Fig. 1 D), as in Fig. 1 B. These results clearly demonstrate that the I-V relation of the open channel is linear, and therefore the outward rectification is a result of a voltage-dependent mechanism that favors channel opening at

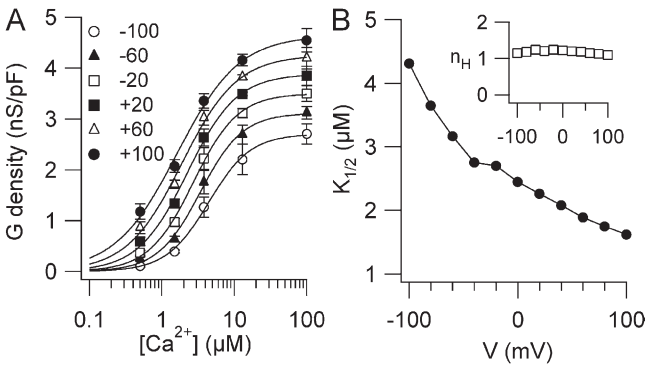

Figure 3. Ca^{2+} sensitivity of TMEM16B. (A) Conductance density calculated from tail currents measured at −100 mV after prepulses between −100 and +100 mV as indicated was plotted versus $[Ca^{2+}]_i$ (n = 3–6). Voltage protocol as in Fig. 1 A. Lines are the fit to the Hill equation (Eq. 1). (B) $K_{1/2}$ and n_H (inset) values plotted versus voltage.

Published March 12, 2012

depolarizing voltages. Thus, TMEM16B is activated by $[Ca^{2+}]_i$ and modulated by voltage at low $[Ca^{2+}]_i$.

To further examine the interplay between $[Ca^{2+}]_i$ and voltage in channel activation, we varied $[Ca^{2+}]_i$ (Fig. 2 A). Steady-state I-V relations measured at low $[Ca^{2+}]_i$ showed an outward rectification that became less pronounced as $[Ca^{2+}]_i$ increased (Fig. 2 B). We calculated a rectification index as the ratio between the steady-state current at +100 and −100 mV at each $[Ca^{2+}]_i$. The rectification index was 4.8 ± 0.2 at 1.5 µM Ca^{2+} and decreased to 1.4 ± 0.2 at 100 µM Ca^{2+}, showing that the I-V relation is Ca^{2+} dependent and becomes more linear as $[Ca^{2+}]_i$ increases (Fig. 2 C).

To analyze the Ca^{2+} dependence of TMEM16B activation at various voltages, we measured the dose–response relations. Tail currents at each $[Ca^{2+}]_i$ were measured at the beginning of the step to −100 mV after prepulses ranging from −100 to +100 mV. Fig. 3 A shows the average conductance densities plotted versus $[Ca^{2+}]_i$ and fit at each voltage by the Hill equation:

$$G = G_{max}\left[Ca^{2+}\right]_i^{nH} / \left(\left[Ca^{2+}\right]_i^{nH} + {K_{1/2}}^{nH}\right), \quad (1)$$

where G is the current density, G_{max} is the maximal current density, $K_{1/2}$ is the half-maximal $[Ca^{2+}]_i$, and n_H is the Hill coefficient.

The Hill coefficient was not voltage dependent with a value of 1.2 at −100 mV and 1.1 at +100 mV. The finding that the Hill coefficient was >1 indicates that the binding of more than one Ca^{2+} ion is necessary to open the channel. $K_{1/2}$ slightly decreased with membrane depolarization from 4.3 µM at −100 mV to 1.6 µM at +100 mV, as illustrated in Fig. 3 B. These data show that the Ca^{2+} sensitivity of TMEM16B is moderately voltage dependent, in agreement with previous results obtained with inside-out patches (Pifferi et al., 2009; Stephan et al., 2009).

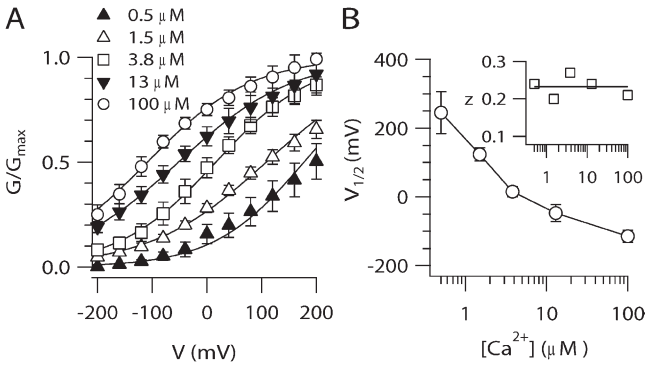

Figure 4. Voltage dependence of TMEM16B. (A) Normalized conductances at the indicated $[Ca^{2+}]_i$ calculated from tail currents at −100 mV after prepulses between −200 and +200 mV were plotted versus the prepulse voltage (n = 4–9). Lines are the fit to the Boltzmann equation (Eq. 2). (B) $V_{1/2}$ and z (inset) values plotted versus $[Ca^{2+}]_i$.

The voltage dependence of steady-state activation (G-V relation) was analyzed by measuring tail currents at the beginning of a step to −100 mV after prepulse voltages between −200 and +200 mV. The range of voltages was extended from the previous voltage protocols to obtain a better estimate of voltage dependence. Fig. 4 A shows the average conductance activated at a given $[Ca^{2+}]_i$ plotted versus membrane voltage and fit by the Boltzmann equation:

$$G / G_{max} = 1 / \left\{1 + \exp\left[z\left(V_{1/2} - V\right)F / RT\right]\right\}, \quad (2)$$

where G/G_{max} is the normalized conductance, z is the equivalent gating charge associated with voltage-dependent channel opening, V is the membrane potential, $V_{1/2}$ is the membrane potential producing half-maximal activation, F is the Faraday constant, R is the gas constant, and T is the absolute temperature.

The maximal conductance density G_{max} was determined by a global fit of G-V relations, and G at each $[Ca^{2+}]_i$ was then normalized to the same G_{max}. Because at the smaller $[Ca^{2+}]_i$ the prediction of G_{max} from the fit could be affected by a large error, we also estimated G_{max} at each $[Ca^{2+}]_i$. G_{max} at 0.5 µM Ca^{2+} was 4.1 ± 0.4 nS/pF, not significantly different from the value of 4.7 ± 0.4 nS/pF at 100 µM Ca^{2+}, indicating that the estimate of G_{max} was little affected by $[Ca^{2+}]_i$. Fig. 4 A shows that increasing

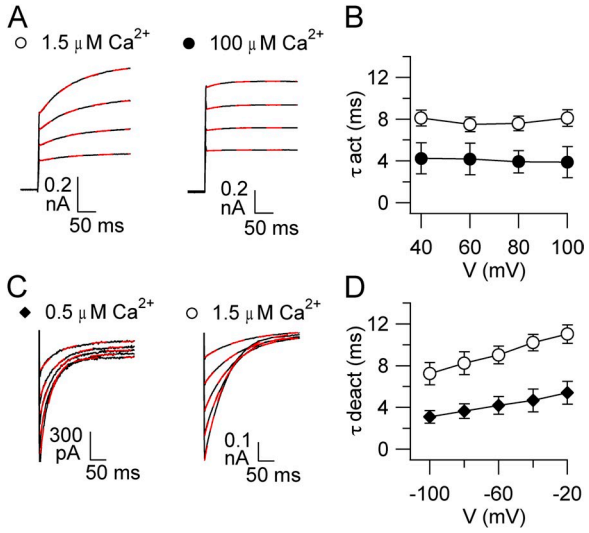

Figure 5. Activation and deactivation kinetics of TMEM16B. (A) Representative recordings at the indicated $[Ca^{2+}]_i$. Voltage protocol as in Fig. 1 A, with voltage steps from a holding voltage of 0 between +40 to +100 mV in 20-mV steps. Red dashed lines are the fit to a single-exponential function. (B) Average activation time constants (τ_{act}) plotted versus voltage (n = 6–8). (C) Representative recordings at the indicated $[Ca^{2+}]_i$. Voltage protocol as in Fig. 1 C, with a prepulse to +100 mV and tail currents induced by voltage steps between −100 and +100 mV in 20-mV steps. Only tail currents are illustrated. Red dashed lines are the fit to a single-exponential function. (D) Average deactivation time constants (τ_{deact}) plotted versus voltage (n = 4–9).

Published March 12, 2012

$[Ca^{2+}]_i$ produced a leftward shift in the G-V relation: $V_{1/2}$ was 124 ± 20 mV at 1.5 µM Ca^{2+} and became −115 ± 18 mV at 100 µM Ca^{2+}, whereas the equivalent gating charge was not largely modified (z = 0.23–0.30). Thus, $V_{1/2}$ decreased as $[Ca^{2+}]_i$ increased, indicating that more channels can be activated by depolarization in the presence of a high $[Ca^{2+}]_i$ (Fig. 4 B). At a given $[Ca^{2+}]_i$, the conductance increased with depolarization, showing that the conductance depends both on $[Ca^{2+}]_i$ and voltage.

Activation and deactivation kinetics are regulated by $[Ca^{2+}]_i$ and voltage

To characterize activation and deactivation kinetics, we analyzed the time-dependent components in response to voltage steps in the presence of a given $[Ca^{2+}]_i$. As shown in Figs. 2 A and 5 A, current activation in response to depolarizing voltage steps had two components: an instantaneous time-independent current, related to the fraction of channels open at the holding voltage of 0 mV, followed by an outward time-dependent relaxation, a

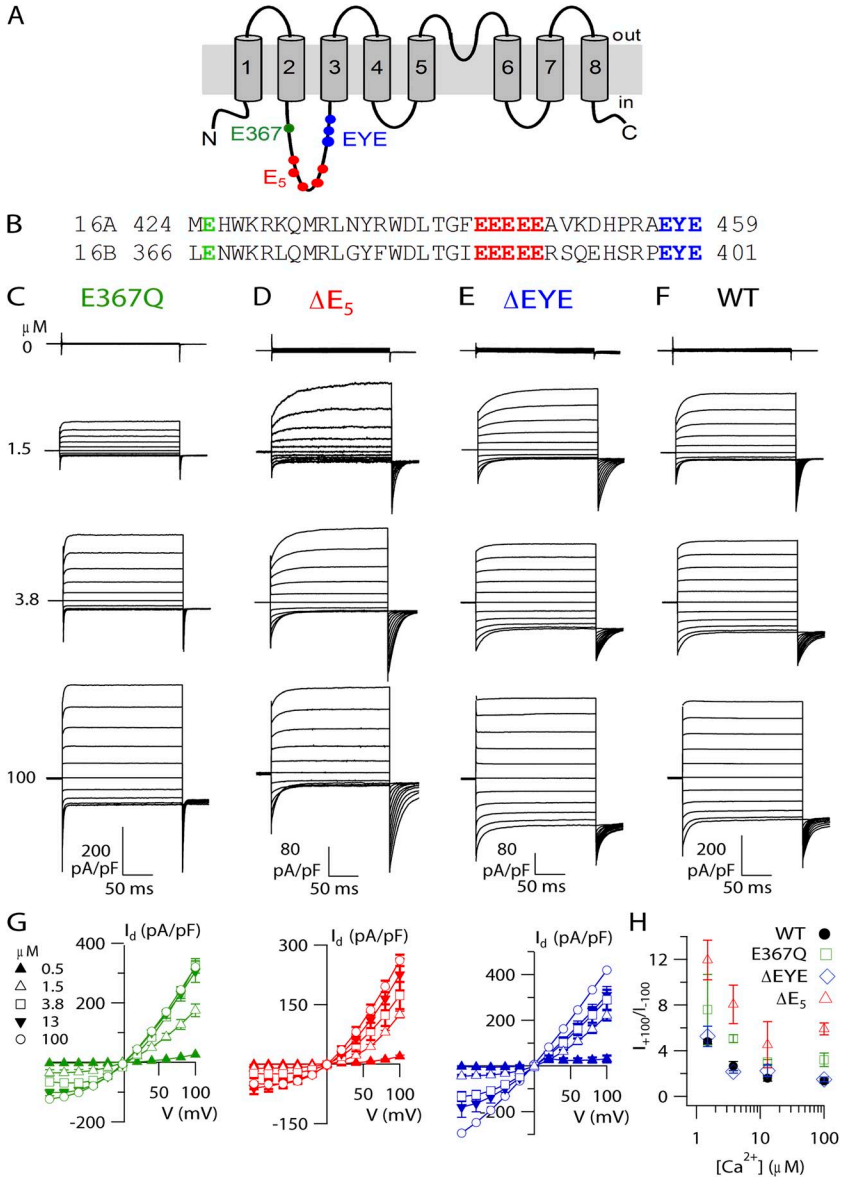

Figure 6. TMEM16B mutations. (A) Predicted topology of TMEM16A and TMEM16B from hydropathy analysis. (B) Alignment between mouse TMEM16A (*a,c*; available from GenBank/EMBL/DDBJ under accession no. NM_178642.4) and the retinal isoform of TMEM16B used in this study (NP_705817.1), with the mutations or deletions highlighted in color. (C–F) Representative recordings at the indicated $[Ca^{2+}]_i$ for E367Q (C), ΔE_5 (D), ΔEYE (E) mutants, and WT (F). Traces for WT are the same as in Fig. 2 A. Voltage protocol as in Fig. 1 A. (G) I-V steady-state relations (n = 3–8). (H) Average ratios between currents measured at +100 and −100 mV plotted versus $[Ca^{2+}]_i$ for each mutant (n = 3–8).

Published March 12, 2012

result of the increase in the fraction of channels opened by depolarization. The time-independent component became larger as voltage or $[Ca^{2+}]_i$ increased.

To examine the activation kinetics, we analyzed the time-dependent component of the current elicited by depolarizing voltage steps. Fig. 5 A shows that most of the time course of time-dependent relaxations was well fit by a single-exponential function. The time constant of current activation, τ_{act}, in the presence of 1.5 µM Ca^{2+} was 8.1 ± 0.8 ms at +100 mV and did not vary as a function of voltage at a given $[Ca^{2+}]_i$ (Fig. 5 B). At +100 mV, τ_{act} at 100 µM Ca^{2+} was 3.9 ± 1.4 ms, significantly smaller than the value of 8.1 ± 0.8 ms at 1.5 µM Ca^{2+}, showing that an increase in $[Ca^{2+}]_i$ accelerated activation.

The time constant of current deactivation (τ_{deact}) was calculated by fitting with a single-exponential function the tail currents obtained after a prepulse at +100 mV by voltage steps ranging between −100 and −20 mV (Fig. 5 C). In the presence of 0.5 µM Ca^{2+}, τ_{deact} was 3.0 ± 0.2 ms at −100 mV and 5.4 ± 0.5 ms at −20 mV, showing that less negative voltages slowed deactivation (Fig. 5 D). At −100 mV, τ_{deact} at 1.5 µM Ca^{2+} was 7.2 ± 0.8 ms, significantly different from the value of 3.0 ± 0.2 ms at 0.5 µM Ca^{2+}, showing that an increase in $[Ca^{2+}]_i$ slowed deactivation.

In summary, the activation kinetics are voltage independent and become faster by increasing $[Ca^{2+}]_i$, whereas the deactivation kinetics are prolonged by depolarization and by increasing $[Ca^{2+}]_i$.

Functional characterization of mutations in the first putative intracellular loop

To investigate the molecular mechanisms responsible for channel activation by Ca^{2+} and by voltage, we performed a site-directed mutagenesis study. Hydropathy analysis indicates that each member of the TMEM16 family has eight transmembrane domains (Fig. 6 A). Analysis of the sequence of TMEM16B does not reveal the presence of any typical voltage sensor or Ca^{2+}-binding domain. However, some acidic amino acids are located in the first putative intracellular loop between transmembrane segment 2 and 3, and we hypothesized that some of them may be involved in Ca^{2+} and/or voltage activation of TMEM16B. As illustrated in Fig. 6 B, we mutated glutamate at position 367 into glutamine (E367Q), deleted the five consecutive glutamate residues $_{386}$EEEEE$_{390}$ (ΔE_5), or deleted $_{399}$EYE$_{401}$ (ΔEYE), and measured their biophysical properties.

Fig. 6 (C–F) illustrates recordings from each mutant channel in the presence of various $[Ca^{2+}]_i$. Similar to WT

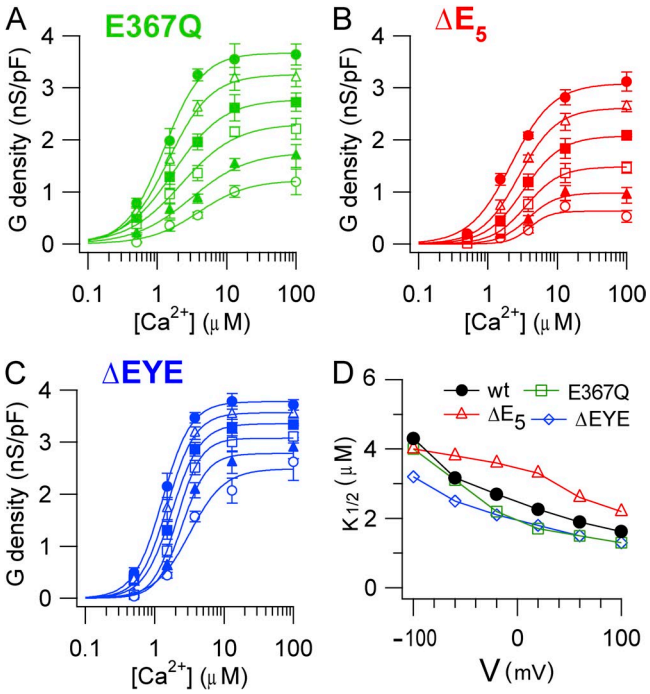

Figure 7. Ca^{2+} sensitivity of TMEM16B mutants. Conductance density calculated from tail currents measured at −100 mV after prepulses between −100 and +100 mV as indicated was plotted versus $[Ca^{2+}]_i$ for E367Q (A; n = 3–6), ΔE_5 (B; n = 3–5), and ΔEYE (C; n = 3–8) mutants. Lines are the fit to the Hill equation (Eq. 1). (D) $K_{1/2}$ values plotted versus voltage for each mutant.

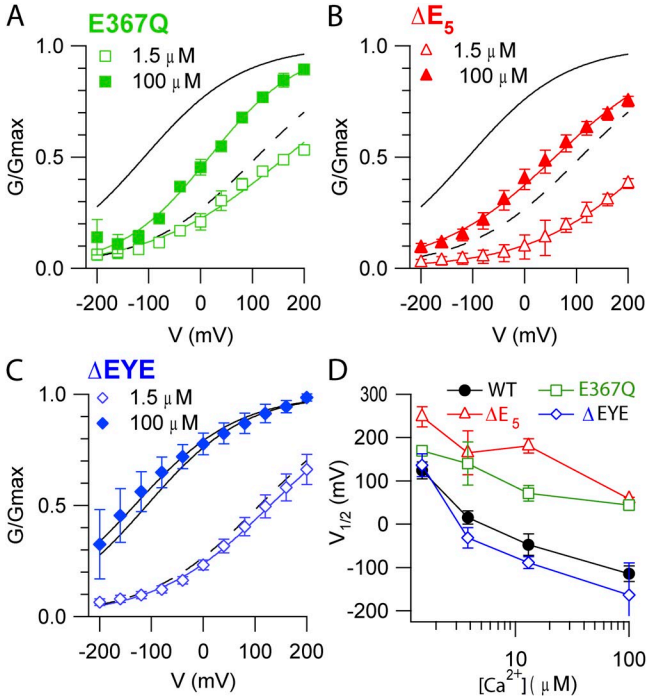

Figure 8. Voltage dependence of TMEM16B mutants. Normalized conductances at the indicated $[Ca^{2+}]_i$ calculated from tail currents at −100 mV after prepulses between −200 and +200 mV were plotted versus the prepulse voltage. Black lines are the fit to the Boltzmann equation (Eq. 2) for WT from Fig. 4 at 100 µM Ca^{2+} (solid line) or at 1.5 µM Ca^{2+} (dashed line). Colored lines are the fits to the Boltzmann equation for E367Q (A; n = 3–4), ΔE_5 (B; n = 3–5), and ΔEYE (C; n = 3–6) mutants. (D) Average $V_{1/2}$ values plotted versus $[Ca^{2+}]_i$.

Published March 12, 2012

(Fig. 2 A), the steady-state I-V relation for each mutant was Ca^{2+} dependent, showing an outward rectification at low $[Ca^{2+}]_i$ that became less pronounced as $[Ca^{2+}]_i$ increased (Fig. 6 G). However, although the overall Ca^{2+} dependence was similar, the rectification index, measured from the ratio between steady-state currents at +100 and −100 mV, was significantly higher at every $[Ca^{2+}]_i$ in E367Q and ΔE_5 mutants than in WT, whereas it remained similar in ΔEYE mutant channel (Fig. 6 H).

The dose–response relations for each mutant channel, evaluated from tail currents as described previously for the WT channel (Fig. 3), were fit by the Hill equation (Fig. 7, A–C). Fig. 7 D shows that $K_{1/2}$ at +100 mV (−100 mV) was 1.6 µM (4.3 µM) in WT, 1.3 µM (4.0 µM) in E367Q, 2.2 µM (4.0 µM) in ΔE_5, and 1.3 µM (3.2 µM) in ΔEYE. The Hill coefficient n_H at +100 mV (−100 mV) was 1.1 (1.2) in WT, 1.6 (1.2) in E367Q, 1.4 (2.9) in ΔE_5, and 2.0 (1.7) in ΔEYE. Thus, the mutations produced only some very small changes in $K_{1/2}$ or n_H, but overall no strong modifications in Ca^{2+} sensitivity were observed.

The G-V relations in mutant channels were measured at each $[Ca^{2+}]_i$ and compared with the corresponding relations in WT channels. Fig. 8 A shows that the E367Q mutation produced a rightward shift of the G-V relation at a given $[Ca^{2+}]_i$ with respect to WT; indeed, $V_{1/2}$ changed from 124 ± 20 mV in WT to 169 ± 6 mV in E367Q at 1.5 µM Ca^{2+}, and from −115 ± 18 mV in WT to 44 ± 8 mV in E367Q at 100 µM Ca^{2+} (Fig. 8 D). The deletion ΔE_5 also shifted the G-V relations to the right (Fig. 8, B and D): $V_{1/2}$ changed from 124 ± 20 mV in WT to 248 ± 39 mV in ΔE_5 at 1.5 µM Ca^{2+}, and from −115 ± 18 mV in WT to 58 ± 15 mV in ΔE_5 at 100 µM Ca^{2+}. Differently from the previous mutants, the ΔEYE deletion did not produce any significant change in the G-V relations (Fig. 8, C and D). The equivalent gating charge for each mutant varied between 0.15 and 0.32, values similar to those of the WT channel (z = 0.23–0.30). Thus, E367Q and the ΔE_5 deletion modified the voltage sensitivity: at a given $[Ca^{2+}]_i$, fewer channels can be open by depolarization compared with WT.

The kinetic properties of activation and deactivation of mutant channels also showed some interesting changes compared with WT channels. Upon depolarizing voltage steps, the activation of mutant channels was still characterized by two components: an instantaneous time-independent current, followed by an outward time-dependent relaxation (Fig. 6), which was well fit by a single-exponential function as in WT channels. In the presence of 1.5 µM Ca^{2+}, τ_{act} at +100 mV was 2.8 ± 0.3 ms in E367Q, faster than 7.5 ± 0.7 ms in the WT channel, whereas it became slower than WT in ΔE_5 (17.7 ± 3.0 ms) and in ΔEYE (25.5 ± 2.3 ms). These results indicate that each mutation altered the time course of activation. Indeed, the time necessary to respond to a depolarization decreased in E367Q, whereas it was progressively prolonged in ΔE_5 and in ΔEYE compared with WT. As in the WT channel, τ_{act} in each mutant was not significantly modified by voltage (Fig. 9 A).

Deactivation kinetics was also well fit by a single-exponential function and, similarly to WT, τ_{deact} showed an increase at less negative voltages for each mutant channel (Fig. 9 B). In the presence of 1.5 µM Ca^{2+}, τ_{deact} at −100 mV was 1.6 ± 0.3 ms in E367Q, smaller than 7.2 ± 0.8 ms in the WT channel, whereas it was not significantly different from WT in ΔE_5 (6.8 ± 0.3 ms) and became larger than WT in ΔEYE (12.3 ± 1.5 ms). The time necessary for channels to close upon repolarization decreased in E367Q but remained similar in ΔE_5, and it was prolonged in ΔEYE compared with WT. Thus, E367Q and ΔEYE mutants also showed a modified time course of deactivation.

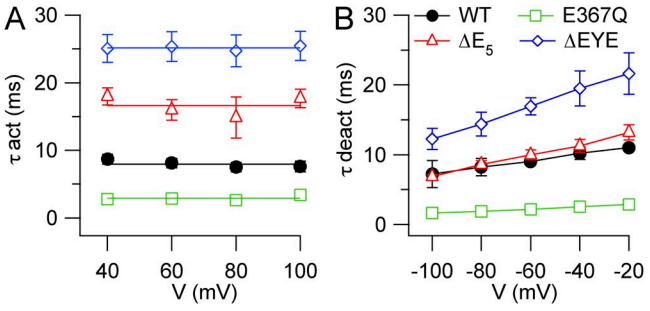

Figure 9. Activation and deactivation kinetics of TMEM16B mutants. Kinetics were measured as explained in Fig. 5. (A) Average activation time constants (τ_{act}) plotted versus voltage for E367Q (n = 5), ΔE_5 (n = 3), and ΔEYE (n = 6) mutants. (B) Average deactivation time constants (τ_{deact}) plotted versus voltage for E367Q (n = 4), ΔE_5 (n = 4), and ΔEYE (n = 5) mutants.

DISCUSSION

Here, we have provided the first site-directed mutagenesis study to investigate structure–function relations of the TMEM16B channel. Because previous studies have shown that TMEM16B in excised inside-out patches has a significant rundown (Pifferi et al., 2009, Fig. 5; Stephan et al., 2009, Fig. 3 A), whereas whole cell recordings are rather stable (Pifferi et al., 2009, Fig. 1 h), we decided to use the whole cell configuration.

We first characterized the WT TMEM16B channel and established one important difference between TMEM16A and TMEM16B activation properties in the absence of $[Ca^{2+}]_i$. Indeed, we found that TMEM16B cannot be activated by voltages up to +200 mV in the absence of Ca^{2+} (32 ± 10 pA/pF; n = 6; not depicted), whereas recent data from Hartzell's laboratory showed that TMEM16A was activated by strong depolarization in the absence of Ca^{2+} (∼140 pA/pF at +200 mV; Fig. 5 A in Xiao et al., 2011). Thus, our data show that TMEM16B needs Ca^{2+} to be activated differently from TMEM16A, which can be activated by voltage also in the absence of Ca^{2+} (Xiao et al., 2011).

Published March 12, 2012

In the presence of Ca^{2+}, dose–response relations for TMEM16A and TMEM16B obtained by different laboratories reported variable values for $K_{1/2}$. For TMEM16A, from inside-out recordings, $K_{1/2}$ at +60 mV (−60 mV) was 0.3 µM (2.6 µM) (Yang et al., 2008), and at +100 mV (−100 mV) it was 0.4 µM (5.9 µM) (Xiao et al., 2011), whereas from whole cell recordings at +100 mV (−40 mV) it was 332 nM (∼700 nM) (Ferrera et al., 2009). For TMEM16B, from previous work in inside-out patches, $K_{1/2}$ at +50 mV (−50 mV) was 3.3 µM (4.9 µM) (Pifferi et al., 2009), and at +40 mV (−40 mV) it was 1.2 µM (1.8 µM) (Stephan et al., 2009), whereas from whole cell recordings we found that $K_{1/2}$ at +40 mV (−40 mV) was 2.0 µM (2.7 µM), and at +100 mV (−100 mV) it was 1.6 µM (4.3 µM) (Fig. 3). Although there are some differences among studies reported from different laboratories, every report showed that the apparent affinity for Ca^{2+} is slightly voltage dependent, with higher apparent Ca^{2+} affinity at positive voltages, and the Hill coefficients are consistently higher than one, indicating that more than a Ca^{2+} ion is necessary to activate the channels. A comparison between TMEM16A and TMEM16B shows a fourfold difference between $K_{1/2}$ values at +100 mV: 0.4 µM (Xiao et al., 2011) for TMEM16A and 1.6 µM for TMEM16B (Fig. 3), indicating a lower apparent affinity for Ca^{2+} of TMEM16B compared with TMEM16A.

A critical question about the function of TMEM16A and TMEM16B is the following: what are the molecular mechanisms responsible for Ca^{2+} and voltage modulation of channel gating in each channel? Galietta's laboratory (Ferrera et al., 2009) has shown that human TMEM16A has various protein isoforms generated by alternative splicing, and it has labeled the four identified alternative segments as *a*, *b*, *c*, and *d*. A rare minimal version of TMEM16A lacking all alternative segments, TMEM16A (0), still shows CaCC properties, although the voltage dependence is reduced, (Caputo et al., 2008; Ferrera et al., 2009, 2011). Ferrera et al. (2009) showed that segment *b* modified the Ca^{2+} sensitivity by nearly fourfold, decreasing the apparent half-effective concentration at +80 mV from 350 to 90 nM, whereas segment *c* affected the voltage dependence but not the Ca^{2+} sensitivity of human TMEM16A (*abc*). Segment *c* is composed of the four amino acids EAVK, which have also been recently deleted from mouse TMEM16A (*ac*) in a study from Hartzell's laboratory (Xiao et al., 2011). Differently from Ferrera et al. (2009), Xiao et al. (2011) found that deletion of EAVK modified both Ca^{2+} and voltage dependence of TMEM16A. The discrepancy between the results can be a result of differences between human TMEM16A (*ab*) and mouse TMEM16A (*a*), and/or to the different techniques, whole cell versus inside-out recordings, used for the experiments in the different laboratories. Although the two studies reached some different conclusions, they both pointed to the relevance of the segment *c* in the regulation of the TMEM16A functional activity.

TMEM16B is expressed in the retina, at the synaptic terminal of photoreceptors (Stöhr et al., 2009; Billig et al., 2011), in the cilia of olfactory sensory neurons, and in the microvilli of vomeronasal sensory neurons (Stephan et al., 2009; Rasche et al., 2010; Sagheddu et al., 2010; Billig et al., 2011; Pifferi et al., 2012). Zhao's laboratory showed that the major TMEM16B olfactory isoform differs from the retinal isoform in the absence of the exon encoding the four amino acids ERSQ in the first putative intracellular loop (Stephan et al., 2009). It is worth pointing out here that segment *c* (EAVK) in TMEM16A is not present in TMEM16B, but that ERSQ residues are located in the corresponding positions in the retinal isoform of TMEM16B (Fig. 6). A comparison between the biophysical properties measured in inside-out patches from the retinal isoform (Pifferi et al., 2009) and from the olfactory isoform (missing ERSQ; Stephan et al., 2009) did not reveal any major difference in the rectification properties and in the dose–response relations between the two isoforms, although we cannot exclude that more detailed biophysical studies may reveal subtle differences. Indeed, the functional properties of additional isoforms for TMEM16B are under investigation (Saidu, S.P., A.B. Stephan, S.M. Caraballo, H. Zhao, and J. Reisert. 2010. Association for Chemoreception Sciences Meeting. Abstr. P68).

Although the amino acidic sequences of both TMEM16A and TMEM16B lack any classical voltage-sensor or Ca^{2+}-binding domain, a series of five consecutive glutamates located in the first putative intracellular loop has been identified as a good candidate to play a role in channel gating. Moreover, we have investigated if other glutamates in the same loop could also be involved in the activation of TMEM16B by Ca^{2+} and voltage. We found that deletion of the five glutamates, ΔE_5, did not greatly affect the apparent affinity for Ca^{2+} (Fig. 7), but it significantly shifted the activation curve to the right. Indeed, $V_{1/2}$ at 1.5 µM Ca^{2+} changed from 124 mV in WT to 248 mV, whereas the equivalent gating charge was not modified. In addition, the time necessary to respond to a depolarization was prolonged in ΔE_5, whereas the deactivation constant was not significantly affected (Fig. 9). Thus, the five consecutive glutamates are involved in the voltage dependence of the TMEM16B channel, whereas they do not seem to play a significant role in the apparent affinity for Ca^{2+}. These results are in agreement with a recent study in TMEM16A, showing that the substitution of the four correspondent glutamates into alanines ($_{444}$EEEE/AAAA$_{447}$) did not greatly affect the apparent affinity for Ca^{2+} but modified the voltage dependence, producing a shift of the activation curve to the right (Xiao et al., 2011).

In the TMEM16B mutant E367Q, both activation and deactivation kinetics were shortened; the dose–response relation for Ca^{2+} was not strongly modified, while the activation curve was shifted to the right. Finally, the deletion ΔEYE produced an increase in the time constants

for activation and deactivation, whereas it did not cause any large change in apparent affinity for Ca^{2+} or in voltage sensitivity.

Collectively, our results indicate that glutamates E367 and $_{386}$EEEEE$_{390}$ in the first putative intracellular loop play a relevant role in the modulation of the voltage dependence of TMEM16B.

Conclusions

In conclusion, we have found evidence that the five consecutive glutamates in the first putative intracellular loop are not involved in Ca^{2+} sensitivity in TMEM16B but have an important role in voltage dependence. Another glutamate in position 367 plays a similar role, further indicating that the first intracellular loop is involved in voltage-dependent activation of TMEM16B.

At present, the location of the Ca^{2+}-binding site in TMEM16A and TMEM16B remains unknown. It is possible that several residues in different regions contribute to bind Ca^{2+} ions, but it cannot be excluded that the Ca^{2+}-binding site is located in an accessory subunit expressed both in HEK 293T cells and in axolotl oocytes. Future work will have to shed light on the intricate mechanisms that couple Ca^{2+} gating and voltage dependence, including intriguing interactions between gating and permeation.

We thank Anna Boccaccio, Arin Marchesi, and Riccardo Scala for discussions; Federica Ferrero for help with cell cultures; and all members of the laboratory for discussions.

This study was supported by grants from the Italian Ministry of Education, University and Research, and from the Italian Institute of Technology.

Christopher Miller served as editor.

Submitted: 27 December 2011
Accepted: 17 February 2012

REFERENCES

Bers, D.M. 2008. Calcium cycling and signaling in cardiac myocytes. *Annu. Rev. Physiol.* 70:23–49. http://dx.doi.org/10.1146/annurev.physiol.70.113006.100455

Billig, G.M., B. Pál, P. Fidzinski, and T.J. Jentsch. 2011. Ca2+-activated Cl− currents are dispensable for olfaction. *Nat. Neurosci.* 14:763–769. http://dx.doi.org/10.1038/nn.2821

Caputo, A., E. Caci, L. Ferrera, N. Pedemonte, C. Barsanti, E. Sondo, U. Pfeffer, R. Ravazzolo, O. Zegarra-Moran, and L.J.V. Galietta. 2008. TMEM16A, a membrane protein associated with calcium-dependent chloride channel activity. *Science.* 322:590–594. http://dx.doi.org/10.1126/science.1163518

Das, S., Y. Hahn, D.A. Walker, S. Nagata, M.C. Willingham, D.M. Peehl, T.K. Bera, B. Lee, and I. Pastan. 2008. Topology of NGEP, a prostate-specific cell:cell junction protein widely expressed in many cancers of different grade level. *Cancer Res.* 68:6306–6312. http://dx.doi.org/10.1158/0008-5472.CAN-08-0870

Duran, C., and H.C. Hartzell. 2011. Physiological roles and diseases of tmem16/anoctamin proteins: are they all chloride channels? *Acta Pharmacol. Sin.* 32:685–692. http://dx.doi.org/10.1038/aps.2011.48

Duran, C., C.H. Thompson, Q. Xiao, and H.C. Hartzell. 2010. Chloride channels: often enigmatic, rarely predictable. *Annu. Rev. Physiol.* 72:95–121. http://dx.doi.org/10.1146/annurev-physiol-021909-135811

Ferrera, L., A. Caputo, I. Ubby, E. Bussani, O. Zegarra-Moran, R. Ravazzolo, F. Pagani, and L.J.V. Galietta. 2009. Regulation of TMEM16A chloride channel properties by alternative splicing. *J. Biol. Chem.* 284:33360–33368. http://dx.doi.org/10.1074/jbc.M109.046607

Ferrera, L., P. Scudieri, E. Sondo, A. Caputo, E. Caci, O. Zegarra-Moran, R. Ravazzolo, and L.J.V. Galietta. 2011. A minimal isoform of the TMEM16A protein associated with chloride channel activity. *Biochim. Biophys. Acta.* 1808:2214–2223. http://dx.doi.org/10.1016/j.bbamem.2011.05.017

Flores, C.A., L.P. Cid, F.V. Sepúlveda, and M.I. Niemeyer. 2009. TMEM16 proteins: the long awaited calcium-activated chloride channels? *Braz. J. Med. Biol. Res.* 42:993–1001. http://dx.doi.org/10.1590/S0100-879X2009005000028

Frings, S., D. Reuter, and S.J. Kleene. 2000. Neuronal Ca2+-activated Cl− channels—homing in on an elusive channel species. *Prog. Neurobiol.* 60:247–289. http://dx.doi.org/10.1016/S0301-0082(99)00027-1

Galietta, L.J.V. 2009. The TMEM16 protein family: a new class of chloride channels? *Biophys. J.* 97:3047–3053. http://dx.doi.org/10.1016/j.bpj.2009.09.024

Hartzell, C., I. Putzier, and J. Arreola. 2005. Calcium-activated chloride channels. *Annu. Rev. Physiol.* 67:719–758. http://dx.doi.org/10.1146/annurev.physiol.67.032003.154341

Hartzell, H.C., K. Yu, Q. Xiao, L.-T. Chien, and Z. Qu. 2009. Anoctamin/TMEM16 family members are Ca2+-activated Cl− channels. *J. Physiol.* 587:2127–2139. http://dx.doi.org/10.1113/jphysiol.2008.163709

Huang, F., X. Wong, and L.Y. Jan. 2012. International Union of Basic and Clinical Pharmacology. LXXXV: calcium-activated chloride channels. *Pharmacol. Rev.* 64:1–15. http://dx.doi.org/10.1124/pr.111.005009

Kleene, S.J. 2008. The electrochemical basis of odor transduction in vertebrate olfactory cilia. *Chem. Senses.* 33:839–859. http://dx.doi.org/10.1093/chemse/bjn048

Kunzelmann, K., P. Kongsuphol, K. Chootip, C. Toledo, J.R. Martins, J. Almaca, Y. Tian, R. Witzgall, J. Ousingsawat, and R. Schreiber. 2011a. Role of the Ca2+-activated Cl− channels bestrophin and anoctamin in epithelial cells. *Biol. Chem.* 392:125–134. http://dx.doi.org/10.1515/BC.2011.010

Kunzelmann, K., Y. Tian, J.R. Martins, D. Faria, P. Kongsuphol, J. Ousingsawat, F. Thevenod, E. Roussa, J. Rock, and R. Schreiber. 2011b. Anoctamins. *Pflugers Arch.* 462:195–208. http://dx.doi.org/10.1007/s00424-011-0975-9

Kunzelmann, K., R. Schreiber, A. Kmit, W. Jantarajit, J.R. Martins, D. Faria, P. Kongsuphol, J. Ousingsawat, and Y. Tian. 2012. Expression and function of epithelial anoctamins. *Exp. Physiol.* 97:184–192.

Lalonde, M.R., M.E. Kelly, and S. Barnes. 2008. Calcium-activated chloride channels in the retina. *Channels (Austin).* 2:252–260. http://dx.doi.org/10.4161/chan.2.4.6704

Leblanc, N., J. Ledoux, S. Saleh, A. Sanguinetti, J. Angermann, K. O'Driscoll, F. Britton, B.A. Perrino, and I.A. Greenwood. 2005. Regulation of calcium-activated chloride channels in smooth muscle cells: a complex picture is emerging. *Can. J. Physiol. Pharmacol.* 83:541–556. http://dx.doi.org/10.1139/y05-040

Patton, C., S. Thompson, and D. Epel. 2004. Some precautions in using chelators to buffer metals in biological solutions. *Cell Calcium.* 35:427–431. http://dx.doi.org/10.1016/j.ceca.2003.10.006

Petersen, O.H. 2005. Ca2+ signalling and Ca2+-activated ion channels in exocrine acinar cells. *Cell Calcium.* 38:171–200. http://dx.doi.org/10.1016/j.ceca.2005.06.024

Petersen, O.H., and A.V. Tepikin. 2008. Polarized calcium signaling in exocrine gland cells. *Annu. Rev. Physiol.* 70:273–299. http://dx.doi.org/10.1146/annurev.physiol.70.113006.100618

Pifferi, S., G. Pascarella, A. Boccaccio, A. Mazzatenta, S. Gustincich, A. Menini, and S. Zucchelli. 2006. Bestrophin-2 is a candidate calcium-activated chloride channel involved in olfactory transduction. *Proc. Natl. Acad. Sci. USA*. 103:12929–12934. http://dx.doi.org/10.1073/pnas.0604505103

Pifferi, S., M. Dibattista, and A. Menini. 2009. TMEM16B induces chloride currents activated by calcium in mammalian cells. *Pflugers Arch.* 458:1023–1038. http://dx.doi.org/10.1007/s00424-009-0684-9

Pifferi, S., V. Cenedese, and A. Menini. 2012. Anoctamin 2/TMEM16B: a calcium-activated chloride channel in olfactory transduction. *Exp. Physiol.* 97:193–199.

Rasche, S., B. Toetter, J. Adler, A. Tschapek, J.F. Doerner, S. Kurtenbach, H. Hatt, H. Meyer, B. Warscheid, and E.M. Neuhaus. 2010. Tmem16b is specifically expressed in the cilia of olfactory sensory neurons. *Chem. Senses.* 35:239–245. http://dx.doi.org/10.1093/chemse/bjq007

Rock, J.R., and B.D. Harfe. 2008. Expression of TMEM16 paralogs during murine embryogenesis. *Dev. Dyn.* 237:2566–2574. http://dx.doi.org/10.1002/dvdy.21676

Sagheddu, C., A. Boccaccio, M. Dibattista, G. Montani, R. Tirindelli, and A. Menini. 2010. Calcium concentration jumps reveal dynamic ion selectivity of calcium-activated chloride currents in mouse olfactory sensory neurons and TMEM16b-transfected HEK 293T cells. *J. Physiol.* 588:4189–4204. http://dx.doi.org/10.1113/jphysiol.2010.194407

Sanders, K.M., M.H. Zhu, F.C. Britton, S.D. Koh, and S.M. Ward. 2012. Anoctamins and gastrointestinal smooth muscle excitability. *Exp. Physiol.* 97:200–206.

Schroeder, B.C., T. Cheng, Y.N. Jan, and L.Y. Jan. 2008. Expression cloning of TMEM16A as a calcium-activated chloride channel subunit. *Cell.* 134:1019–1029. http://dx.doi.org/10.1016/j.cell.2008.09.003

Scudieri, P., E. Sondo, L. Ferrera, and L.J. Galietta. 2012. The anoctamin family: TMEM16A and TMEM16B as calcium-activated chloride channels. *Exp. Physiol.* 97:177–183. http://dx.doi.org/10.1113/expphysiol.2011.058198

Stephan, A.B., E.Y. Shum, S. Hirsh, K.D. Cygnar, J. Reisert, and H. Zhao. 2009. ANO2 is the cilial calcium-activated chloride channel that may mediate olfactory amplification. *Proc. Natl. Acad. Sci. USA.* 106:11776–11781. http://dx.doi.org/10.1073/pnas.0903304106

Stöhr, H., J.B. Heisig, P.M. Benz, S. Schöberl, V.M. Milenkovic, O. Strauss, W.M. Aartsen, J. Wijnholds, B.H.F. Weber, and H.L. Schulz. 2009. TMEM16B, a novel protein with calcium-dependent chloride channel activity, associates with a presynaptic protein complex in photoreceptor terminals. *J. Neurosci.* 29:6809–6818. http://dx.doi.org/10.1523/JNEUROSCI.5546-08.2009

Wray, S., T. Burdyga, and K. Noble. 2005. Calcium signalling in smooth muscle. *Cell Calcium.* 38:397–407. http://dx.doi.org/10.1016/j.ceca.2005.06.018

Xiao, Q., K. Yu, P. Perez-Cornejo, Y. Cui, J. Arreola, and H.C. Hartzell. 2011. Voltage- and calcium-dependent gating of TMEM16A/Ano1 chloride channels are physically coupled by the first intracellular loop. *Proc. Natl. Acad. Sci. USA.* 108:8891–8896. http://dx.doi.org/10.1073/pnas.1102147108

Yang, Y.D., H. Cho, J.Y. Koo, M.H. Tak, Y. Cho, W.-S. Shim, S.P. Park, J. Lee, B. Lee, B.-M. Kim, et al. 2008. TMEM16A confers receptor-activated calcium-dependent chloride conductance. *Nature.* 455:1210–1215. http://dx.doi.org/10.1038/nature07313

Interactions between permeation and gating

in the TMEM16B/anoctamin2 calcium-activated chloride channel

Giulia Betto[1*], O. Lijo Cherian[1*], Simone Pifferi[1*],Valentina Cenedese[1,#], Anna Boccaccio[2], Anna Menini[1]

[1]Neurobiology Group, SISSA, International School for Advanced Studies, Trieste, Italy

[2]Istituto di Biofisica, CNR, Genova, Italy

[*]These authors contributed equally to this paper and are listed in alphabetical order

[#]present address: Netherlands Institute for Neuroscience (NIN), Amsterdam, Netherlands

Corresponding author:

Anna Boccaccio

Istituto di Biofisica - IBF

Consiglio Nazionale delle Ricerche - CNR

Via De Marini 6, 16149 Genova, Italy

phone : +39 010 6475 891, Fax: +39 010 6475500

boccaccio@ge.ibf.cnr.it

KEY WORDS: Ca^{2+}-activated Cl^- channel, patch clamp, ANO2, ion selectivity

RUNNING TITLE: Permeation and gating of TMEM16B/anoctamin2

Abstract

At least two members of TMEM16/anoctamin family, TMEM16A (also known as anoctamin1) and TMEM16B (also known as anoctamin2), encode Ca^{2+}-activated Cl^- channels (CaCCs), which are found in various cell types and mediate numerous physiological functions. Here, we used whole-cell and excised inside-out patch-clamp to investigate the relationship between anion permeation and gating, two processes typically viewed as independent, in TMEM16B expressed in HEK 293T cells. The permeability ratio sequence determined by substituting Cl^- with other anions (P_x/P_{Cl}) was $SCN^- > I^- > NO_3^- > Br^- > Cl^- > F^-$ > gluconate. When external Cl^- was substituted with other anions, TMEM16B activation and deactivation kinetics at 0.5μM Ca^{2+} were modified according to the sequence of permeability ratios, with anions more permeant than Cl^- slowing both activation and deactivation and anions less permeant than Cl^- accelerating them. Moreover, replacement of external Cl^- with gluconate, or sucrose, shifted the voltage dependence of steady-state activation (G_V relation) to more positive potentials, whereas substitution of extracellular or intracellular Cl^- with SCN^- shifted G-V to more negative potentials. Dose-response relationships for Ca^{2+} in the presence of different extracellular anions indicated that apparent affinity for Ca^{2+} at +100mV increased with increasing permeability ratio. The apparent affinity for Ca^{2+} in the presence of intracellular SCN^- also increased compared with that in Cl^-. Our results provide the first evidence that TMEM16B gating is modulated by permeant anions and provide the basis for future studies aimed at identifying the molecular determinants of TMEM16B ion selectivity and gating.

INTRODUCTION

Permeation and gating properties in most ion channels have been traditionally considered to be independent, with the opening and closing the ion channel (gating) as a separate process from ion entrance and passage in the channel pore (permeation). However, several reports on many ion channels, have described interactions between permeation and gating, suggesting that these two processes are not always independent (Hille, 2001).

Ca^{2+}-activated Cl^- channels (CaCCs) play important physiological functions, including regulation of cell excitability, fluid secretion, smooth muscle contraction and block of polyspermy in some oocytes (for reviews, see Frings et al., 2000; Hartzell et al., 2005; Leblanc et al., 2005; Petersen, 2005; Wray et al., 2005; Lalonde et al., 2008; Duran et al., 2010; Berg et al., 2012; Huang et al., 2012a). Evidence that anions modify gating of endogenous CaCCs was reported in several cell types. Indeed, partial replacement of Cl^- with other anions caused alterations in CaCCs kinetics or conductance in lacrimal gland cells (Evans and Marty, 1986), parotid secretory cells (Ishikawa and Cook, 1993; Perez-Cornejo et al., 2004), portal vein smooth muscle cells (Greenwood and Large, 1999), and *Xenopus* oocytes (Centinaio et al., 1997; Kuruma and Hartzell, 2000; Qu and Hartzell, 2000). Moreover, Qu and Hartzell (2000) showed that the sensitivity for Ca^{2+} of CaCCs in *Xenopus* oocytes depended on the permeant anion, indicating that the permeant anion is able to affect channel gating.

The molecular identity of CaCCs has been controversial for a long time, but there is now a general consensus that at least two members of the TMEM16 (anoctamin) gene family, TMEM16A/anoctamin1 and TMEM16B/anoctamin2, encode for CaCCs (Caputo et al., 2008; Schroeder et al., 2008; Yang et al., 2008; Pifferi et al., 2009; Stephan et al., 2009; Stöhr et al., 2009*)*. TMEM16A is expressed in secretory cells, smooth muscle cells and in several other cell

types (Huang et al., 2009; 2012a), including supporting cells in the olfactory and vomeronasal epithelium (Billig et al., 2011, Dauner et al., 2012; Dibattista et al., 2012; Maurya and Menini, 2014) and microvilli of vomeronasal sensory neurons (Dibattista et al., 2012). TMEM16B is expressed at the synaptic terminal of photoreceptors (Stöhr et al., 2009; Billig et al., 2011; Dauner et al., 2013), in hippocampal cells (Huang et al., 2012b), in the cilia of olfactory sensory neurons, and in the microvilli of vomeronasal sensory neurons (Stephan et al., 2009; Hengl et al., 2010; Rasche et al., 2010; Sagheddu et al., 2010; Billig et al., 2011; Dauner et al., 2012; Dibattista et al., 2012; Maurya and Menini, 2014). Studies with knockout mice for TMEM16A or TMEM16B (Rock and Harfe, 2008; Billig et al., 2011), or knockdown of these channels further confirmed a reduction in CaCC activity (for reviews, see Flores et al., 2009; Galietta, 2009; Hartzell et al., 2009; Kunzelmann et al., 2011, 2012; Pifferi et al., 2012; Sanders et al., 2012; Scudieri et al., 2012; Huang et al., 2012a).

At present little is known about the structure-function relations for TMEM16A and TMEM16B. Bioinformatic models based on hydropathy analysis indicate that TMEM16 proteins have eight putative transmembrane domains (Caputo et al., 2008; Schroeder et al., 2008; Yang et al., 2008). In TMEM16A, the first putative intracellular loop contains regions that are involved both in the Ca^{2+} and voltage-dependence (Caputo et al., 2008; Ferrera et al., 2009, 2011; Xiao et al., 2011). In TMEM16B, some glutamic acids in the first putative intracellular loop contribute to voltage-dependence (Cenedese et al., 2012). A recent study identified splice variants for TMEM16B and found that N terminal sequences affect Ca^{2+} sensitivity (Ponissery Saidu et al., 2013).

A region located between transmembrane domains 5 and 6 was proposed to form a re-entrant loop exposed to the extracellular membrane side and to be part of the channel pore. Indeed,

mutations of some basic aminoacids in this region of TMEM16A, such as R621E, altered ion selectivity (Yang et al., 2008), although another study did not confirm the change in ion selectivity with this mutation (Yu et al., 2012). The same group proposed a different topology in which a re-entrant loop is exposed to the intracellular membrane side of the membrane also forming the third intracellular loop. Indeed, mutagenesis of two aminoacids in this region, E702 and E705, largely modified Ca^{2+} sensitivity of TMEM16A (Yu et al., 2012). Experiments with chimeras between TMEM16A and TMEM16B support the finding that the third intracellular loop is important for Ca^{2+} sensitivity (Scudieri et al., 2013). At present, no mutations significantly altering ion selectivity have been found (Yu et al., 2012).

Recent studies reported that anions modify gating of TMEM16A. Ferrera et al. (2011) showed that membrane conductance increased at all voltages when extracellular Cl^- was replaced with I^- or SCN^-. Xiao et al. (2011) found that voltage-dependent gating of TMEM16A was facilitated by anions with high permeability or by an increase in extracellular Cl^-.

Here, we investigate how extracellular and intracellular anions affect gating in TMEM16B and show the presence of a strong coupling between permeation and gating.

MATERIALS AND METHODS

Heterologous expression

Full-length mouse TMEM16B cDNA in pCMV-Sport6 mammalian expression plasmid was obtained from RZPD (Berlin, Germany; clone identification: IRAVp968H1167D; accession number NP_705817.1). This is the retinal isoform with the same start site of the olfactory isoform used in Stephan et al. (2009) and contained the exon 14 (Ponissery Saidu et al., 2013, named exon 13 in Stephan et al., 2009). 2 μg cDNA was transfected into HEK 293T cells using FuGENE-6 or X-tremeGENE 9 (Roche Applied Science, Mannheim, Germany). Cells were cotransfected with 0.2 μg pEGFP–C1 (Clontech, Mountain View, CA, USA) for fluorescent identification of transfected cells.

Electrophysiology

Electrophysiological recordings were performed in the whole-cell or inside-out patch-clamp configurations between 48 and 72 hours from transfection, as previously described (Pifferi et al., 2006, 2009; Cenedese et al., 2012). Patch pipettes, made of borosilicate glass (WPI, Sarasota, FL) with a PP-830 puller (Narishige, Tokyo, Japan), had resistance of about 3-5 MΩ or 1-2 MΩ respectively for whole-cell or inside-out experiments. Currents were recorded with an Axopatch 1D or Axopatch 200B amplifier controlled by Clampex 9 or 10 via a Digidata 1332A or 1440 (Axon Instruments, or Molecular Devices, Union City, CA, USA). Data were low-pass filtered at 4 or 5 kHz and sampled at 10 kHz. Experiments were performed at room temperature (20-25^{o}C). The bath was grounded via a 1 or 3 M KCl agar salt bridge connected to a Ag/AgCl reference electrode. A modified rapid solution exchanger (Perfusion Fast-Step SF-77B; Warner

Instruments Corp., USA) was used to expose cells or excised membrane patches to different solutions.

In whole-cell recordings, one stimulation protocol consisted of voltage steps of 200 ms duration from a holding potential of 0 mV ranging from -100 to +100 mV (or from -200 to +200 mV), followed by a step to -100 mV. A single-exponential function was fitted to tail currents to extrapolate the tail current value at the beginning of the step to -100 mV. The conductance, G, was calculated as $G = I_t / (V_t - V_{rev})$, where I_t is the tail current, V_t is the tail voltage, -100mV, V_{rev} is the current reversal potential.

To estimate V_{rev}, channels were activated by a 200 ms pulse to +100 mV and then rapidly closed by application of hyperpolarizing steps. Single-exponential functions were fitted to tail currents to extrapolate the tail current value at each voltage step. Tail current values were plotted as a function of voltage and the V_{rev} was estimated from a linear fit in a ± 20 mV interval around V_{rev}.

In inside-out recordings, currents were recorded after the initial rundown, as described in Pifferi et al. (2009). Moreover, to allow the current to partially inactivate, patches were pre-exposed to the various Ca^{2+} concentrations for 500 ms before applying voltage protocols (Pifferi et al., 2009). Stimulation protocols consisted of a +100 mV voltage step of 200 ms duration from a holding potential of 0 mV followed by a step to -100 mV, or by double voltage ramps from -100 to +100 mV and back to -100 mV at 1 mV/ms rate and the two current-voltage relations were averaged. The dose-response curves were obtained by exposing the patches for one second to solutions with increasing free Ca^{2+} concentrations. Leak currents measured in nominally 0 Ca^{2+} solutions were subtracted.

Ionic solutions

The same solutions were used for whole-cell and inside-out recordings, unless otherwise indicated. The standard extracellular solution contained (in mM): 140 NaCl, 5 KCl, 2 $CaCl_2$, 1 $MgCl_2$, 10 glucose, and 10 HEPES, pH 7.4. The standard intracellular solutions contained (in mM): 140 CsCl, 10 HEPES, 10 HEDTA (or 5 EGTA), pH 7.2, and no added Ca^{2+} for the nominally 0 Ca^{2+} solution, or various amounts of $CaCl_2$, as calculated with the program WinMAXC (C. Patton), to obtain free Ca^{2+} in the range between 0.18 and 100 μM (Patton et al., 2004). The intracellular solution with 1 mM Ca^{2+} contained (in mM): 140 NaCl, 10 HEPES, 1 $CaCl_2$, pH 7.2

Cl^- in the extracellular solution was substituted with other anions by replacing NaCl on an equimolar basis (unless otherwise indicated) with NaX, where X is the substituted anion.

The control extracellular solution (140 mM Cl) used in Fig. 4 contained (in mM) 140 NaCl, 2.5 K_2SO_4, 2 $CaSO_4$, 1 $MgSO_4$ and 10 HEPES, pH 7.4. For the 11 mM Cl^- and 1 mM Cl^- solutions, NaCl was replaced on an equimolar basis with Na-gluconate or sucrose. The osmolarity was adjusted with sucrose.

In the extracellular solutions containing NaF divalent cations were omitted. When NaF was tested in the presence of 1mM Ca^{2+} at the intracellular side of inside-out patches, no current was measured, probably due to the insolubility of CaF_2.

When the patch pipette contained SCN^-, I^-, Br^-, a 1 M KCl agar salt bridge was used to connect the Ag/AgCl wire to the recording solutions.

Applied voltages were not corrected for liquid junction potentials.

All chemicals were purchased from Sigma (Milano, Italy), except K_2SO_4 from Carlo Erba (Rodano (MI), Italy) and $CaSO_4$ from JT Baker (Milano, Italy).

Data analysis

Data are presented as mean ± SEM, with n indicating the number of cells or patches. Statistical significance was determined using paired or unpaired t-tests, or ANOVA, as appropriate. When a statistically significant difference was determined with ANOVA, a post hoc Tukey's test was used to evaluate which data groups showed significant differences. P values <0.05 were considered significant. Data analysis and figures were made with Igor Pro software (Wavemetrics, Lake Oswego, OR, USA). For the sake of clarity in the figures the capacitative transients of some traces were trimmed**.**

RESULTS

Anion selectivity of TMEM16B

To determine the selectivity of TMEM16B to anions, we measured currents in the presence of various extracellular anions by replacing 140 mM NaCl in the Ringer solution with the Na salt of other anions. Fig. 1 A shows representative whole-cell recordings at 0.5 μM Ca^{2+} in the presence of Cl^-, after replacement of Cl^- with the indicated anions, and in Cl^- after wash out. Steady-state I-V relations are plotted in Fig. 1 B. To obtain a better estimate of V_{rev} we also measured tail currents (Fig. 1 C-D). When Cl^- was replaced with gluconate, the outward currents decreased and V_{rev} shifted to positive values, revealing a lower permeability of gluconate than Cl^-. On the contrary, in the presence of SCN^-, I^-, NO_3^- and Br^-, the outward currents were larger than those measured in Cl^- and V_{rev} shifted to negative values, indicating a higher permeability of the substituted anions than Cl^-. Permeability ratios (P_X/P_{Cl}) were: SCN^- (3.0) > I^- (2.6) >NO_3^- (2.3) > Br^- (1.7) > Cl^- (1.0) > F^- (0.5) > gluconate (0.2). Fig. 1 E-F shows that the selectivity of TMEM16B estimated both from permeability ratios (P_X/P_{Cl}) and from chord conductance ratios (G_X/G_{Cl}) had the same sequence: SCN^- > I^- > NO_3^- > Br^- > Cl^- > F^- > gluconate.

To obtain a direct comparison of selectivity in whole-cell and inside-out configurations, we also performed experiments in inside-out patches with different anions in the pipette solution, at the extracellular side of the membrane patch. Fig. 2 A shows currents activated at 1.5 μM Ca^{2+} using voltage ramps from -100 to +100 mV, in the presence of the indicated extracellular anions. P_X/P_{Cl} were: SCN^- (18.2) > I^- (7.1) >NO_3^- (4.1) > Br^- (2.3) > Cl^- (1.0) > F^- (0.3) > gluconate (0.1). The sequence of P_X/P_{Cl} in inside-out patches was the same as that measured in whole-cell experiments, although the value of P_X/P_{Cl} for some anions was significantly higher when

measured in inside-out than in whole-cell recordings (see Discussion).

Moreover, we compared selectivity when anions were replaced at the extracellular or intracellular side of inside-out patches and showed that for each internal or external anion P_X/P_{Cl} was not significantly different (Fig. 2 B; data for intracellular I^-, NO_3^-, Br^- are from Pifferi et al., 2009).

We plotted P_X/P_{Cl} for extracellular anion substitution versus ionic radius (Fig. 2 C) or free energy of hydration (Fig. 2 D) of the test anion X. These plots show that P_X/P_{Cl} increases with the ionic radius, with the exception of F^- and gluconate. On the other side, P_X/P_{Cl} increases monotonically as the free energy of hydration decreases, indicating that the facility with which the anion enters the channel is related to its free energy of hydration.

Activation and deactivation kinetics

To characterize activation and deactivation kinetics in the presence of various anions, we analyzed the time-dependent components in response to voltage steps in whole-cell recordings at 0.5 μM Ca^{2+}. We measured the activation kinetics of currents in response to a voltage step to +100 mV from 0 mV holding voltage. The current in Cl^- had an instantaneous component, related to the fraction of channels open at 0 mV, followed by a time-dependent component due to the increase in channel opening at +100 mV. The time-dependent component was fit by a single-exponential function to calculate the time constant of activation, τ_{act}. Fig. 3 A shows superimposed normalized currents from the same cell in Cl^- or with the indicated extracellular anion. No time-dependent component at +100 mV was observed when Cl^- was replaced with gluconate or F^- (not shown). On average, τ_{act} at +100 mV in the presence of 0.5 μM Ca^{2+} was 7.7 ± 0.4 ms in Cl^-, while it became slower with more permeant anions: 28 ± 3 ms in SCN^-, 14.8 ±

1.2 ms in I^-, 12.5 ± 1.0 ms in NO_3^-, 11.1 ± 1.4 ms in Br^-. The average τ_{act} is plotted as a function of P_X/P_{Cl} in Fig. 3 C, showing that more permeant anions significantly prolonged the time course of activation increasing the time necessary to respond to a depolarization compared to Cl^-.

To examine the deactivation kinetics, we calculated the time constant of current deactivation (τ_{deact}) by fitting with a single exponential function the tail currents obtained by a voltage step to -60 mV after a prepulse at +100 mV. Fig. 3 B shows superimposed normalized currents from the same cells of Fig. 3 A. In the presence of 0.5 μM Ca^{2+}, the average τ_{deact} at -60 mV was 4.6 ± 0.3 ms in Cl^-, while it became faster with less permeant anions: 2.3 ± 0.5 ms in F^-, 1.9 ± 0.2 ms in gluconate, and slower with more permeant anions 23.3 ± 4.8 ms in SCN^-, 9.3 ± 1.4 ms in I^-, 7.5 ± 0.5 ms in NO_3^-, 5.8 ± 0.9 ms in Br^-. The average τ_{deact} is plotted as a function of P_X/P_{Cl} in Fig. 3 C, showing that the deactivation kinetics prolonged as a function of permeability ratios.

Voltage dependence

To investigate the effect of anions on the voltage dependence of channel activation in whole-cell recordings, we extended voltage steps from -200 to +200 mV to obtain a better estimate of voltage dependence (Fig. 4). The voltage dependence of steady-state activation (G-V relation) was analyzed measuring tail currents at the beginning of a step to -100 mV after the prepulse voltage steps. The conductance was plotted versus membrane voltage and fit by the Boltzmann equation:

$$G = G_{max} / \{1 + \exp [z (V_{1/2} - V) F/RT]\}, \quad (1)$$

where G is the conductance, z is the equivalent gating charge associated with voltage dependent channel opening, V is the membrane potential, $V_{1/2}$ is the membrane potential producing half-maximal activation, F is the Faraday constant, R is the gas constant, and T is the

absolute temperature. G_{max} was evaluated for each cell from a global fit of G-V relations in control, after anion substitutions, and after wash out.

In a first set of experiments, we decreased the extracellular Cl^- concentration from 140 mM to 11 mM or 1 mM by replacing Cl^- with equimolar concentrations of the less permeant anion gluconate, in the presence of 1.5 μM Ca^{2+} (Fig. 4 A, B). Fig. 4 C shows that the decrease of $[Cl^-]_o$ produced a rightward shift of the G-V relation. From a global fit of G-V relations with the same G_{max} and equivalent gating charge (z), $V_{1/2}$ significantly changed from 79 ± 13 mV in 140 mM Cl^-, to 187 ± 14 mV in 11 mM $[Cl^-]_o$. When Cl^- was further decreased to 1 mM, $V_{1/2}$ was 205 ± 17 mV, not significantly different from $V_{1/2}$ value in 11 mM. The average z value was 0.29±0.02 (n=10). Similar results were obtained when $[Cl^-]_o$ was reduced by partial substitution with sucrose: $V_{1/2}$ changed from 70 ± 19 mV in 140 mM Cl^-, to 209 ± 23 mV in 11 mM Cl^-, and 199 ± 23 mV in 1 mM Cl^-, confirming that the shift was due to $[Cl^-]_o$ reduction rather than to the presence of gluconate (Fig. 4 D).

These results show that $V_{1/2}$ increased when extracellular Cl^- was reduced by substitution with gluconate or with sucrose, indicating that less channels can be activated by depolarization when the external Cl^- concentration is reduced. The opposite trend, consisting of a leftward shift of the G-V relation at a given $[Ca^{2+}]_i$, was observed when Cl^- was partially replaced by the more permeant anion SCN^- (Fig. 5). Indeed, in the presence of 0.5 μM Ca^{2+} (Fig. 5A-C) or 1.5 μM Ca^{2+} (Fig. 5D-F), the substitution of Cl^- with SCN^- produced a leftward shift of the G-V relations. Upon a further increase of Ca^{2+} concentration to 13 μM (Fig. 5G-H), the substitution of Cl^- with SCN^- caused an almost complete activation of the current at all membrane potentials in all the experiments, preventing the possibility to numerically estimate $V_{1/2}$, which was shifted to very negative potentials << -200 mV (Fig. 5G-H).

Data from several cells at 0.5 or 1.5 μM Ca^{2+} are summarized in Fig. 5I, where average $V_{1/2}$ are shown. At 0.5 μM Ca^{2+}, the average $V_{1/2}$ significantly changed from 195 ± 19 mV in Cl^- to 11 ± 35 mV in SCN^- (n=4). At 1.5 μM Ca^{2+}, the average $V_{1/2}$ significantly changed from 84 ± 20 mV in Cl^- to -189 ± 20 mV in SCN^- (n=9;in some experiments with SCN^- at 1.5 μM Ca^{2+}, in which the current was fully activated and $V_{1/2}$ could not be evaluated, we considered $V_{1/2}$ = -250 mV). The average z value was not significantly different: 0.33 ± 0.04 and 0.26 ± 0.01 respectively in 0.5 and 1.5 μM Ca^{2+}.

To investigate whether the leftward shift of the G-V relation was specific to SCN^- or was present also with other anions more permeant than Cl^-, we performed experiments changing the external anion from Cl^- to NO_3^- in the presence of 1.5 μM Ca^{2+} (representative recordings not shown). A leftward shift of the G-V relation was observed also with NO_3^- and the average $V_{1/2}$ significantly changed from 52 ± 16 mV in Cl^- to -101 ± 18 mV in NO_3^- (n=6), as shown in the right columns of Fig. 5 I.

Thus, $V_{1/2}$ decreased in the presence of SCN^- or NO_3^-, indicating that more channels can be activated by depolarization in the presence of some anions more permeant than Cl^-.

Ca^{2+} dependence

To investigate whether different anions modify the Ca^{2+} dependence of TMEM16B activation we measured dose-response relations. The best technique to measure the Ca^{2+}-dependence of TMEM16B is to use excised inside-out patches, because channels can be activated by several $[Ca^{2+}]_i$ in the same patch, and the leakage current in the absence of Ca^{2+} can be subtracted from each measurement. However, as we have previously shown, the current induced by TMEM16B present a rundown in activity in inside-out patches (Pifferi et al., 2009), limiting the number of

recordings that can be compared on the same patch. For this reason, we measured currents activated by various $[Ca^{2+}]_i$ at only two voltage steps of 100 or -100 mV, as shown in Fig. 6 A. Currents in the presence of each extracellular anion were measured at the end of each voltage step by taking the average current between 150 and 190 ms, normalized to the maximal current at the same voltage and plotted versus $[Ca^{2+}]_i$ (Fig. 6 B). Data were fitted by the Hill equation:

$$I/I_{max} = [Ca^{2+}]_i^{n_H} / ([Ca^{2+}]_i^{n_H} + K_{1/2}^{n_H}) \quad (2)$$

where I is the current, I_{max} is the maximal current, $K_{1/2}$ is the half-maximal $[Ca^{2+}]_i$, and n_H is the Hill coefficient.

Average $K_{1/2}$ values at +100 mV were lower for anions more permeant than Cl^-, while increased for less permeant anions (Fig 6 B,C,E). At -100 mV, average $K_{1/2}$ value for SCN^- was smaller than the value in Cl^-, whereas there was no significant difference for values between the other anions and Cl^- (Fig. 6 C). Moreover, we observed a significant increase for Hill coefficient values (n_H) both at -100 and +100 mV for NO_3^-, I^- and SCN^- compared to Cl^- (Fig. 6 D).

These results indicate that, at +100 mV, a lower $[Ca^{2+}]_i$ is sufficient to activate 50% of the maximal current in the presence of external anions more permeant than Cl^-, while a higher $[Ca^{2+}]_i$ is required for less permeant anions.

To further investigate how external SCN^- modifies the Ca^{2+}-dependence of TMEM16B compared with Cl^-, we measured dose-response relations in whole-cell recordings at different voltages and compared the results with values measured with voltage ramps in inside-out patches (Fig. 7). The whole-cell configuration has the advantage of allowing the comparison of recordings with different extracellular anions in the same cell, but has the disadvantage that different $[Ca^{2+}]_i$ have to be tested on different cells. To compare currents from different cells, current densities were calculated by dividing current amplitudes by the cell capacitance. Fig. 7 A

shows whole-cell currents at various $[Ca^{2+}]_i$ in external Cl^- or SCN^-. In each cell, at a given $[Ca^{2+}]_i$, both inward and outward currents in SCN^- significantly increased with respect to those in Cl^-. Dose-response relations in whole-cell were analyzed by measuring tail currents at the beginning of the step to -100 mV after prepulses ranging from -100 to +100 mV in steps of 20 mV. Average conductance densities in the presence of external Cl^- or SCN^- were calculated, plotted versus $[Ca^{2+}]_i$ and fit at each voltage by the Hill equation:

$$G = G_{max} [Ca^{2+}]_i^{n_H} / ([Ca^{2+}]_i^{n_H} + K_{1/2}^{n_H}) \quad (3)$$

where G is the conductance density, G_{max} is the maximal conductance density, $K_{1/2}$ is the half-maximal $[Ca^{2+}]_i$, and n_H is the Hill coefficient.

The comparison between dose-response relations at +100 and -100 mV in external Cl^- and SCN^- is illustrated in Fig. 7 B. At +100 mV, $K_{1/2}$ was 1.2 μM in Cl^- and decreased to 0.4 μM in SCN^-. Fig. 7 C shows that $K_{1/2}$ slightly decreased as a function of voltage from 7.6 μM at -100 mV to 1.2 μM at +100 mV in Cl^-, and from 1.1 μM at -100 mV to 0.4 μM at +100 mV in SCN^-. The Hill coefficient in Cl^- was not voltage dependent, with a value of 1.1 both at -100 and +100 mV, while in SCN^- n_H was 2.2 at -100 mV and 3.5 at +100 mV (Fig. 7 D). Similar results were obtained from experiments in the inside-out configuration. Currents at various $[Ca^{2+}]_i$ were activated with voltage ramps with Cl^- (Fig. 7 E) or SCN^- (Fig. 7 F) in the patch pipette.

Normalized dose-response relations were fit with the Hill equation (eq. 2, Fig. 7 G). Fig. 7 H-I show that $K_{1/2}$ and n_H values at different voltages were similar in inside-out and in whole cell configurations, further confirming that external SCN^- increased the apparent Ca^{2+} affinity at all voltages compared to Cl^-, and increased n_H at some positive voltages.

To determine if SCN^- modifies channel gating also from the intracellular side, we measured the voltage dependence of activation in whole-cell recordings in the presence SCN^- instead of

Cl^- at 0.5 μM Ca^{2+} (Fig. 8 A). G-V relations showed that $V_{1/2}$ was -0.4 ± 11 mV in intracellular SCN^- (n=11; z = 0.33 ± 0.01), while it was 195 ± 19 mV in intracellular Cl^- (Fig. 8 B-C, for Cl^- data from Fig. 5 I).

Moreover, we measured dose-response relations for Ca^{2+} in inside-out patches in the presence of SCN^- in the bathing solution (Fig. 8 D). The comparison between dose-response relations at +100 and -100 mV in intracellular Cl^- and SCN^- is illustrated in Fig. 8 E. At +100 mV, $K_{1/2}$ was 2.2 ± 0.1 μM in Cl^- and decreased to 0.85 ± 0.06 μM in SCN^-, at –100 mV $K_{1/2}$ was 6.4 ± 0.4 μM in Cl^- and 3.3 ± 0.3 μM in SCN^-. The Hill coefficient in Cl^- was not voltage dependent, with a value of 1.41 ± 0.06 at -100 and 1.4 ± 0.3 at +100 mV, while in SCN^- n_H was 1.90 ± 0.06 at -100 mV and 2.2 ± 0.2 at +100 mV.

These results show that not only extracellular, but also intracellular SCN^- affects gating of TMEM16B by producing a leftward shift of the voltage dependence and an increase of the apparent affinity for Ca^{2+}.

DISCUSSION

In this study, we have provided evidence that, in the TMEM16B channel, permeant anions modulate the kinetics of current activation and deactivation, as well as the voltage and apparent Ca^{2+}-sensitivity. Indeed, extracellular anions more permeant than Cl^- prolonged both τ_{act} and τ_{deact} at low Ca^{2+}, shifted $V_{1/2}$ toward more negative values, and decreased $K_{1/2}$, favoring channel's opening. In contrast, extracellular anions less permeant than Cl^- shortened τ_{deact}, shifted $V_{1/2}$ toward more positive values, and increased $K_{1/2}$, contributing to channel closure. Moreover, a decrease of extracellular Cl^- by replacement with sucrose, also shortened τ_{deact} (not shown), and shifted $V_{1/2}$ toward more positive values, favoring the closed state of the channel. Overall, these results indicate that the most permeant anions and Cl^- itself favor the open state of TMEM16B.

Furthermore, we investigated the effect of replacing Cl^- with SCN^- at the intracellular side of the channel and found similar gating modifications as from the extracellular side.

Anion selectivity

The sequence of permeability ratios measured in whole-cell recordings when extracellular Cl^- was replaced with other anions was: SCN^- (3.0) > I^- (2.6) >$NO3^-$ (2.3) > Br^- (1.7) > Cl^- (1.0) > F^- (0.5) >gluconate (0.2). Moreover, the sequence of relative chord conductance followed the same order. Both sequences are in agreement, for the corresponding anions, with measurements obtained by Adomaviciene et al. (2013, see Fig. 4) on TMEM16B and TMEM16A.

The order of anions in the sequence was the same when measurements were obtained both from whole-cell and inside-out patches. However, permeability ratios in inside-out patches were:

SCN^- (18.2) > I^- (7.1) >NO_3^- (4.1) > Br^- (2.3) > Cl^- (1.0) > F^- (0.3) >gluconate (0.1), showing larger differences among anions than in whole-cell recordings. Indeed, we measured a difference in V_{rev} when anions were exchanged in the whole-cell or inside-out configurations. For example, when external Cl^- was replaced with SCN^-, the average V_{rev} in whole-cell was -27 ± 2 mV, whereas in the same ionic conditions with SCN^- in the pipette, V_{rev} in inside-out was -70 ± 1 mV. We measured a less negative V_{rev} in whole-cell than in inside-out recordings also with the other anions more permeant than Cl^-. This difference may be due to several reasons, including the loss of some intracellular factor after patch excision, such as calmodulin, and/or ion accumulation effects due to restricted ion diffusion altering the ion concentration gradient. If SCN^- or other anions entering the cell accumulated at the intracellular side of the membrane, the concentration gradient between intracellular and extracellular side would decrease, producing a less negative V_{rev} value. The differences we observed are consistent with anion accumulation at the intracellular surface membrane in whole-cell, whereas the continuous flow of solutions containing Cl^- in inside-out membrane patches is likely to prevent or reduce the possibility of anion accumulation at the intracellular side of the membrane. In addition, we cannot exclude a difference induced by effects following patch excision. Jung et al. (2013) reported that the anion selectivity of TMEM16A is dynamically regulated by the Ca^{2+}/calmodulin complex, while the effect of Ca^{2+}/calmodulin on selectivity of TMEM16B has not been investigated yet. In any case, despite the difference in some values of permeability ratios, we obtained the same sequence for anion permeability ratios measured with different patch-clamp configurations, confirming that the permeability ratios sequence for TMEM16B follows the Hofmeister sequence or lyotropic sequence, in which anions with lower dehydration energy (lyotropos) have higher permeability compared to anions with higher dehydration energy (Wright and Diamond, 1977; Zhang and

Cremer, 2006). As previously pointed out, "the relationship between anion permeability and anion energy of hydration supports the notion that anion dehydration is the limiting step in permeation" (Dawson et al. 1999; Linsdell et al. 2000).

Activation and deactivation kinetics

We found that anions more permeant than Cl^- slowed both the activation and deactivation time constants at 0.5 μM Ca^{2+}. τ_{act} at +100 mV was 7.7 ± 0.4 ms in Cl^- and almost doubled to 14.8 ± 1.2 ms in I^-. τ_{deact} at -60 mV was 4.6 ± 0.3 ms in Cl^-, also increased twice to 9.3 ± 1.4 ms in I^-. For anions less permeant than Cl^-, currents activated by depolarizing voltage steps lost any time-dependence, while the τ_{deact} were shortened in gluconate, τ_{deact} at -60 mV decreased to 1.9 ± 0.2 ms.

These results can be compared with the limited number of previous studies investigating the effects of permeant anions on endogenous CaCCs. Although some differences in permeability sequences were reported in different cells, in each case there was a correlation between changes in kinetics and permeability ratios.

Evans and Marty (1986) reported the following sequence of permeability ratios for CaCCs in isolated cells from lacrimal glands when Cl^- was replaced with some extracellular anions: I^- (2.71) > NO_3^- (2.39) > Br^- (1.59) > Cl^- (1) > F^- (0.18) > isethionate (0.11) = methanesulphonate (0.11) > glutamate (0.05). The same authors investigated current kinetics at 0.5 μM Ca^{2+}, and showed that replacement of extracellular Cl^- with the two most permeant anions in these cells, I^- or NO_3^-, led to significant alterations of both τ_{act} at +20 mV and τ_{deact} at -60 mV. The value of τ_{act} in Cl^- was 241 ± 53 ms and was shortened of 0.91 and 0.83 times in I^- and NO_3^-, respectively. The value of τ_{deact} was 170 ± 45 ms in Cl^- and increased 1.54 and 1.38 times in I^- and NO_3^-,

respectively. Other anions such as Br^-, isethionate, methanesulphonate or glutamate did not significantly modified current kinetics indicating that "the more permeant the anion, the greater was its effect on channel kinetics" (Evans and Marty, 1986).

Greenwood and Large (1999) studied the effects of extracellular anions on the deactivation kinetics of CaCCs in smooth muscle cells isolated from rabbit portal vein with the perforated patch clamp technique. The sequence of permeability ratios was: $SCN^- > I^- > Br^- > Cl^- > >$ isethionate. The same authors reported that τ_{deact} was prolonged by the external anions SCN^-, I^- and Br^-, which were more permeant than Cl^-, while it was accelerated by the less permeant anion isethionate. Indeed, τ_{deact} was 97 ± 7 ms in Cl^-, 278 ± 19 ms in SCN^-, 157 ± 37 ms in I^-, and 67 ± 5 ms in isethionate, showing a strong correlation between permeability ratios and changes in kinetics of deactivation, suggesting that gating is linked to permeability.

In another study, Perez-Cornejo (2004) obtained whole-cell recordings from acinar cells dissociated from rat parotid gland and measured the following permeability ratios: SCN^- (4.3) > I^- > (2.6) > NO_3^- (2.0) > Br^- (1.6) > Cl^- (1) > F^- (0.3) > aspartate (0.1) > glutamate (0.05). Kinetics of current activation and deactivation were measured in the presence of 250 nM Ca^{2+}. Activation kinetics increased about fourfold in SCN^- and about twofold in NO_3^-. Deactivation kinetics increased about threefold in SCN^- and about twofold in NO_3^-, while decreased in F^-. As in previous studies, the effects on kinetics largely followed the order of the permeability sequence, with anions with permeability ratios > 1 producing larger effects. Also in this case SCN^- efficacy was much larger than what observed with the other more permeant anions, an effect consistent with the high permeability of SCN^-.

Although results from CaCCs on different cells are heterogeneous, all share the same property that τ_{act} and τ_{deact} were affected by extracellular permeant anions according with their

permeability ratios, similarly to our results. τ_{deact} was prolonged or shortened by anions more or less permeant than Cl^-, respectively. One important difference from our results is that we found that τ_{act} for the TMEM16B current was prolonged by anions more permeant than Cl^-, whereas in the previous work on endogenous CaCCs, τ_{act} was shortened (Evans and Marty, 1986; Perez-Cornejo, 2004). This difference may be due to the difference in channel proteins, as TMEM16A is most likely the CaCCs expressed in lacrimal glands and in parotid acinar cells and/or by the $[Ca^{2+}]_i$. Indeed, we measured τ_{act} at 0.5 μM Ca^{2+}, a concentration at which the TMEM16B current induced by depolarization has a clear time-dependent component, while as $[Ca^{2+}]_i$ increases the time-dependent component decreases and most current has an instantaneous change to the new level (Fig. 7 A). Thus, differences in τ_{act} may be explained by different Ca^{2+}-dependencies of the time-dependent component among CaCCs.

Voltage and Ca^{2+} dependence of activation.

We measured the voltage dependent activation of TMEM16B at low Ca^{2+} concentrations showing that the substitution of both intra- and extracellular Cl^- with the more permeant SCN^- caused a leftward shift of the G-V relation. Also the Cl^- itself is affecting TMEM16B voltage dependence, since its substitution with sucrose caused a shift of $V_{1/2}$ to more positive values. Furthermore, dose-response relations Ca^{2+} showed that the sensitivity for Ca^{2+} depends on the permeant anion, and that $K_{1/2}$ at +100 mV decreases as a function of permeability ratios.

Also these results can be compared with the small number of previous studies which have investigated the effect of permeant anions on endogenous CaCCs.

Ishikawa and Cook (1993) recorded in whole-cell from sheep parotid secretory cells and measured the following permeability ratios: SCN^- (1.80) > I^- (1.09) > Cl^- (1) > NO_3^- (0.92) >

Br^- (0.75). These authors analysed current amplitudes and showed that both outward and inward currents increased when Cl^- was replaced with SCN^-, remained similar in I^-, and decreased both with NO_3^- and Br^-. Thus, the conductance changes followed the order of the permeability sequence. Perez-Cornejo (2004) measured G-V relations in the presence of anions more permeant than Cl^-, fit the normalized conductance with the Boltzmann equation, and reported that G-V relations were shifted towards more negative voltages with respect to the value in Cl^-. The shift was larger for anions with higher permeability ratios. Anions with permeability ratios < 1 were not tested. Qu and Hartzell (2000) compared dose-response for Ca^{2+} in inside-out patches from Xenopus oocytes, in the presence of Cl^- or SCN^- at the intracellular side. By fitting the data with the Hill equation, they found that at 0 mV, the Ca^{2+} concentration producing 50% of the maximal current was 279 nM in Cl^-, while it decreased of about twofold, 131 nM, in SCN^-, indicating that a lower $[Ca^{2+}]_i$ is sufficient to open the channels in the presence of the more permeant anion SCN^-, compared to Cl^-. These results show that anions more permeant than Cl^- favor channel opening, whereas less permeant anions favor channel closure, in agreement with our results.

TMEM16A and TMEM16B

After the discovery that TMEM16A and TMEM16B are CaCCs, some studies reported the effect of some permeant anion on TMEM16A, whereas this is the first study on TMEM16B.

Xiao et al. (2011) obtained whole-cell recordings from HEK293 cell expressing the TMEM16A(ac) isoform and showed that replacement of extracellular Cl^- with NO_3^- or SCN^- shifted G-V relations to more negative voltages. Moreover, replacement of increasing concentrations of extracellular Cl^- with gluconate or sucrose, shifted the G-V relations toward

increasingly more positive voltages. τ_{act} and τ_{deact} were not reported. These results are in agreement with our data.

Ferrera et al. (2011) reported that whole-cell recordings from Fischer rat thyroid cells stably expressing the TMEM16A(abc) showed an increase or decrease in conductance when extracellular Cl^- was replaced with more or less permeant anions, respectively. Indeed, the conductance increased about twofold in I^- and SCN^-, while decreased of about 50% in gluconate. Interestingly, the same authors showed that the isoform TMEM16A(0) had some differences in selectivity compared to TMEM16A(abc). P_I/P_{Cl} increased from 3.6 for TMEM16A(abc) to 4.7 for TMEM16A(0) and P_{SCN}/P_{Cl} increased from 3.4 for TMEM16A(abc) to 5.6 for TMEM16A(0). Furthermore, the membrane conductance in I^- and SCN^- increased about sixfold compared to Cl for TMEM16A(0), to be compared with a twofold increase in TMEM16A(abc). τ_{act} and τ_{deact} were not reported. It is likely that a comparison of the regions of the two isoforms may help to shed light on the molecular mechanism at the basis of the effect of permeant anion on gating.

How are permeant anions modifying gating in these channels? Greenwood and Large (1999) first suggested that the slower deactivation measured with more permeant anions could be explained if the more permeant anion favors the channel open state, for example by increasing the mean open time, possibly with a mechanism similar to the "foot in the door", originally observed in potassium channels (Armstrong, 1971) and afterwards confirmed in various other ion channels, where the most permeant ions stabilized the open conformation (Yellen, 1997). Our results could be explained by this mechanism, as the most permeant anions also produce an increase in the apparent open probability.

Overall, we found that permeant anions affected the voltage dependence, and the apparent

Ca^{2+} affinity, but not the voltage sensitivity as measured by the equivalent gating charge *z*. However, it is likely that permeant anions play a more complex role in addition to an increase in open probability. We observed that the substitution of Cl^- with SCN^- both at the extracellular and intracellular side produced a shift of the G-V relation toward more negative values, an increase of the apparent Ca^{2+} affinity, but also a reduction in the voltage dependence of the apparent Ca^{2+} affinity (Fig. 7 C, H), and an increase of the Hill coefficient at positive voltages. These results could suggest that more permeant ion can bind with higher affinity than Cl^- to an allosteric binding site (inside or outside the pore) that may control the gate of the channel.

Interestingly, effect of permeant anions on gating is not novel for Cl^- channels, since it is well known that anion occupancy of the pore is strictly coupled to fast gating in CLC Cl^- channels. For these channels, the movement of the permeating anion in the pore contributes to the voltage dependence of the channel opening (Chen and Miller, 1996; Pusch et al., 1995; Pusch, 1996). However, the ion selectivity sequence for CLC Cl^- channels, $Cl^- > Br^- > I^-$, is very different from that for TMEM16B, and there is no evidence for sequence conservation patterns among CLC and TMEM16 families (Duran et al., 2010), indicating that the molecular mechanisms underlying the effect of permeant anions on gating may be rather different.

Recent work showed that the TMEM16A channel can be gated by direct binding of Ca^{2+} to the TMEM16A protein, rather than by binding to an accessory Ca^{2+} binding protein or through phosphorylation (Yu et al., 2012, 2014; Terashima et al., 2013). Moreover, mutation of two glutamic acids, E702 and E705, greatly modified the Ca^{2+} sensitivity of the channel and contributed to the revision of the topology of the channel (Yu et al., 2012), a topology that received further support by results obtained with chimeric proteins between TMEM16A and TMEM16B (Scudieri et al., 2013). Yu et al. (2012) also obtained data consistent with aminoacids

625 to 630 contributing to an outer vestibule at the extracellular side of the membrane, with aminoacids beyond 635 located deep in the putative pore. To determine if these aminoacids are part of the permeation pathway and modify ion selectivity, Yu et al. (2012) measured the permeability and conductance ratios between I^- and Cl^- after replacement of several aminoacids between 625 and 639 with cysteine, but did not find any significant alteration in ion selectivity. Thus, at present determinants of ion selectivity are still unknown. Future work will have to determine which regions of the protein contribute to the permeation pathway, which aminoacids are critical for ion selectivity, and how permeant anions modify gating at the molecular level. Moreover, as TMEM16A and TMEM16B have several important differences and none of the chimeras recently produced had properties reproducing those of TMEM16B (Scudieri et al., 2013), it is likely that the molecular determinants of modifications of gating by permeant anions in the two channels may have some differences.

ACKNOWLEDGMENTS

We thank Sara Migliarini (University of Pisa) for the help with molecular biology, and all members of the laboratory for discussions. This study was supported by a grant from the Italian Ministry of Education, University and Research (MIUR). S.P. is a recipient of an EU Marie Curie Reintegration Grant (OLF-STOM n.334404).

REFERENCES

Adomaviciene, A., K. Smith, H. Garnett, and P. Tammaro. 2013. Putative pore-loops of TMEM16/anoctamin channels affect channel density in cell membranes. *J Physiol*. 591:487–505.

Armstrong, C. 1971. Interaction of tetraethylammonium ion derivatives with the potassium channels of giant axons. *J Gen Physiol*. 58:413–37.

Berg, J., H. Yang, and L. Jan. 2012. Ca2+-activated Cl- channels at a glance. *J Cell Sci*. 125:1367–71.

Billig, G.M., B. Pál, P. Fidzinski, and T.J. Jentsch. 2011. Ca2+-activated Cl− currents are dispensable for olfaction. *Nat. Neurosci.* 14:763–769.

Caputo, A., E. Caci, L. Ferrera, N. Pedemonte, C. Barsanti, E. Sondo, U. Pfeffer, R. Ravazzolo, O. Zegarra-Moran, and L.J.V. Galietta. 2008. TMEM16A, a membrane protein associated with calcium-dependent chloride channel activity. *Science*. 322:590–594.

Cenedese, V., G. Betto, F. Celsi, O.L. Cherian, S. Pifferi, and A. Menini. 2012. The voltage dependence of the TMEM16B/anoctamin2 calcium-activated chloride channel is modified by mutations in the first putative intracellular loop. *J. Gen. Physiol.* 139:258–94.

Centinaio, E., E. Bossi, and A. Peres. 1997. Properties of the Ca^{2+}-activated Cl- current of Xenopus oocytes. *Cell Mol Life Sci*. 53:604–10.

Chen, T., and C. Miller. 2008. Nonequilibrium gating and voltage dependence of the ClC-0 Cl- channel. *J Gen Physiol*. 108:237–50.

Dauner, K., J. Lissmann, S. Jeridi, and F. Möhrlen. 2012. Expression patterns of anoctamin 1 and anoctamin 2 chloride channels in the mammalian nose. *Cell Tissue Res*. 347:327–41.

Dauner, K., C. Möbus, S. Fring, and F. Möhrlen. 2013. Targeted expression of anoctamin calcium-activated chloride channels in rod photoreceptor terminals of the rodent retina. *Invest. Ophthalmol. Vis. Sci.* 54:3126–36.

Dawson, D., S. Smith, and M. Mansoura. 1999. CFTR: mechanism of anion conduction. *Physiol. Rev.* 79:S47–75.

Dibattista, M., A. Amjad, D.K. Maurya, C. Sagheddu, G. Montani, R. Tirindelli, and A. Menini. 2012. Calcium-activated chloride channels in the apical region of mouse vomeronasal sensory neurons. *J. Gen. Physiol.* 140:3–15.

Duran, C., C.H. Thompson, Q. Xiao, and H.C. Hartzell. 2010. Chloride channels: often enigmatic, rarely predictable. *Annu. Rev. Physiol.* 72:95–121.

Evans, M.G., and A. Marty. 1986. Calcium-dependent chloride currents in isolated cells from rat lacrimal glands. *J. Physiol. (Lond.)*. 378:437–460.

Ferrera, L., A. Caputo, I. Ubby, E. Bussani, O. Zegarra-Moran, R. Ravazzolo, F. Pagani, and L.J.V. Galietta. 2009. Regulation of TMEM16A chloride channel properties by alternative splicing. *J. Biol. Chem.* 284:33360–33368.

Ferrera, L., P. Scudieri, E. Sondo, A. Caputo, E. Caci, O. Zegarra-Moran, R. Ravazzolo, and L.J.V. Galietta. 2011. A minimal isoform of the TMEM16A protein associated with chloride channel activity. *Biochim. Biophys. Acta*. 1808:2214–2223.

Flores, C.A., L.P. Cid, F.V. Sepúlveda, and M.I. Niemeyer. 2009. TMEM16 proteins: the long awaited calcium-activated chloride channels? *Braz. J. Med. Biol. Res.* 42:993–1001.

Frings, S., D. Reuter, and S.J. Kleene. 2000. Neuronal Ca^{2+} -activated Cl^- channels--homing in on an elusive channel species. *Prog. Neurobiol.* 60:247–289.

Galietta, L.J.V. 2009. The TMEM16 protein family: a new class of chloride channels? *Biophys. J.* 97:3047–3053.

Greenwood, I.A., and W.A. Large. 1999. Modulation of the decay of Ca^{2+}-activated C^{l-} currents in rabbit portal vein smooth muscle cells by external anions. *J. Physiol. (Lond.)*. 516 (Pt 2):365–376.

Hartzell, C., I. Putzier, and J. Arreola. 2005. Calcium-activated chloride channels. *Annu. Rev. Physiol.* 67:719–758.

Hartzell, H.C., K. Yu, Q. Xiao, L.-T. Chien, and Z. Qu. 2009. Anoctamin/TMEM16 family members are Ca2+-activated Cl- channels. *J. Physiol. (Lond.)*. 587:2127–2139.

Hengl, T., H. Kaneko, K. Dauner, K. Vocke, S. Frings, and F. Möhrlen. 2010. Molecular components of signal amplification in olfactory sensory cilia. *Proc. Natl. Acad. Sci. U.S.A.* 107:6052–6057.

Hille, B. 2001. Ion Channel of Excitable Membranes. Sinauer Associates, Inc, Sunderland, MA. 572pp.

Huang, F., J.R. Rock, B.D. Harfe, T. Cheng, X. Huang, Y.N. Jan, and L.Y. Jan. 2009. Studies on expression and function of the TMEM16A calcium-activated chloride channel. *Proc. Natl. Acad. Sci. U.S.A.* 106:21413–21418.

Huang, F., X. Wong, and L.Y. Jan. 2012a. International Union of Basic and Clinical Pharmacology. LXXXV: Calcium-Activated Chloride Channels. *Pharmacol. Rev.* 64:1–15.

Huang, W., S. Xiao, F. Huang, B. Harfe, Y. Jan, and L. Jan. 2012b. Calcium-activated chloride channels (CaCCs) regulate action potential and synaptic response in hippocampal neurons. *Neuron*. 74:179–92.

Ishikawa, T., and D. Cook. 1993. A Ca^{2+}-activated Cl^- current in sheep parotid secretory cells. *The Journal of Membrane Biology*. 135:261–271.

Jung, J., J.H. Nam, H.W. Park, U. Oh, J.H. Yoon, and M.G. Lee. 2013. Dynamic modulation of ANO1/TMEM16A HCO_3^- permeability by Ca^{2+}/calmodulin. *Proc. Natl. Acad. Sci. U.S.A.* 110:360–365.

Kunzelmann, K., Y. Tian, J. Martins, D. Faria, P. Kongsuphol, J. Ousingsawat, L. Wolf, and R. Schreiber. 2012. Airway epithelial cells--functional links between CFTR and anoctamin dependent Cl- secretion. *Int J Biochem Cell Biol*. 44:1897–900.

Kunzelmann, K., R. Schreiber, A. Kmit, W. Jantarajit, J.R. Martins, D. Faria, P. Kongsuphol, J. Ousingsawat, and Y. Tian. 2011. Expression and function of epithelial anoctamins. *Exp. Physiol.* 97:184–92.

Kuruma, A., and H.C. Hartzell. 2000. Bimodal control of a Ca^{2+}-activated Cl^- channel by different Ca^{2+} signals. *J. Gen. Physiol.* 115:59–80.

Lalonde, M.R., M.E. Kelly, and S. Barnes. 2008. Calcium-activated chloride channels in the retina. *Channels (Austin)*. 2:252–260.

Leblanc, N., J. Ledoux, S. Saleh, A. Sanguinetti, J. Angermann, K. O'Driscoll, F. Britton, B.A. Perrino, and I.A. Greenwood. 2005. Regulation of calcium-activated chloride channels in smooth muscle cells: a complex picture is emerging. *Can. J. Physiol. Pharmacol.* 83:541–556.

Linsdell, P., A. Evagelidis, and J. Hanrahan. 2000. Molecular determinants of anion selectivity in the cystic fibrosis transmembrane conductance regulator chloride channel pore. *Biophys. J.* 78:2973–82.

Maurya, D., and A. Menini. 2014. Developmental expression of the calcium-activated chloride channels TMEM16A and TMEM16B in the mouse olfactory epithelium. *Dev Neurobiol. in press* doi: 10.1002/dneu.22159

Patton, C., S. Thompson, and D. Epel. 2004. Some precautions in using chelators to buffer metals in biological solutions. *Cell Calcium*. 35:427–431.

Perez-Cornejo, P., and J. Arreola. 2004. Regulation of Ca^{2+}-activated chloride channels by cAMP and CFTR in parotid acinar cells. *Biochem. Biophys. Res. Commun.* 316:612–617.

Petersen, O.H. 2005. Ca^{2+} signalling and Ca^{2+}-activated ion channels in exocrine acinar cells. *Cell Calcium*. 38:171–200.

Pifferi, S., V. Cenedese, and A. Menini. 2012. Anoctamin 2/TMEM16B: a calcium-activated chloride channel in olfactory transduction. *Exp. Physiol.* 97:193–199.

Pifferi, S., M. Dibattista, and A. Menini. 2009. TMEM16B induces chloride currents activated by calcium in mammalian cells. *Pflugers Arch.* 458:1023–1038.

Pifferi, S., G. Pascarella, A. Boccaccio, A. Mazzatenta, S. Gustincich, A. Menini, and S. Zucchelli. 2006. Bestrophin-2 is a candidate calcium-activated chloride channel involved in olfactory transduction. *Proc. Natl. Acad. Sci. U.S.A.* 103:12929–12934.

Ponissery Saidu, S., A.B. Stephan, A.K.Talaga, H. Zhao, and J. Reisert. 2013. Channel properties of the splicing isoforms of the olfactory calcium-activated chloride channel Anoctamin 2. *J Gen Physiol.* 141(6):691-703.

Pusch, M. 1996. Knocking on channel's door. The permeating chloride ion acts as the gating charge in ClC-0. *J Gen Physiol*. 108:233–6.

Pusch, M., Ludewig U., Rehfeldt A. and T. Jentsch. 1995. Gating of the voltage-dependent chloride channel CLC-0 by the permeant anion. *Nature*. 373(6514):527-31..

Qu, Z., and H.C. Hartzell. 2000. Anion permeation in Ca^{2+}-activated Cl^- channels. *J. Gen. Physiol.* 116:825–844.

Rasche, S., B. Toetter, J. Adler, A. Tschapek, J.F. Doerner, S. Kurtenbach, H. Hatt, H. Meyer, B. Warscheid, and E.M. Neuhaus. 2010. Tmem16b is specifically expressed in the cilia of olfactory sensory neurons. *Chem. Senses*. 35:239–245.

Rock, J.R., and B.D. Harfe. 2008. Expression of TMEM16 paralogs during murine embryogenesis. *Dev. Dyn.* 237:2566–2574.

Sagheddu, C., A. Boccaccio, M. Dibattista, G. Montani, R. Tirindelli, and A. Menini. 2010. Calcium concentration jumps reveal dynamic ion selectivity of calcium-activated chloride currents in mouse olfactory sensory neurons and TMEM16b-transfected HEK 293T cells. *J. Physiol. (Lond.)*. 588:4189–4204.

Sanders, K.M., M.H. Zhu, F. Britton, S.D. Koh, and S.M. Ward. 2012. Anoctamins and gastrointestinal smooth muscle excitability. *Exp. Physiol.* 97:200–206.

Schroeder, B.C., T. Cheng, Y.N. Jan, and L.Y. Jan. 2008. Expression cloning of TMEM16A as a calcium-activated chloride channel subunit. *Cell*. 134:1019–1029.

Scudieri, P., E. Sondo, E. Caci, R. Ravazzolo, and L. Galietta. 2013. TMEM16A-TMEM16B chimaeras to investigate the structure-function relationship of calcium-activated chloride channels. *Biochem. J*. 452:443–55.

Scudieri, P., E. Sondo, L. Ferrera, and L.J.V. Galietta. 2012. The anoctamin family: TMEM16A and TMEM16B as calcium-activated chloride channels. *Exp. Physiol.* 97:177–183.

Smith, S.S., E.D. Steinle, M.E. Meyerhoff, and D.C. Dawson.1999. Cystic fibrosis transmembrane conductance regulator. Physical basis for lyotropic anion selectivity patterns. *J. Gen. Physiol.* 114(6):799-818.

Stephan, A.B., E.Y. Shum, S. Hirsh, K.D. Cygnar, J. Reisert, and H. Zhao. 2009. ANO2 is the cilial calcium-activated chloride channel that may mediate olfactory amplification. *Proc. Natl. Acad. Sci. U.S.A.* 106:11776–11781.

Stöhr, H., J.B. Heisig, P.M. Benz, S. Schöberl, V.M. Milenkovic, O. Strauss, W.M. Aartsen, J. Wijnholds, and H.L. Schulz. 2009. TMEM16B, a novel protein with calcium-dependent chloride channel activity, associates with a presynaptic protein complex in photoreceptor terminals. *J. Neurosci.* 29:6809–6818.

Terashima, H., A. Picollo, and A. Accardi. 2013. Purified TMEM16A is sufficient to form Ca^{2+}-activated Cl^- channels. *Proc. Natl. Acad. Sci. U.S.A.* 110:19354–9.

Wray, S., T. Burdyga, and K. Noble. 2005. Calcium signalling in smooth muscle. *Cell Calcium*. 38:397–407.

Wright, E., and J. Diamond. 1977. Anion selectivity in biological systems. *Physiol. Rev.* 57:109–56.

Xiao, Q., K. Yu, P. Perez-Cornejo, Y. Cui, J. Arreola, and H.C. Hartzell. 2011. Voltage- and calcium-dependent gating of TMEM16A/Ano1 chloride channels are physically coupled by the first intracellular loop. *Proc. Natl. Acad. Sci. U.S.A.* 108:8891–8896.

Yang, Y.D., H. Cho, J.Y. Koo, M.H. Tak, Y. Cho, W.-S. Shim, S.P. Park, J. Lee, B. Lee, B.-M. Kim, et al. 2008. TMEM16A confers receptor-activated calcium-dependent chloride conductance. *Nature*. 455:1210–1215.

Yellen, G. 1997. Single channel seeks permeant ion for brief but intimate relationship. *J Gen Physiol*. 110:83–5.

Yu, K., C. Duran, Y.Y. Cui, and H.C. Hartzell. 2012. Explaining calcium-dependent gating of anoctamin-1 chloride channels requires a revised topology. *Circ Res*. 110:990–9.

Yu, K., J. Zhu, Z. Qu, Y. Cui, and H. Hartzell. 2014. Activation of the Ano1 (TMEM16A) chloride channel by calcium is not mediated by calmodulin. *J Gen Physiol*. 143:253–67.

Zhang, Y., and P. Cremer. 2006. Interactions between macromolecules and ions: The Hofmeister series. *Curr. Opin. Chem. Biol.* 10:658–63.

FIGURE LEGENDS

Figure 1. Extracellular anion selectivity in whole cell recordings. (A) Representative whole-cell voltage-clamp recordings obtained with an intracellular solution containing 0.5 μM Ca^{2+}. Voltage steps of 200 ms duration were given from a holding voltage of 0 mV to voltages between −100 and +100 mV in 20 mV steps followed by a step to −100 mV, as indicated in the top part of the panel. Each cell was exposed to a control solution containing NaCl (black traces), NaX where X was the indicated anion, followed by wash out in NaCl (grey traces). (B) Steady state I-V relations measured at the end of the voltage steps from the cells shown at the left in control (squares), NaX (circles), or after wash out from the NaX solution (triangles). (C-D) Representative recordings from two cells at 0.5 μM Ca^{2+} obtained with a voltage protocol consisting of a prepulse to +100 mV from a holding voltage of 0 mV, followed by voltage steps between (C) -60 mV and +70 mV, or (D) -60 mV to +20 mV in 10 mV steps. Only current recordings every 20 mV are shown in C. I-V relations measured from tail currents in Cl^- (squares) or in the indicated anion (circles) are shown on the right of each cell. (E) Average permeability ratios (P_X/P_{Cl}) calculated with the Goldman-Hodgkin-Katz equation (n = 11-14). (F) Average chord conductance ratios (G_X/G_{Cl}) measured in a 40 mV interval around V_{rev} per each anion (n = 4-14).

Figure 2. Anion selectivity in inside-out patches. (A) Current-voltage relations in 1.5 μM Ca^{2+} obtained from a ramp protocol in inside-out membrane patches. In each patch, the pipette solution contained 140 mM NaCl or the Na salt of the indicated anion. Leakage currents measured in 0 Ca^{2+} were substracted. (B) Comparison of average permeability ratios (P_X/P_{Cl})

calculated with the Goldman-Hodgkin-Katz equation with different anions in the internal (*n* = 5-6, data for intracellular I^-, NO_3^-, Br^- are from Pifferi et al., 2009) or external solution (*n* = 6-12, as experiments shown in panel A). (C-D) Permeability ratios (P_X/P_{Cl}), obtained from experiments as in panel A, plotted versus ionic radius (C) or free energy of hydration (D) of the extracellular anion. Ionic radius and free energy of hydration were taken from Table I of Smith et al. (1999)

Figure 3. Activation and deactivation kinetics in whole-cell with various extracellular anions. **(**A-B) Normalized single traces from whole-cell currents in the presence of extracellular NaCl or the Na salt of the indicated anion in 0.5 μM Ca^{2+}. Voltage protocol similar to Fig. 1 C-D, with a voltage step to +100 mV (A) from a holding voltage of 0 mV and followed by a step to −60 mV (B). Trace in gluconate in panel A is not shown because at the test potential there is a negligible time dependent component. (C) Current activation and deactivation were fitted with a single exponential (fit not shown for clarity). Average activation time constants (τ_{act}) at +100 mV, and deactivation time constants (τ_{deact}) at -60 mV, plotted versus permeability ratios (*n* = 8-14, * $p<0.05$; ** $p<0.01$, paired t-test with Cl^-).

Figure 4. Changes of voltage-dependence in whole-cell when extracellular Cl^- was substituted with less permeant gluconate or sucrose. **(**A) Representative whole-cell voltage-clamp recordings at 1.5 μM Ca^{2+}. The same cell was exposed to a solution containing NaCl (black traces), Na-gluconate (green and blue traces), and back to NaCl (grey traces). Voltage steps of 200 ms duration were given from a holding voltage of 0 mV to voltages between −200 and +200 mV in 40 mV steps followed by a step to −100 mV. (B) Steady state I-V relations measured at the end of the voltage steps from the cell shown at the left normalized to the control value at +200 mV.

Control values are represented by black filled squares, wash out by grey empty triangles, 11 mM and 1 mM Cl^- respectively by the green and blue filled circles. (C) Normalized conductances calculated from tail currents at -100 mV after prepulses between -200 mV and +200 mV plotted versus the prepulse voltage for the experiment shown in A. Symbols as in (B). Lines are the fit to the Boltzmann equation (eq. 1). (D-E) Average $V_{1/2}$ values in the presence of gluconate (D; n = 10), or sucrose (E; n = 3) at the indicated $[Cl^-]_o$ (** $p<0.01$, Tukey's test after ANOVA for repeated measurements).

Figure 5. Changes of voltage-dependence in whole-cell when extracellular Cl^- was substituted with more permeant anions. (A, D, G) Representative whole-cell voltage-clamp recordings at the indicated $[Ca^{2+}]_i$. The same cell was exposed to a solution containing NaCl (black traces), NaSCN (red traces), and back to NaCl (grey traces). Voltage steps of 200 ms duration were given from a holding voltage of 0 mV to voltages between −200 and +200 mV in 40 mV steps followed by a step to −100 mV, as indicated in the top part of panel A. (B, E, H) Steady state I-V relations measured at the end of the voltage steps from the cell shown at the left in control (squares), NaSCN (circles), and after wash out (triangles). (C, F) Normalized conductances calculated from tail currents at -100 mV after prepulses between -200 mV and +200 mV plotted versus the prepulse voltage. Symbols as in (B, E). Lines are the fit to the Boltzmann equation (eq. 1). (I) Average $V_{1/2}$ values at 0.5 μM Ca^{2+} (n = 4) or 1.5 μM Ca^{2+} (n = 9 in Cl^-, 6 in NO_3^-) for Cl^-, SCN^-, or NO_3^- (** $p<0.01$ paired t test).

Figure 6. Ca^{2+} sensitivity in inside-out patches with various extracellular anions. (A) Each row shows current traces from the same inside-out patch with the indicated anion in the pipette. The cytoplasmic side was exposed to $[Ca^{2+}]_i$ ranging from 0.18 μM to 1 mM. Voltage steps of 200 ms duration were given from a holding voltage of 0 mV to +100 mV followed by a 200 ms step to −100 mV. Leakage currents measured in 0 Ca^{2+} were subtracted. (B) Dose–response relations of activation by Ca^{2+} obtained by normalized currents at -100 or +100 mV, fitted to the Hill equation (eq. 2). Black lines are the fit to the Hill equation in external Cl^-. (C) Comparison of the average $K_{1/2}$ values at -100 mV or +100 mV in the presence of various anions (n = 5-13, ** $p<0.01$ comparison with Cl^- by Tukey's test after ANOVA). (D) Comparison of the average n_H values at -100 mV or +100 mV in the presence of various anions (n = 5-13, ** $p<0.01$ comparison with Cl^- by Tukey's test after ANOVA). (E) Average $K_{1/2}$ values at +100 mV plotted versus permeability ratios.

Figure 7. Comparison of Ca^{2+} sensitivity in whole-cell and inside-out patches. (A) Whole-cell recordings obtained with various $[Ca^{2+}]_i$ in extracellular Cl^- or SCN^-. Same cell were recorded in Cl^- or SCN^- for each $[Ca^{2+}]_i$. Voltage protocol as in Fig. 1 A. (B) Comparison of dose-responses in Cl^- or SCN^- at -100 and +100 mV in whole-cell obtained from conductance density calculated from tail currents plotted versus $[Ca^{2+}]_i$ (n = 3–5). Lines are the fit to the Hill equation (eq. 3). (C-D) Average $K_{1/2}$ and n_H values from whole-cell recordings plotted versus voltage. (E-F) Currents in an inside-out patch activated by voltage ramps at the indicated $[Ca^{2+}]_i$ in symmetrical Cl^- (E) or in extracellular SCN^- (F). Leakage currents measured in 0 Ca^{2+} were subtracted. (G) Comparison of dose-responses in Cl^- or SCN^- obtained by normalized currents at -100 or +100 mV, fitted to the Hill equation (eq. 2). (H-I) Average $K_{1/2}$ and n_H values from inside-out patch

recordings plotted versus voltage (n = 6-7).

Figure 8. Effect of intracellular SCN^-. (A) Whole-cell recordings at 0.5 μM Ca^{2+} with a standard intracellular solution containing Cl^- (same traces of Fig. 5 A) or SCN^-. Voltage steps as in Fig. 5. (B) Normalized conductances calculated from tail currents at -100 mV after prepulses between -200 mV and +200 mV plotted versus the prepulse voltage for the experiments shown in A. Lines are the fit to the Boltzmann equation (eq. 1). (C) Average $V_{1/2}$ values in the presence of Cl^- (n = 4, same data of Fig. 5 I) or SCN^- (n = 11, ** $p<0.01$ unpaired t-test). (D) Traces from an inside-out patch with SCN^- at the intracellular side. $[Ca^{2+}]_i$ ranged from 0.18 μM to 100 μM. Voltage steps of 200 ms duration were given from a holding voltage of 0 mV to +100 mV followed by a 200 ms step to −100 mV. Leakage currents measured in 0 Ca^{2+} were subtracted. (E) Dose–response relations of activation by Ca^{2+} obtained by normalized currents at -100 or +100 mV (n = 11), fitted to the Hill equation (eq. 2). Black lines are the fit to the Hill equation in symmetrical Cl^- solutions.

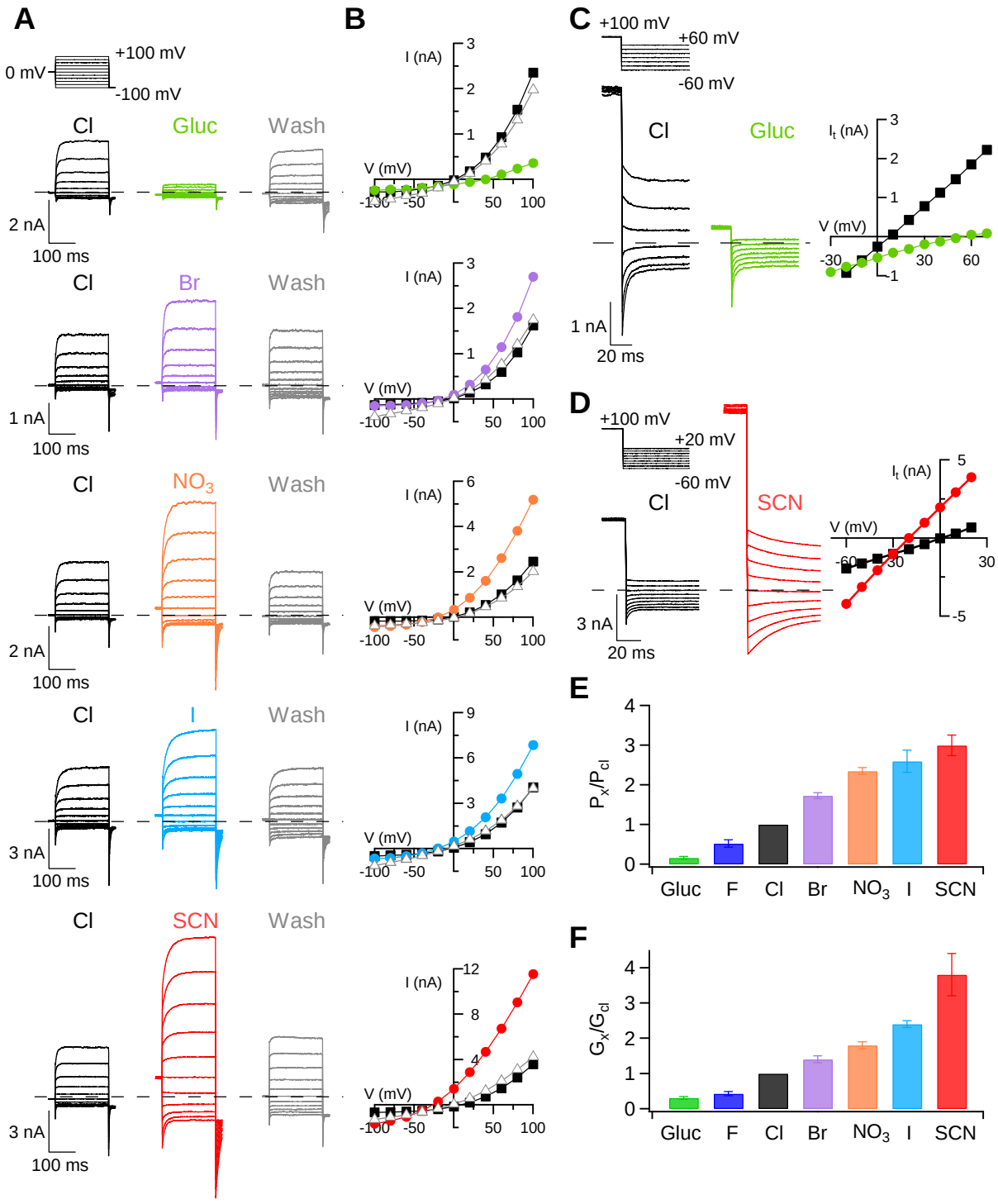
A
0 mV
+100 mV
-100 mV
Cl
Gluc
Wash
2 nA
100 ms
Br
1 nA
NO3
I
3 nA
SCN
B
I (nA)
V (mV)
C
+60 mV
-60 mV
It (nA)
D
+20 mV
E
Px/Pcl
Gluc
F
Cl
Br
NO3
I
SCN
F
Gx/Gcl

Figure 1

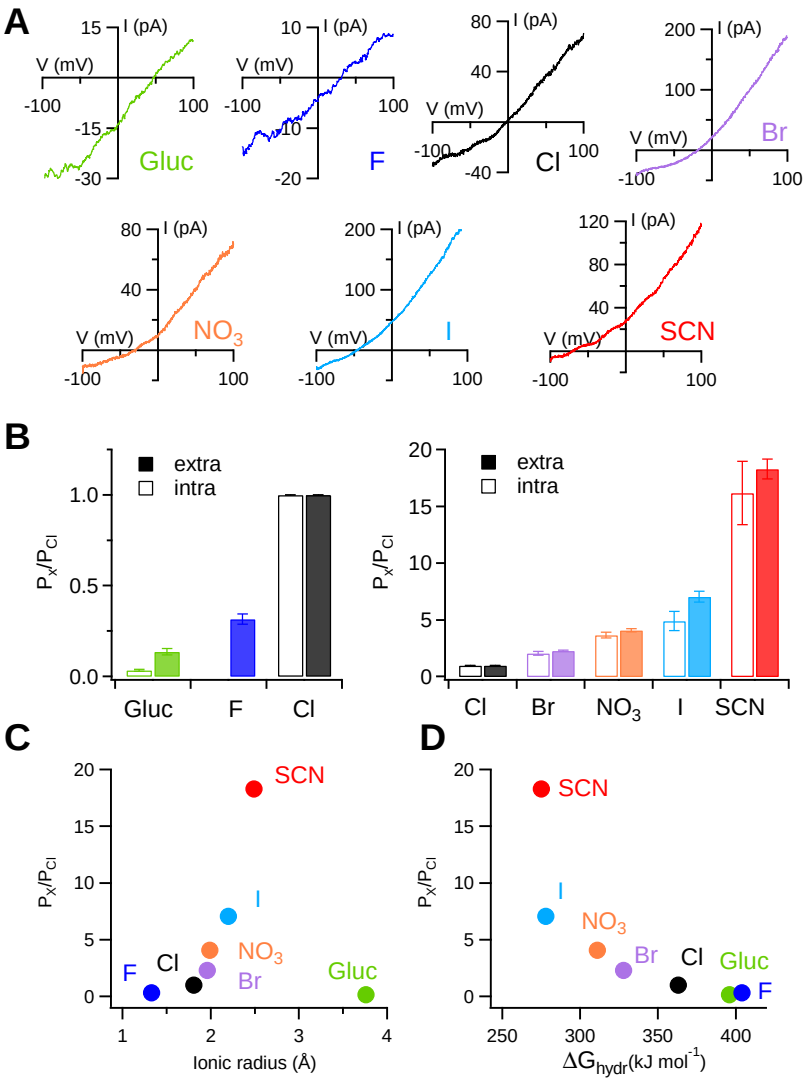
A
I (pA)
V (mV)
Gluc
F
Cl
Br
NO3
I
SCN
B
extra
intra
PX/PCl
Gluc
F
Cl
Br
NO3
I
SCN
C
Ionic radius (Å)
D
ΔGhydr(kJ mol-1)

Figure 2

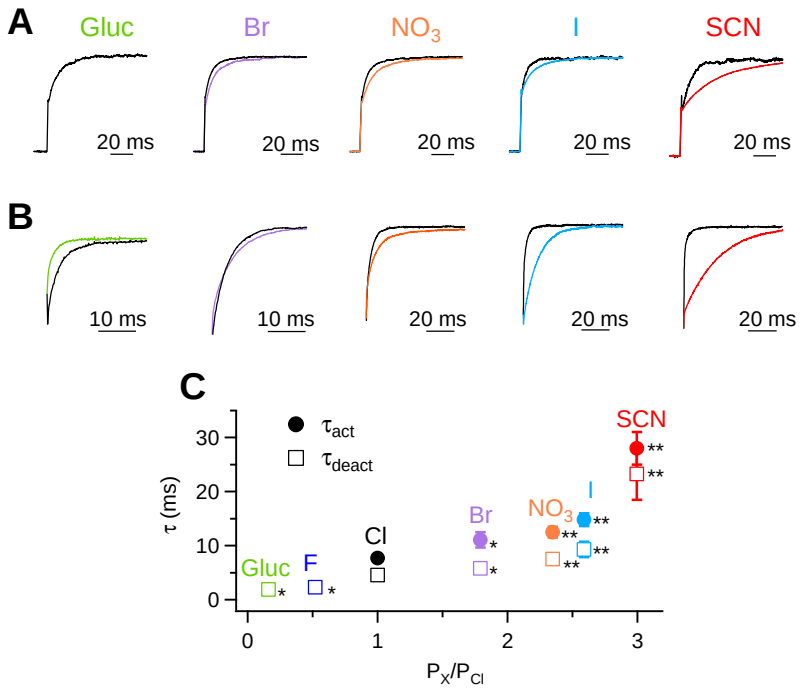
A
Gluc
Br
NO3
I
SCN
20 ms
20 ms
20 ms
20 ms
20 ms
B
10 ms
10 ms
20 ms
20 ms
20 ms
C
τact
τdeact
τ (ms)
30
20
10
0
0
1
2
3
PX/PCl
Gluc
F
Cl
Br
NO3
I
SCN
*
**

Figure 3

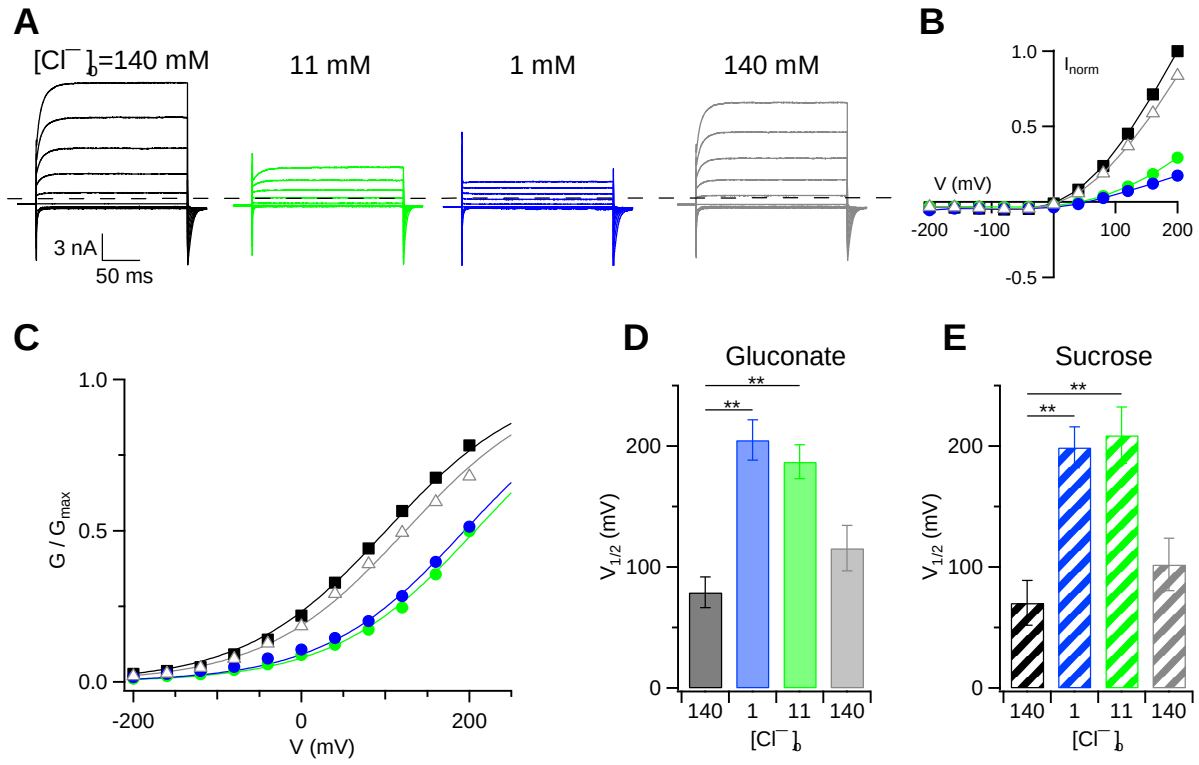
A
[Cl⁻]b=140 mM
11 mM
1 mM
140 mM
3 nA
50 ms
B
1.0
0.5
-0.5
Inorm
V (mV)
-200
-100
100
200
C
1.0
0.5
0.0
G / Gmax
-200
0
200
V (mV)
D
Gluconate
**
**
200
100
0
V1/2 (mV)
140
1
11
140
[Cl⁻]b
E
Sucrose
**
**
200
100
0
V1/2 (mV)
140
1
11
140
[Cl⁻]b

Figure 4

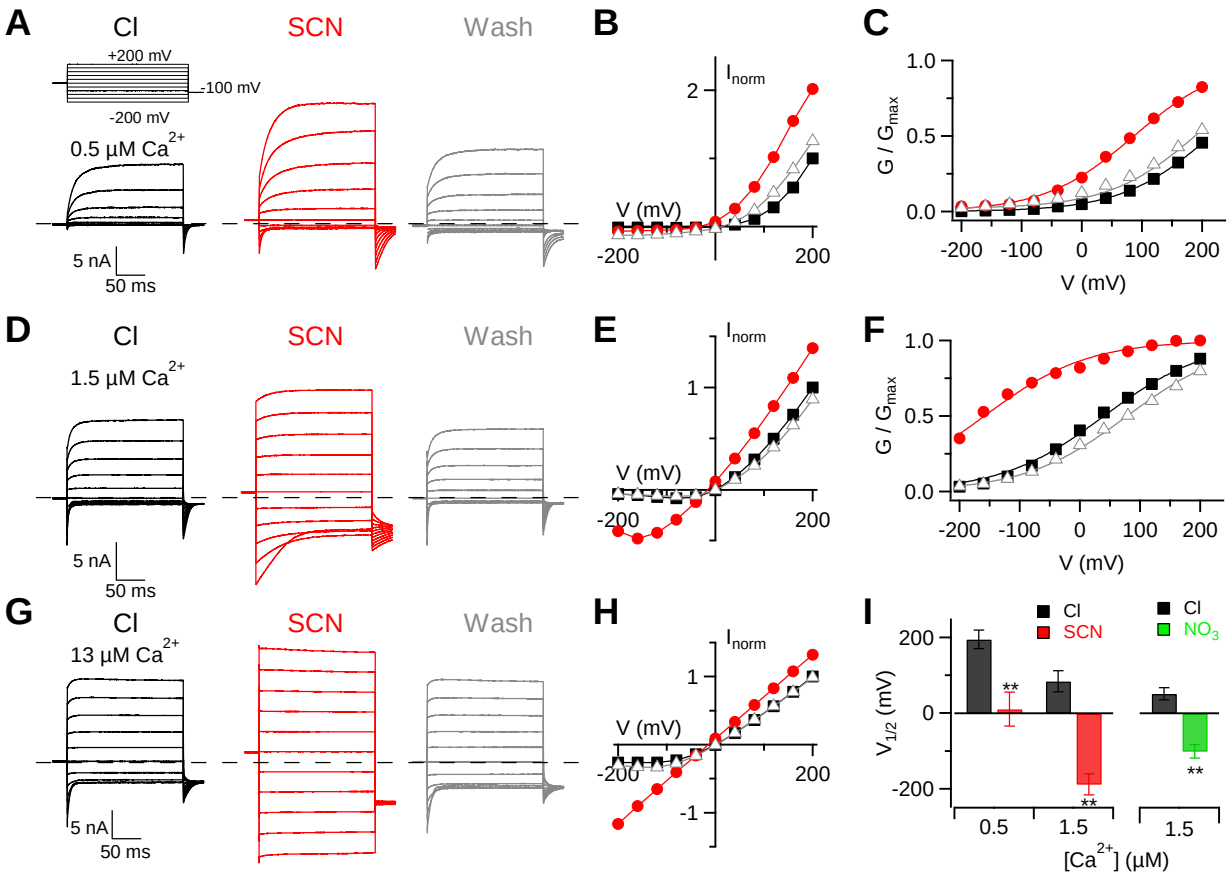
A
Cl
SCN
Wash
+200 mV
-100 mV
-200 mV
0.5 µM Ca2+
5 nA
50 ms
B
Inorm
2
V (mV)
-200
200
C
G / Gmax
1.0
0.5
0.0
-200 -100 0 100 200
V (mV)
D
Cl
SCN
Wash
1.5 µM Ca2+
5 nA
50 ms
E
Inorm
1
V (mV)
-200
200
F
G / Gmax
1.0
0.5
0.0
-200 -100 0 100 200
V (mV)
G
Cl
SCN
Wash
13 µM Ca2+
5 nA
50 ms
H
Inorm
1
V (mV)
-200
200
-1
I
Cl
SCN
Cl
NO3
200
0
-200
V1/2 (mV)
**
**
**
0.5
1.5
1.5
[Ca2+] (µM)

Figure 5

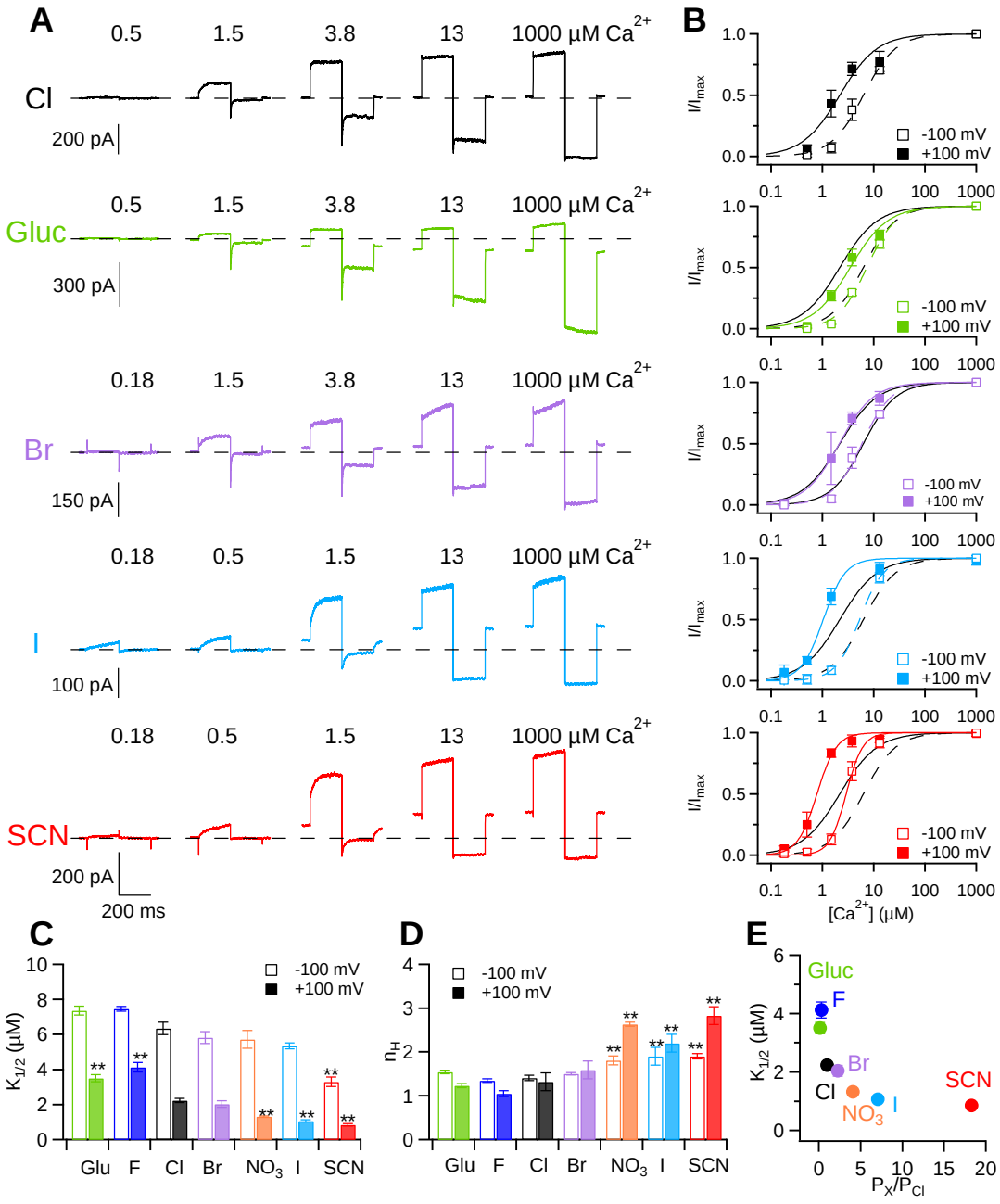
A
0.5
1.5
3.8
13
1000 µM Ca2+
Cl
200 pA
Gluc
300 pA
0.18
Br
150 pA
I
100 pA
SCN
200 pA
200 ms
B
I/Imax
-100 mV
+100 mV
[Ca2+] (µM)
C
K1/2 (µM)
Glu
F
Cl
Br
NO3
I
SCN
D
nH
E
PX/PCl

Figure 6

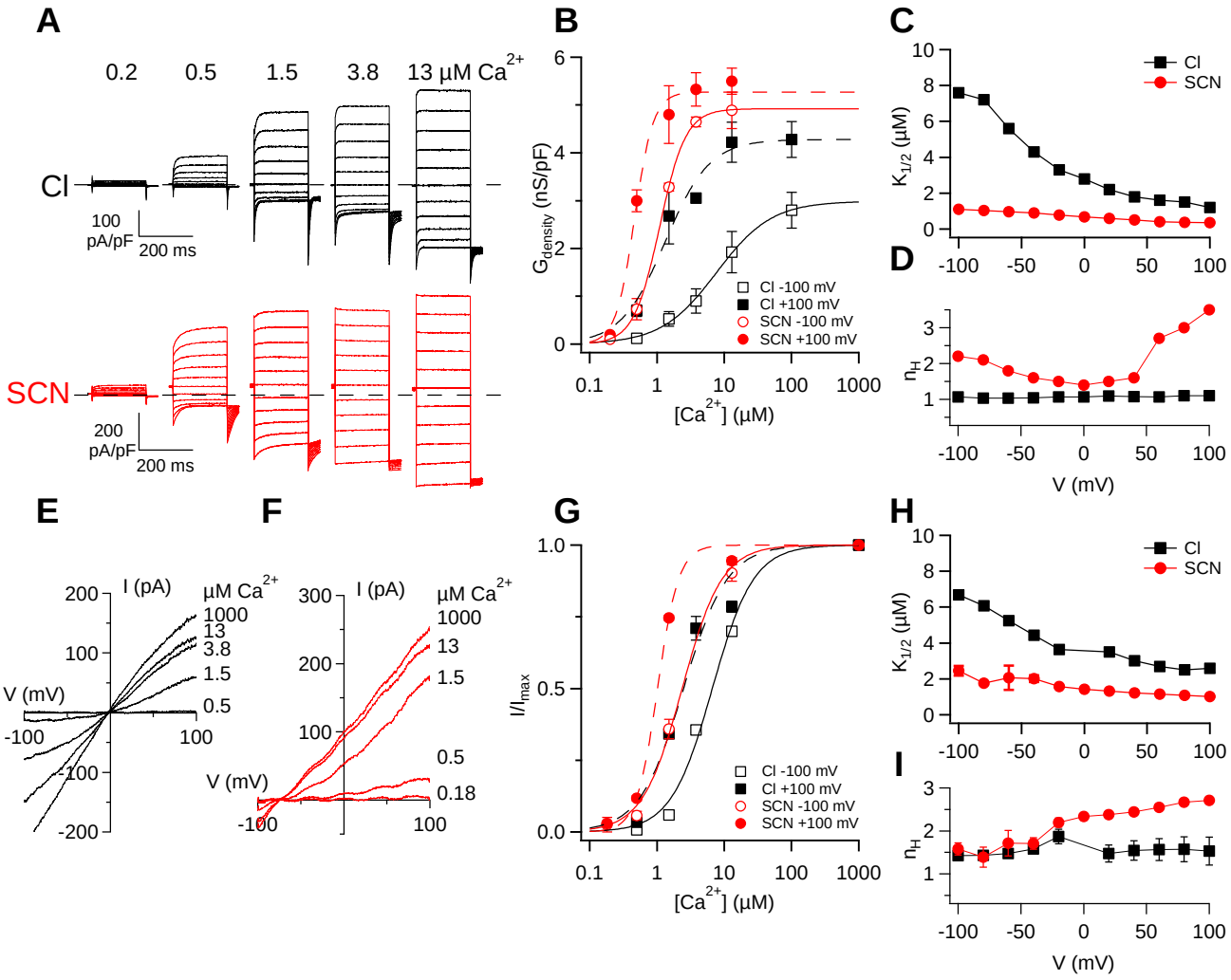
A
0.2
0.5
1.5
3.8
13 µM Ca2+
Cl
100 pA/pF
200 ms
SCN
200 pA/pF
200 ms
B
Gdensity (nS/pF)
Cl -100 mV
Cl +100 mV
SCN -100 mV
SCN +100 mV
[Ca2+] (µM)
C
K1/2 (µM)
Cl
SCN
D
nH
V (mV)
E
I (pA)
µM Ca2+
1000
13
3.8
1.5
0.5
V (mV)
F
I (pA)
µM Ca2+
1000
13
1.5
0.5
0.18
V (mV)
G
I/Imax
Cl -100 mV
Cl +100 mV
SCN -100 mV
SCN +100 mV
[Ca2+] (µM)
H
K1/2 (µM)
Cl
SCN
I
nH
V (mV)

Figure 7

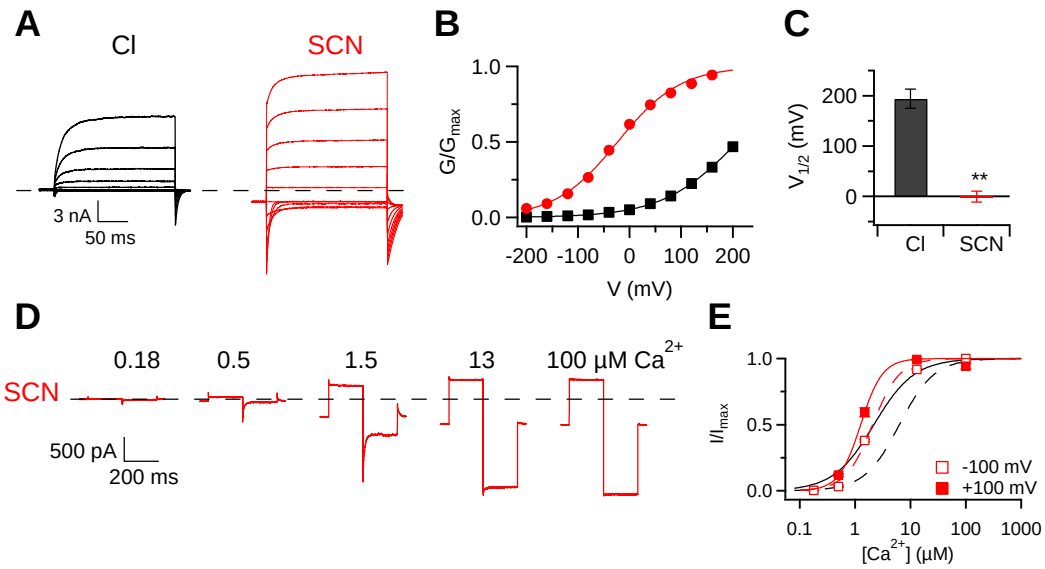
A
Cl
SCN
3 nA
50 ms
B
1.0
0.5
0.0
G/Gmax
-200 -100 0 100 200
V (mV)
C
200
100
0
V1/2 (mV)
**
Cl
SCN
D
0.18
0.5
1.5
13
100 µM Ca2+
SCN
500 pA
200 ms
E
1.0
0.5
0.0
I/Imax
-100 mV
+100 mV
0.1 1 10 100 1000
[Ca2+] (µM)

Figure 8

5. DISCUSSION

The molecular mechanisms underlying TMEM16A and TMEM16B gating by Ca^{2+} and membrane potential remain an open question. TMEM16A and TMEM16B channels share 60% of aminoacid identity (Yang et al., 2008). By alignment between their sequences, we identified a series of acidic amino acids in the first intracellular loop ($_{367}E_{386}$, $_{386}EEEEE_{390}$ and $_{399}EYE_{401}$) that are highly conserved. We thought that these aminoacids could be good candidates to play a role in channel gating.

We found that deletion of the five consecutive glutamates, ΔE_5, did not change the apparent Ca^{2+} affinity of the channel but it shifted the activation curve to more positive voltages. In particular, $V_{1/2}$ at 1.5 μM Ca^{2+} changed from 124 mV in wild type to 248 mV in ΔE_5. Our results are in agreement with the work of Xiao et al. (2011), who showed that the substitution of the four glutamates into alanines ($_{444}EEEE/AAAA_{447}$) in TMEM16A did not greatly affect the apparent affinity for Ca^{2+} but modified the voltage dependence, producing a shift in the activation curve to the right (Xiao et al., 2011). The second mutant we have studied is E367Q. In this case, both activation and deactivation kinetics were faster than in wild type, the activation curve was shifted to more positive voltages, while the dose-response relation for Ca^{2+} was not affected.

Finally, we studied the deletion ΔEYE. This deletion produced an increase in the time constants for activation and deactivation, while it did not cause any large change in apparent affinity for Ca^{2+} or in voltage dependence.

Differently from what Xiao et al. (2011) reported on TMEM16A, we found that TMEM16B is not activated in the absence of Ca^{2+}.

Previous observations showed that the gating of CaCCs in *Xenopus* oocytes and salivary glands are affected by permeant anions (Perez-Cornejo and Arreola, 2004; Qu and Hartzell, 2000). Xiao et al. (2011), showed the effect of some permeant anion on TMEM16A obtained using whole cell recording from HEK293 cell expressing the TMEM16A (*ac*) isoform and showed that the

replacements of Cl^- with NO_3^- or SCN^- shifted the conductance-voltage relation to more negative voltages. Ferrera et al. (2011), demonstrated that TMEM16A (*abc*) stably expressed in Fisher rat thyroid showed an increase or decrease in conductance when extracellular Cl^- was replaced with more o less permeant anions, respectively. They also reported that there were differences in selectivity between the isoform (*0*): P_I/P_{Cl} increased from 3.6 for the isoform (*abc*) to 4.7 for TMEM16A (*0*) and P_{SCN}/P_{Cl} increased from 3.4 (*abc*) to 5.6 (*0*).

We performed, for the first time, experiments to test the influence of permeant anions on the gating of TMEM16B.

We found that permeant anions affected the voltage dependence and the apparent Ca^{2+} affinity but not the voltage sensitivity of the channel. The substitution of Cl^- with the more permeant anion SCN^- both at the extracellular and intracellular side of the membrane produced a shift in the activation curve toward more negative values, an increase of the apparent Ca^{2+} affinity and a reduction in the voltage dependence of the apparent Ca^{2+} affinity and a small increase of the Hill coefficient at positive voltages. These results could suggest that anions more permeant than Cl^- can bind with higher affinity than Cl^- to an allosteric binding site that may control the gate of the channel. Moreover, anions more permeant than Cl^- slowed both activation and deactivation constants at 0.5 μM Ca^{2+}.

We can conclude that the gating of TMEM16B, as well as TMEM16A, is controlled by a complex interplay among $[Ca^{2+}]_i$, membrane potential and permeant anions.

6. BIBLIOGRAPHY

Adomaviciene, A., K. Smith, H. Garnett, and P. Tammaro. 2013. Putative pore-loops of TMEM16/anoctamin channels affect channel density in cell membranes. *J Physiol*. 591:487–505.

Almaça, J., Y. Tian, F. Aldehni, J. Ousingsawat, P. Kongsuphol, J.R. Rock, B.D. Harfe, R. Schreiber, and K. Kunzelmann. 2009. TMEM16 proteins produce volume-regulated chloride currents that are reduced in mice lacking TMEM16A. *J. Biol. Chem.* 284:28571–28578.

Arreola, J., J.E. Melvin, and T. Begenisich. 1996. Activation of calcium-dependent chloride channels in rat parotid acinar cells. *J. Gen. Physiol.* 108:35–47.

Barish, M.E. 1983. A transient calcium-dependent chloride current in the immature Xenopus oocyte. *J. Physiol. (Lond.)*. 342:309–325.

Billig, G.M., B. Pál, P. Fidzinski, and T.J. Jentsch. 2011. Ca2+-activated Cl− currents are dispensable for olfaction. *Nat. Neurosci.* 14:763–769.

Boccaccio, A., and A. Menini. 2007. Temporal development of cyclic nucleotide-gated and Ca2+ -activated Cl- currents in isolated mouse olfactory sensory neurons. *J. Neurophysiol.* 98:153–160.

Caputo, A., E. Caci, L. Ferrera, N. Pedemonte, C. Barsanti, E. Sondo, U. Pfeffer, R. Ravazzolo, O. Zegarra-Moran, and L.J.V. Galietta. 2008. TMEM16A, a membrane protein associated with calcium-dependent chloride channel activity. *Science*. 322:590–594.

De Castro, F., E. Geijo-Barrientos, and R. Gallego. 1997. Calcium-activated chloride current in normal mouse sympathetic ganglion cells. *J. Physiol. (Lond.)*. 498 (Pt 2):397–408.

Chung, M.-K., A.D. Güler, and M.J. Caterina. 2008. TRPV1 shows dynamic ionic selectivity during agonist stimulation. *Nat. Neurosci.* 11:555–564.

Dauner, K., J. Lissmann, S. Jeridi, and F. Möhrlen. 2012. Expression patterns of anoctamin 1 and anoctamin 2 chloride channels in the mammalian nose. *Cell Tissue Res*. 347:327–41.

Dauner, K., C. Möbus, S. Fring, and F. Möhrlen. 2013. Targeted expression of anoctamin calcium-activated chloride channels in rod photoreceptor terminals of the rodent retina. *Invest. Ophthalmol. Vis. Sci.* 54:3126–36.

Dibattista, M., A. Amjad, D.K. Maurya, C. Sagheddu, G. Montani, R. Tirindelli, and A. Menini. 2012. Calcium-activated chloride channels in the apical region of mouse vomeronasal sensory neurons. *J. Gen. Physiol.* 140:3–15.

Duran, C., and H.C. Hartzell. 2011. Physiological roles and diseases of Tmem16/Anoctamin proteins: are they all chloride channels? *Acta Pharmacol. Sin.* 32:685–692.

Espinosa, I., C.-H. Lee, M.K. Kim, B.-T. Rouse, S. Subramanian, K. Montgomery, S. Varma, C.L. Corless, M.C. Heinrich, K.S. Smith, et al. 2008. A novel monoclonal antibody against DOG1 is a sensitive and specific marker for gastrointestinal stromal tumors. *Am. J. Surg. Pathol.* 32:210–218.

Fallah, G., T. Römer, S. Detro-Dassen, U. Braam, F. Markwardt, and G. Schmalzing. 2011. TMEM16A(a)/anoctamin-1 shares a homodimeric architecture with CLC chloride channels. *Mol. Cell Proteomics*. 10:M110.004697.

Ferrera, L., A. Caputo, and L.J.V. Galietta. 2010. TMEM16A protein: a new identity for Ca(2+)-dependent Cl^- channels. *Physiology (Bethesda)*. 25:357–363.

Ferrera, L., A. Caputo, I. Ubby, E. Bussani, O. Zegarra-Moran, R. Ravazzolo, F. Pagani, and L.J.V. Galietta. 2009. Regulation of TMEM16A chloride channel properties by alternative splicing. *J. Biol. Chem.* 284:33360–33368.

Ferrera, L., P. Scudieri, E. Sondo, A. Caputo, E. Caci, O. Zegarra-Moran, R. Ravazzolo, and L.J.V. Galietta. 2011. A minimal isoform of the TMEM16A protein associated with chloride channel activity. *Biochim. Biophys. Acta*. 1808:2214–2223.

Flores, C.A., L.P. Cid, F.V. Sepúlveda, and M.I. Niemeyer. 2009. TMEM16 proteins: the long awaited calcium-activated chloride channels? *Braz. J. Med. Biol. Res.* 42:993–1001.

Frings, S., D. Reuter, and S.J. Kleene. 2000. Neuronal Ca2+ -activated Cl- channels--homing in on an elusive channel species. *Prog. Neurobiol.* 60:247–289.

Galietta, L.J.V. 2009. The TMEM16 protein family: a new class of chloride channels? *Biophys. J.* 97:3047–3053.

Galindo, B.E., and V.D. Vacquier. 2005. Phylogeny of the TMEM16 protein family: some members are overexpressed in cancer. *Int. J. Mol. Med.* 16:919–924.

Greenwood, I.A., and W.A. Large. 1999. Modulation of the decay of Ca2+-activated Cl- currents in rabbit portal vein smooth muscle cells by external anions. *J. Physiol. (Lond.)*. 516 (Pt 2):365–376.

Grubb, S., K. Poulsen, C. Juul, T. Kyed, T. Klausen, E. Larsen, and E. Hoffmann. 2013. TMEM16F (Anoctamin 6), an anion channel of delayed Ca(2+) activation. *J Gen Physiol*. 141:585–600.

Hartzell, C., I. Putzier, and J. Arreola. 2005. Calcium-activated chloride channels. *Annu. Rev. Physiol.* 67:719–758.

Hartzell, H.C., K. Yu, Q. Xiao, L.-T. Chien, and Z. Qu. 2009. Anoctamin/TMEM16 family members are Ca2+-activated Cl- channels. *J. Physiol. (Lond.)*. 587:2127–2139.

Hengl, T., H. Kaneko, K. Dauner, K. Vocke, S. Frings, and F. Möhrlen. 2010. Molecular components of signal amplification in olfactory sensory cilia. *Proc. Natl. Acad. Sci. U.S.A.* 107:6052–6057.

Herness, M.S., and X.D. Sun. 1999. Characterization of chloride currents and their noradrenergic modulation in rat taste receptor cells. *J. Neurophysiol.* 82:260–271.

Huang, W., S. Xiao, F. Huang, B. Harfe, Y. Jan, and L. Jan. 2012. Calcium-activated chloride channels (CaCCs) regulate action potential and synaptic response in hippocampal neurons. *Neuron*. 74:179–92.

Huang, X., T.E. Godfrey, W.E. Gooding, K.S. McCarty Jr, and S.M. Gollin. 2006. Comprehensive genome and transcriptome analysis of the 11q13 amplicon in human oral cancer and synteny to the 7F5 amplicon in murine oral carcinoma. *Genes Chromosomes Cancer*. 45:1058–1069.

Jentsch, T.J. 2002. Chloride channels are different. *Nature*. 415:276–277.

Kashyap, M.K., A. Marimuthu, C.J.H. Kishore, S. Peri, S. Keerthikumar, T.S.K. Prasad, R. Mahmood, S. Rao, P. Ranganathan, R.C. Sanjeeviah, et al. 2009. Genomewide mRNA profiling of esophageal squamous cell carcinoma for identification of cancer biomarkers. *Cancer Biol. Ther.* 8:36–46.

Katoh, M., and M. Katoh. 2003. FLJ10261 gene, located within the CCND1-EMS1 locus on human chromosome 11q13, encodes the eight-transmembrane protein homologous to C12orf3, C11orf25 and FLJ34272 gene products. *Int. J. Oncol.* 22:1375–1381.

Khakh, B.S., and H.A. Lester. 1999. Dynamic selectivity filters in ion channels. *Neuron*. 23:653–658.

Kidd, J.F., and P. Thorn. 2000. Intracellular Ca2+ and Cl- channel activation in secretory cells. *Annu. Rev. Physiol.* 62:493–513.

Kleene, S.J. 1993. Origin of the chloride current in olfactory transduction. *Neuron*. 11:123–132.

Kleene, S.J. 2008. The electrochemical basis of odor transduction in vertebrate olfactory cilia. *Chem. Senses*. 33:839–859.

Kleene, S.J., and R.C. Gesteland. 1991. Calcium-activated chloride conductance in frog olfactory cilia. *J. Neurosci.* 11:3624–3629.

Kunzelmann, K., P. Kongsuphol, F. Aldehni, Y. Tian, J. Ousingsawat, R. Warth, and R. Schreiber. 2009. Bestrophin and TMEM16-Ca(2+) activated Cl(-) channels with different functions. *Cell Calcium*. 46:233–241.

Kunzelmann, K., P. Kongsuphol, K. Chootip, C. Toledo, J.R. Martins, J. Almaca, Y. Tian, R. Witzgall, J. Ousingsawat, and R. Schreiber. 2011. Role of the Ca2+ -activated Cl- channels bestrophin and anoctamin in epithelial cells. *Biol. Chem.* 392:125–134.

Kurahashi, T., and K.W. Yau. 1994. Olfactory transduction. Tale of an unusual chloride current. *Curr. Biol.* 4:256–258.

Kuruma, A., and H.C. Hartzell. 2000. Bimodal control of a Ca(2+)-activated Cl(-) channel by different Ca(2+) signals. *J. Gen. Physiol.* 115:59–80.

Lalonde, M.R., M.E. Kelly, and S. Barnes. 2008. Calcium-activated chloride channels in the retina. *Channels (Austin)*. 2:252–260.

Large, W.A., and Q. Wang. 1996. Characteristics and physiological role of the Ca(2+)-activated Cl- conductance in smooth muscle. *Am. J. Physiol.* 271:C435–454.

Leblanc, N., J. Ledoux, S. Saleh, A. Sanguinetti, J. Angermann, K. O'Driscoll, F. Britton, B.A. Perrino, and I.A. Greenwood. 2005. Regulation of calcium-activated chloride channels in smooth muscle cells: a complex picture is emerging. *Can. J. Physiol. Pharmacol.* 83:541–556.

Maurya, D., and A. Menini. 2013. Developmental expression of the calcium-activated chloride channels TMEM16A and TMEM16B in the mouse olfactory epithelium. *Dev Neurobiol.*

Melvin, J.E., D. Yule, T. Shuttleworth, and T. Begenisich. 2005. Regulation of fluid and electrolyte secretion in salivary gland acinar cells. *Annu. Rev. Physiol.* 67:445–469.

Miledi, R. 1982. A calcium-dependent transient outward current in Xenopus laevis oocytes. *Proc. R. Soc. Lond., B, Biol. Sci.* 215:491–497.

Nilius, B., J. Prenen, T. Voets, K. Van den Bremt, J. Eggermont, and G. Droogmans. 1997. Kinetic and pharmacological properties of the calcium-activated chloride-current in macrovascular endothelial cells. *Cell Calcium*. 22:53–63.

Patton, C., S. Thompson, and D. Epel. 2004. Some precautions in using chelators to buffer metals in biological solutions. *Cell Calcium*. 35:427–431.

Perez-Cornejo, P., and J. Arreola. 2004. Regulation of Ca(2+)-activated chloride channels by cAMP and CFTR in parotid acinar cells. *Biochem. Biophys. Res. Commun.* 316:612–617.

Pifferi, S., V. Cenedese, and A. Menini. 2012. Anoctamin 2/TMEM16B: a calcium-activated chloride channel in olfactory transduction. *Exp. Physiol.* 97:193–199.

Pifferi, S., M. Dibattista, and A. Menini. 2009. TMEM16B induces chloride currents activated by calcium in mammalian cells. *Pflugers Arch.* 458:1023–1038.

Ponissery Saidu, S., A. Stephan, A. Talaga, H. Zhao, and J. Reisert. 2013. Channel properties of the splicing isoforms of the olfactory calcium-activated chloride channel Anoctamin 2. *J Gen Physiol*. 141:691–703.

Qu, Z., and H.C. Hartzell. 2000. Anion permeation in Ca(2+)-activated Cl(-) channels. *J. Gen. Physiol.* 116:825–844.

Qu, Z., and H.C. Hartzell. 2001. Functional geometry of the permeation pathway of Ca2+-activated Cl-channels inferred from analysis of voltage-dependent block. *J. Biol. Chem.* 276:18423–18429.

Qu, Z., R. Wei, and H. Hartzell. 2003. Characterization of Ca2+-activated Cl- currents in mouse kidney inner medullary collecting duct cells. *Am J Physiol Renal Physiol*. 285:326–35.

Rasche, S., B. Toetter, J. Adler, A. Tschapek, J.F. Doerner, S. Kurtenbach, H. Hatt, H. Meyer, B. Warscheid, and E.M. Neuhaus. 2010. Tmem16b is specifically expressed in the cilia of olfactory sensory neurons. *Chem. Senses*. 35:239–245.

Reisert, J., P.J. Bauer, K.-W. Yau, and S. Frings. 2003. The Ca-activated Cl channel and its control in rat olfactory receptor neurons. *J. Gen. Physiol.* 122:349–363.

Rock, J.R., and B.D. Harfe. 2008. Expression of TMEM16 paralogs during murine embryogenesis. *Dev. Dyn.* 237:2566–2574.

Romanenko, V.G., M.A. Catalán, D.A. Brown, I. Putzier, H.C. Hartzell, A.D. Marmorstein, M. Gonzalez-Begne, J.R. Rock, B.D. Harfe, and J.E. Melvin. 2010. Tmem16A encodes the Ca2+-activated Cl- channel in mouse submandibular salivary gland acinar cells. *J. Biol. Chem.* 285:12990–13001.

Sagheddu, C., A. Boccaccio, M. Dibattista, G. Montani, R. Tirindelli, and A. Menini. 2010. Calcium concentration jumps reveal dynamic ion selectivity of calcium-activated chloride currents in mouse olfactory sensory neurons and TMEM16b-transfected HEK 293T cells. *J. Physiol. (Lond.)*. 588:4189–4204.

Sanders, K.M., M.H. Zhu, F. Britton, S.D. Koh, and S.M. Ward. 2012. Anoctamins and gastrointestinal smooth muscle excitability. *Exp. Physiol.* 97:200–206.

Schild, D., and D. Restrepo. 1998. Transduction mechanisms in vertebrate olfactory receptor cells. *Physiol. Rev.* 78:429–466.

Schreiber, M., and L. Salkoff. 1997. A novel calcium-sensing domain in the BK channel. *Biophys. J.* 73:1355–1363.

Schreiber, R., I. uliyakina, P. Kongsuphol, R. Warth, M. Mirza, J. Martins, and K. Kunzekmann. 2010. Expression and function of epithelial anoctamins. *J Biol Chem*. 285:7838–45.

Schroeder, B.C., T. Cheng, Y.N. Jan, and L.Y. Jan. 2008. Expression cloning of TMEM16A as a calcium-activated chloride channel subunit. *Cell*. 134:1019–1029.

Scott, R., K. Sutton, A. Griffin, S. Stapleton, and K. Currie. 1995. Aspects of calcium activated chloride currents: a neuronal perspective. *Pharmacol Ther*. 66:535–65.

Scudieri, P., E. Sondo, E. Caci, R. Ravazzolo, and L. Galietta. 2013. TMEM16A-TMEM16B chimaeras to investigate the structure-function relationship of calcium-activated chloride channels. *Biochem J.* 452:443–55.

Scudieri, P., E. Sondo, L. Ferrera, and L.J.V. Galietta. 2012. The anoctamin family: TMEM16A and TMEM16B as calcium-activated chloride channels. *Exp. Physiol.* 97:177–183.

Sheridan, J.T., E.N. Worthington, K. Yu, S.E. Gabriel, H.C. Hartzell, and R. Tarran. 2011. Characterization of the oligomeric structure of the Ca(2+)-activated Cl- channel Ano1/TMEM16A. *J. Biol. Chem.* 286:1381–1388.

Stephan, A.B., E.Y. Shum, S. Hirsh, K.D. Cygnar, J. Reisert, and H. Zhao. 2009. ANO2 is the cilial calcium-activated chloride channel that may mediate olfactory amplification. *Proc. Natl. Acad. Sci. U.S.A.* 106:11776–11781.

Stöhr, H., J.B. Heisig, P.M. Benz, S. Schöberl, V.M. Milenkovic, O. Strauss, W.M. Aartsen, J. Wijnholds, and H.L. Schulz. 2009. TMEM16B, a novel protein with calcium-dependent chloride channel activity, associates with a presynaptic protein complex in photoreceptor terminals. *J. Neurosci.* 29:6809–6818.

Suzuki, J., M. Umeda, P.J. Sims, and S. Nagata. 2010. Calcium-dependent phospholipid scrambling by TMEM16F. *Nature*. 468:834–838.

Taylor, R., and S. Roper. 1994. Ca(2+)-dependent Cl- conductance in taste cells from Necturus. *J. Neurophysiol.* 72:475–478.

Terashima, H., A. Picollo, and A. Accardi. 2013. Purified TMEM16A is sufficient to form Ca2+-activated Cl- channels. *Proc. Natl. Acad. Sci. U.S.A.* 110:19354–9.

Tian, Y., P. Kongsuphol, M. Hug, J. Ousingsawat, R. Witzgall, R. Schreiber, and K. Kunzelmann. 2011. Calmodulin-dependent activation of the epithelial calcium-dependent chloride channel TMEM16A. *FASEB J.* 25:1058–1068.

Tien, J., H. Lee, D.J. Minor, and L. Jan. 2013. Identification of a dimerization domain in the TMEM16A calcium-activated chloride channel (CaCC). *Proc. Natl. Acad. Sci. U.S.A.* 110:6352–7.

Verkman, A.S., and L.J.V. Galietta. 2009. Chloride channels as drug targets. *Nat Rev Drug Discov*. 8:153–171.

West, R.B., C.L. Corless, X. Chen, B.P. Rubin, S. Subramanian, K. Montgomery, S. Zhu, C.A. Ball, T.O. Nielsen, R. Patel, et al. 2004. The novel marker, DOG1, is expressed ubiquitously in gastrointestinal stromal tumors irrespective of KIT or PDGFRA mutation status. *Am. J. Pathol.* 165:107–113.

White, M.M., and M. Aylwin. 1990. Niflumic and flufenamic acids are potent reversible blockers of Ca2(+)-activated Cl- channels in Xenopus oocytes. *Mol. Pharmacol.* 37:720–724.

Xiao, Q., K. Yu, P. Perez-Cornejo, Y. Cui, J. Arreola, and H.C. Hartzell. 2011. Voltage- and calcium-dependent gating of TMEM16A/Ano1 chloride channels are physically coupled by the first intracellular loop. *Proc. Natl. Acad. Sci. U.S.A.* 108:8891–8896.

Yang, H., A. Kim, T. David, D. Palmer, T. Jin, J. Tien, F. Huang, T. Cheng, S. Coughlin, Y. Jan, et al. 2012. TMEM16F forms a Ca2+-activated cation channel required for lipid scrambling in platelets during blood coagulation. 151:111–22.

Yang, Y.D., H. Cho, J.Y. Koo, M.H. Tak, Y. Cho, W.-S. Shim, S.P. Park, J. Lee, B. Lee, B.-M. Kim, et al. 2008. TMEM16A confers receptor-activated calcium-dependent chloride conductance. *Nature*. 455:1210–1215.

Yu, K., C. Duran, Y.Y. Cui, and H.C. Hartzell. 2012. Explaining calcium-dependent gating of anoctamin-1 chloride channels requires a revised topology. *Circ Res*. 110:990–9.

Yu, K., J. Zhu, Z. Qu, Y. Cui, and H. Hartzell. 2014. Activation of the Ano1 (TMEM16A) chloride channel by calcium is not mediated by calmodulin. Yu K, Zhu J, Qu Z, Cui YY, Hartzell HC. *J Gen Physiol*. 143:253–67.